Technische Universität München

WACKER-Lehrstuhl für Makromolekulare Chemie

Copolymerization of Propylene Oxide and CO_2 with Salen-type Catalysts; Polymerization Activities and Polymer Microstructure

Khalifah Ahmad Salmeia

Vollständiger Abdruck der von der Fakultät für Chemie der Technischen Universität München zur Erlangung des akademischen Grades eines

Doktors der Naturwissenschaften

genehmigten Dissertation.

Vorsitzender: Univ.-Prof. Dr. Klaus Köhler

Prüfer der Dissertation: 1. Univ.-Prof. Dr. Dr. h. c. Bernhard Rieger

2. Univ.-Prof. Dr. Fritz E. Kühn

Die Dissertation wurde am 04.03.2013 bei der Technischen Universität München eingereicht und durch die Fakultät für Chemie am 08.04.2013 angenommen.

اهداء

الى امي الحنونة و اخي و اخواتي

الى زوجتي الغالية و ابنتي قرة عيني

الى روح والدي الطاهرة

اهدي هذا العمل

مع كل الحب

DEDICATION

To My Mother & Brother & Sisters

To My Wife and My Daughter

To The Soul of My Father

I Dedicate This Work

With Love

List of Abbreviations

BDI	β-diiminate
BINOL	1,1`-Bi-2-naphthol
^{n}BuTBD	7-Butyl-1,5,7-triazabicyclo[4.4.0]dec-5-ene
$^{n}Bu_4NCl$	Tetrabutylammonium chloride
$^{n}Bu_4NI$	Tetrabutylammonium iodide
$^{n}Bu_4NNO_3$	Tetrabutylammonium nitrare
CHO	Cyclohexene oxide
cPC	Cyclic propylene carbonate
DMAP	4-(Dimethylamino)pyridine
DMAQ	(N,N-dimethylamino)quinoline
ee	Enantiomeric excess
ESI-MS	Electospray ionization mass spectrometry
FRET	Fluorescence Resonance Energy Transfet
$I(\lambda)$	Fluorescence spectrum
K_{rel}	Relative rate reaction for the substrate enantiomers
MALDI	Matrix-assisted laser desorption/ionization
M_n	Average Molecular number
MTBD	7-Methyl-1,5,7-triazabicyclo[4.4.0]dec-5-ene
M_w	Average molecular weight
NMR	Nuclear Magnatic Resonance
PCHC	Poly(cyclohexene carbonate)
PDI	Polydispersity index
PO	Propylene oxide

PPC	Poly(propylene carbonate)
[PPN]Cl	Bis(triphenylphosphine)iminium chloride
R_0	Förster distance
rac	Racemic
SO	Styrene oxide
TBD	1,5,7-Triazabicyclo[4.4.0]dec-5-ene
ToF	Time-of-Flight mass spectrometer
TOF	Turn over frequency
TON	Turn over number
TCSPC	Time Correlated Single Photon Counting
Φ	Quantum yield
τ	Fluorescence lifetime
τ_{DA}	Life time of the donor in presence of the acceptor

List of Contents

1. Introduction

1.1 Carbon Dioxide: from Waste to Chemical Feedstock

Carbon dioxide (CO_2) is the chief greenhouse gas (GHG) that results from human activities and causes global warming and climate change. Climate change is the global challenge that has to be addressed throughout the current century. Since about 1850, rapid growth of CO_2 emission has risen due to the fossil fuels combustion as global dominated energy supply. As a consequence, concentrations of CO_2 have continued to grow and by the end of 2010 had reached 390 ppm, or 39% above preindustrial levels.[1] On the other hand, infrastructure that directly releases GHGs and the infrastructure that contributes to the production of devices that emit GHGs are two important overlapped infrastructural components that have a crucial effect on the atmosphere with respect to GHG emission.[2] However, scenarios of global CO_2 emissions were developed if no additional CO_2-emitting devices were built, allowing all the existing CO_2-emitting devices to live out their normal lifetimes. It has been estimated, cumulatively, that 496 gigatonnes of CO_2 will be emitted with respect to burn rates of fossil fuels by existing infrastructure between 2010 and 2060 to stabilize around twice pre-industrial levels (415 to 550 ppm), taking into consideration the amount of carbon in fossil fuel reserves that not yet burned.[2-4] Limitations up to this point has been depleting conventional oil fields, the oil that freely flows from underground reservoir of its own or with a minimum of encouragement, such as pumping it out or pushing it out using natural mechanisms. For example, oil production of the United States, peaked in 1970 as rising output from newly discovered fields failed to compensate for declines in old fields.[5,6] Carbon dioxide, besides being a natural gas and biomass, will be one of the most abundant carbon sources in the future, since fossil sources (coal, petroleum) are limited. The use of CO_2 as a chemical feedstock will almost certainly not reduce its atmospheric concentration significantly; however, it may provide access to high-value products from a nontoxic, renewable, and low-

cost resource.[7] The potential use of CO_2 as an alternative feedstock for the chemical industry is shown in **Scheme 1.1**.

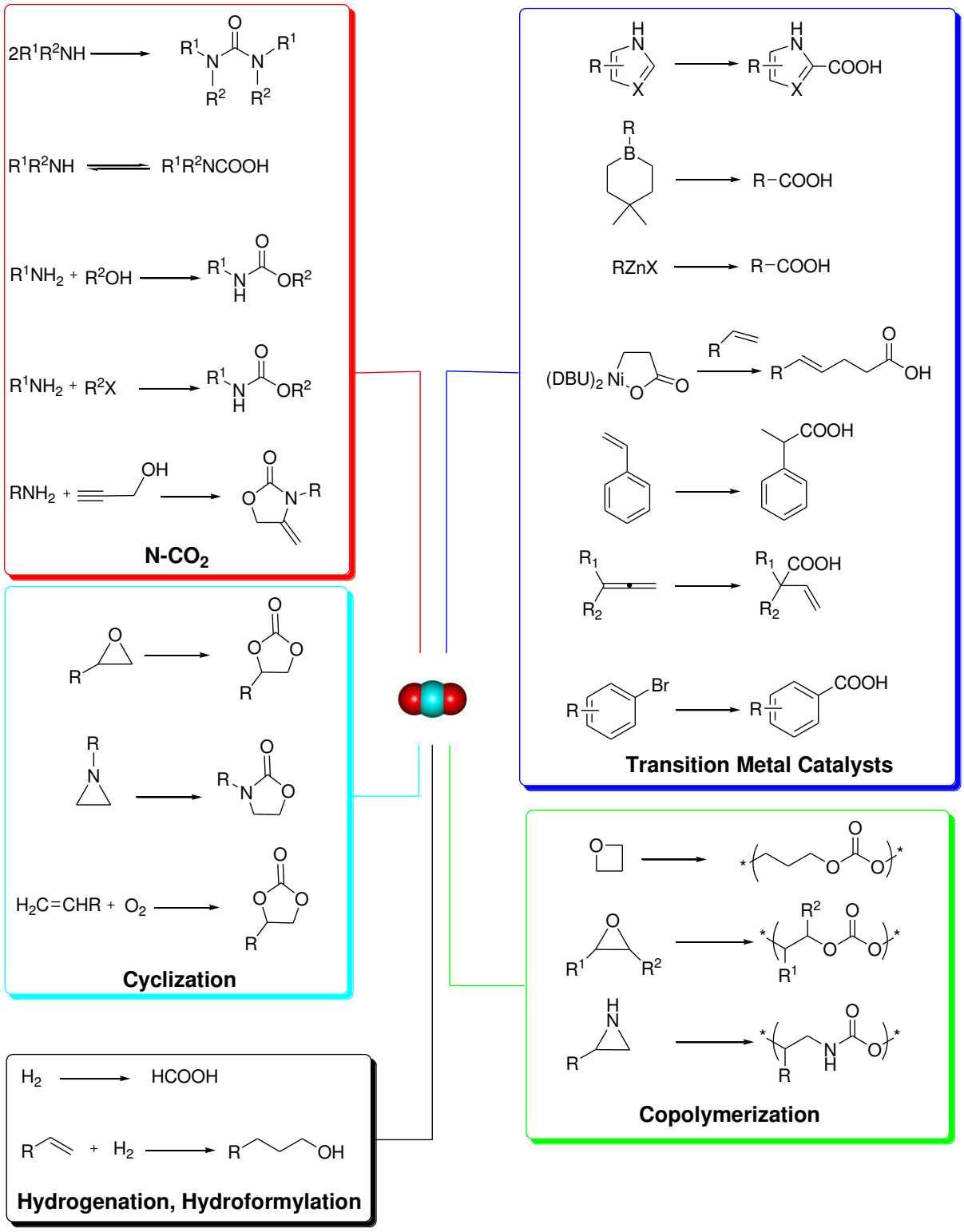

Scheme 1.1: Application of CO_2 in chemical syntheses.[7-10]

Fixation of CO_2 into polycarbonates can reduce the CO_2 atmospheric concentration, by the sustainable long term biodegradation of polymer material and solve CO_2 emission and global warming.[11] Synthesis of polycarbonates from carbon dioxide has been studied ever since the pioneering efforts of Inoue and co-workers.[12,13] On the other hand, the safety and toxicity concerns associated with the production of conventional polycarbonate could enable widespread opportunities for such material. Furthermore, the properties of this material need to be improved. However, the catalysts used for CO_2 copolymerization have a major effect on the physical and chemical properties of polycarbonates, as a consequence, improving the catalysts activity and selectivity offer tremendous potential for producing copolymers from CO_2 with broad properties.[14]

1.2 CO_2 and Epoxide Copolymerization Reaction

Transformation CO_2 into useful chemicals has been explored in recent decades. Despite many successful approaches of CO_2 activation, high energy is required to activate the thermodynamically stable CO_2.[9] In general, catalyst systems have been considered to promote the reactivity of CO_2 toward copolymerization (**Scheme 1.2**). The pioneered successful approach was based on using organometallic compounds as catalysts for copolymerization of epoxide with CO_2.[12,13]

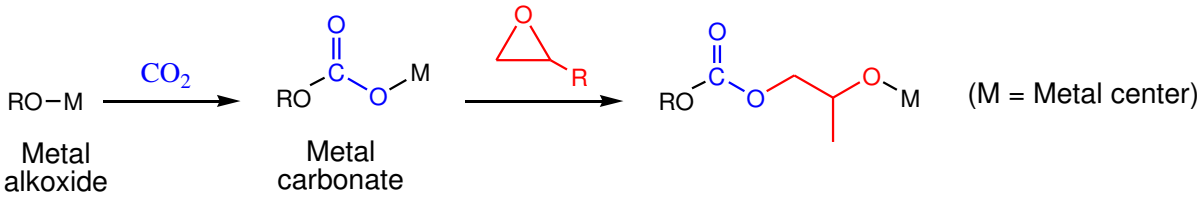

Scheme 1.2: CO_2 and epoxide reaction with metal alkoxide and metal carbonate, respectively.

Other active catalysts were also developed for copolymerization of CO_2 and epoxides. For example, the $ZnEt_2$ catalytic system toward CO_2 and epoxide copolymerization was improved by using $ZnEt_2$/dihydroxy or trihydroxy phenol systems.[15-18] The catalytic activities of $ZnEt_2$/dihydric phenol systems were attributed to the presence of the proposed Et(-Zn-O-

C_6H_5-O-) group related to amount of ethane evolved.[19] Inoue and co-workers tested a new catalytic system consisting of $ZnEt_2$ and dicarboxylic acids or hydroxy carboxylic acids for CO_2/PO copolymerization.[20] Furthermore, different zinc dicarboxylates systems have been reported.[21-24] It is noteworthy that all the above zinc carboxylate catalysts are either slightly or not active toward PO copolymerization with CO_2. On the other hand, zinc glutarate catalyst was found the most active heterogeneous catalyst for copolymerization of CO_2 and PO, producing high molecular weight PPC in a high yield. The catalytic activity of zinc glutarate was attributed primarily to the morphological structure (which includes crystallinity and crystal size) rather than the surface area.[23] However, the heterogeneous nature of these catalytic systems limited the mechanistic understanding of the active species in such systems. Therefore, Darensbourg and co-workers synthesized an active homogenous catalysts afforded from reaction of substituted phenol derivatives with a solution of Zn^{II}(bis-(trimethylsilyl) amide)$_2$ in THF or diethyl ether.[25,26]

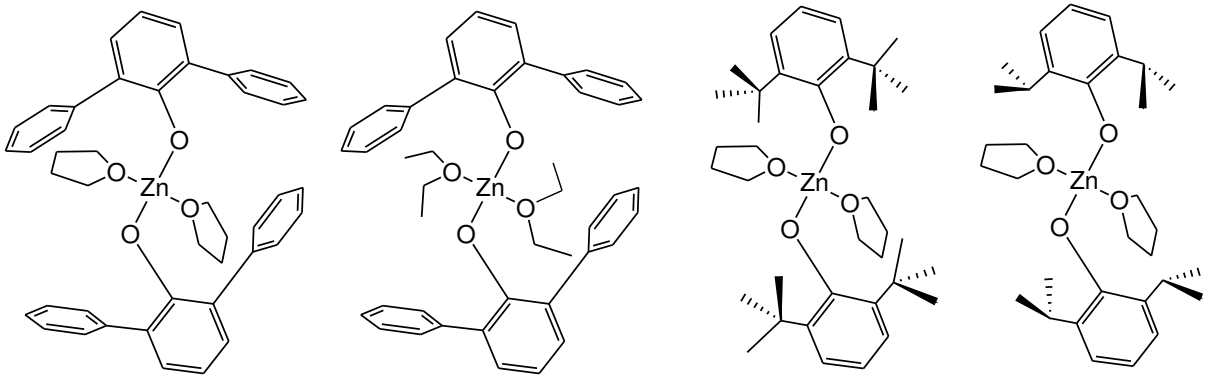

Figure 1.1: Structure of zinc phenoxide catalysts (**1-4**) for copolymerization of CHO and CO_2.

These homogenous zinc phenoxide catalysts (**1-4**) (**Figure 1.1**) were found only selective for CHO copolymerization with CO_2.[26] It was found, that the trend in catalytic activity of these catalysis is a balance between an electron-rich metal center, which is more reactive toward both epoxide ring-opening and CO_2 insertion processes, and the steric hindrance about the

metal center.[25] On the other hand, phosphine derivatives of the monomeric zinc phenoxide complexes, $(phenoxide)_2ZnL_n$ have been investigated for the copolymerization of CHO and CO_2, resulting in poly(cyclohexene carbonate) (PCHC) with low ether linkages units.[25,27,28] In 1998, Coates and co-workers have discovered a new class of well-defined, highly active catalysts for the synthesis of highly alternated, high molecular weight, and monodispersed carbon dioxide/epoxide copolymers.[29] The catalysts have been synthesized by deprotonation of the *β*-diimine ligand (**Figure 1.2**) (BDI-H, derived from 2,6-substituted aniline) with n-butyllithium followed by a subsequent reaction with zinc acetate yields [(BDI)ZnOAc] (**5**) which exists in equilibrium between its monomeric and dimeric structure, whereas it exists as the acetate-bridged dimer in the solid state. However, Reaction of BDI-H with $ZnEt_2$ gives [(BDI)ZnEt], which produces [(BDI)ZnOMe] (**6**) upon reaction with methanol.[29]

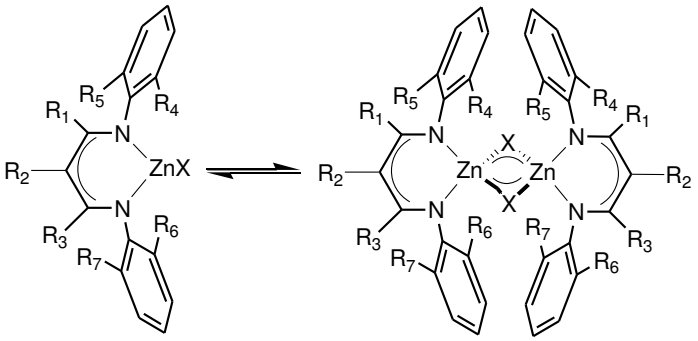

Cat.	X	R_1=R_3	R_2	R_4 =R_5 = R_6 = R_7
5	OAc	Me	H	^{i}Pr
6	OMe	Me	H	^{i}Pr

Cat.	X	R_1	R_2	R_3	R_4 =R_5	R_6 = R_7
7	OAc	Me	H	CF_3	Et	^{i}Pr

Cat.	X	R_1=R_3	R_2	R_4 =R_6	R_5 = R_7
8	OMe	Me	H	^{i}Pr	Et

Cat.	X	R_1=R_3	R_2	R_4 =R_5 = R_6 = R_7
9a	OS(O)Et	Me	H	^{i}Pr
9b	OS(O)Et	Me	H	Et

Cat.	X	R_1=R_3	R_2	R_4 =R_6	R_5 = R_7
9c	OS(O)Et	Me	H	^{i}Pr	Me

Figure 1.2: Structure of ZnBDI catalysts (**5-9**) for copolymerization of CHO and CO_2.

Catalysts **5** and **6** were found active catalyst for copolymerization of CHO with CO_2 with TOF 247 and 224, respectively at moderate reaction temperature and low CO_2 pressure. Furthermore, the polymers produced are of high molecular weight and exhibit very narrow polydispersities, consistent with a living polymerization process. On the other hand, catalyst **7** has shown a significantly higher activity than any other reported catalyst for PPC copolymer with TOF equal 235 at 25 °C reaction temperature and 100 psi CO_2 pressure.[30] Catalyst **7,** as

well, exhibited catalytic activity (TOF = 37 h^{-1}) for the alternating copolymerization of limonene oxide with CO_2. Catalyst **7** is suitable for the enchainment of many different polycarbonate blocks. The minimal influence of monomer variations on chain propagation permits the synthesis of various block copolymers with functionalities including protected alcohol, lipophilic, hydrophilic, and fluorophilic groups in a single chain.[31] In addition, the interchangeability of blocks makes this method well-suited for controlled block copolymer synthesis so that it is now possible to prepare polycarbonates with a wide range of block combinations. It exhibits and maintains superior selectivity for tran-(R)-limonene oxide (% trans in copolymer = 98.9%). The alternating polycarbonate copolymer produced from a cis/trans mixture of limonene oxide is highly regio- and stereoregular. High molecular weight copolymer can be produced using longer reaction times and higher [limonene oxide]/[Zn] ratios.[32] Owing to the well-defined nature of β-diiminate (BDI) zinc complexes (**5**, **6**) for the synthesis of aliphatic polycarbonates, Coates et al. studied different BDI ligand complexes, with varying N-aryl substituents and bridging structures.[33] The optimal catalytic activity occurs with **8**, which crystallized as the methoxide-bridged dimer where the isopropyl substituents adopt cis geometry, producing PCHC with low molecular weight distribution of 1.14 and a turnover frequency of 257 h^{-1}. Rieger and co-workers have reported in 2003 a new and simple strategy to yield active single-component catalysts (**9a-c)** in quantitative yield.[34] The essential feature of the structures **9a-c** is the ethylsulfinate ligand [(BDI)ZnOS(O)-Et] that results from a quantitative insertion of dry SO_2 into the Zn-carbon bond. In addition to the behavior of this initiating group, the influence of BDI-H ligands of variable steric demand on the copolymerization reaction was also discussed. The chemical structure of complex **9a** has been confirmed by single crystal X-ray diffraction. The dimeric **9a** exists in solution in equilibrium with its mononuclear analogue. That is, variable temperature ^1H NMR measuremnts in toluene revealed two sets of resonances whose intensities vary with temperature. The set that becomes more intense with higher temperatures is assigned to the

monomeric complex. Polymerization experiments with the single-component catalysts **9a**-**9c** were performed in neat CHO at 10 bar of CO_2 pressure. All the complexes have shown catalytic activity toward CHO copolymerization with CO_2 (TOF = 135-165, same reaction condition). During the prior copolymerization studies of CHO and CO_2, Coates et a1. found that the complex **8** exhibits superior activity.[33] Therefore they believed that further modification of the ligand geometry could provide an optimal active site for monomer enchainment to result in dramatically improved activities. To probe this, complexes with ligands bearing different aryl groups were synthesized.[35] Unsymmetrical ligands were synthesized by refluxing two different anilines (one equivalent of each) plus one equivalent of 2,4-pentanedione in acidic ethanol. Isolation of the unsymmetrical ligands was accomplished through repeated crystallization from ethanol. Cyanation of the ligands and complex synthesis gave complexes **10a**-**10e** (**Figure 1.3**).

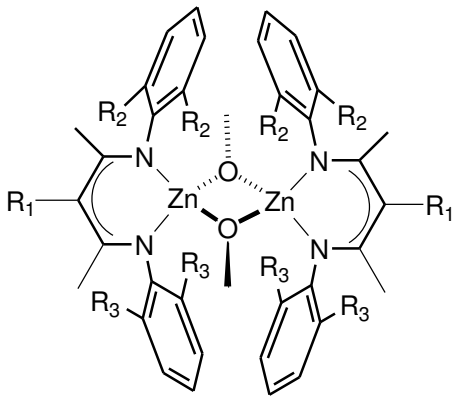

Catalyst	R_1	R_2	R_3
10a	H	Et	Et
10b	CN	Et	Et
10c	CN	Et	^{i}Pr
10d	CN	Me	^{i}Pr

Figure 1.3: Dimeric Structure of Zn BDI complexes (**10a-10d**).

Catalyst **10c** and **10d** showed the highest catalytic activity toward CHO with CO_2 (TOF = 2170 and 2290 h^{-1}, respectively) at 50 °C and 100 psi CO_2 pressure.

In 2005, Kröger and Döring and co-workers have developed a new synthetic route towards chelating imidoester ligands with functional groups on ligand backbone. Generally, the procedure should allow for a wide range of substituents on the ligand. Zinc acetate complexes of these ligands (**11a**-**11e**) (**Figure 1.4**) catalyze the copolymerization of CO_2 and cyclohexene oxide, showing high activities (TOF up to 210 h^{-1}). [36,37] All of these complexes

exist in their monomeric form in solution, whereas the dimeric form is confirmed by single crystal X-ray diffraction.

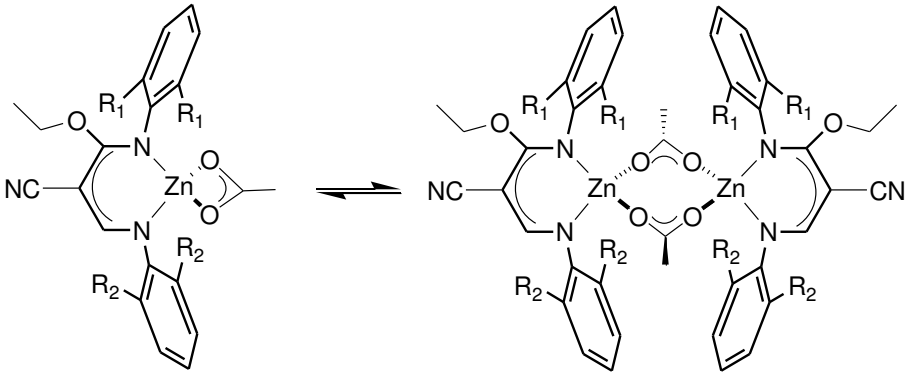

Catalyst	R_1	R_2
11a	^{i}Pr	^{i}Pr
11b	^{i}Pr	Et
11c	Et	^{i}Pr
11d	^{i}Pr	Me
11e	Me	^{i}Pr

Figure 1.4: Monomeric and dimeric structures of catalysts **11**.

On the other hand, the tetramer structures of such analogues compounds have been synthesized.[38] The catalytic activity of such tetramers was found less active than the dimer forms.

1.3 Stereocenters of Epoxides Monomers

The common epoxides that are used for copolymerization with CO_2 are propylene oxide (PO), cyclohexene oxide (CHO) and styrene oxide (SO). All of these monomers contain stereo-centers around the methine carbons which afford different stereoconfigurations (**Scheme 1.3**). The ring-opening of the epoxides during the copolymerization reaction with CO_2 can happen either on the methylene group which retains the chirality of the stereocenter, or on the methine group which leads to either retention ring-opening via S_N^1-type reaction mechanism or inversion ring-opening via S_N^2-type reaction mechanism. Chiral catalysts create new chiral centers in the main chain of the resulting polymers with control of the absolute configuration (**Scheme 1.3**). Precedents for such a methodology are ring-opening polymerization of epoxide or episulfide.[39]

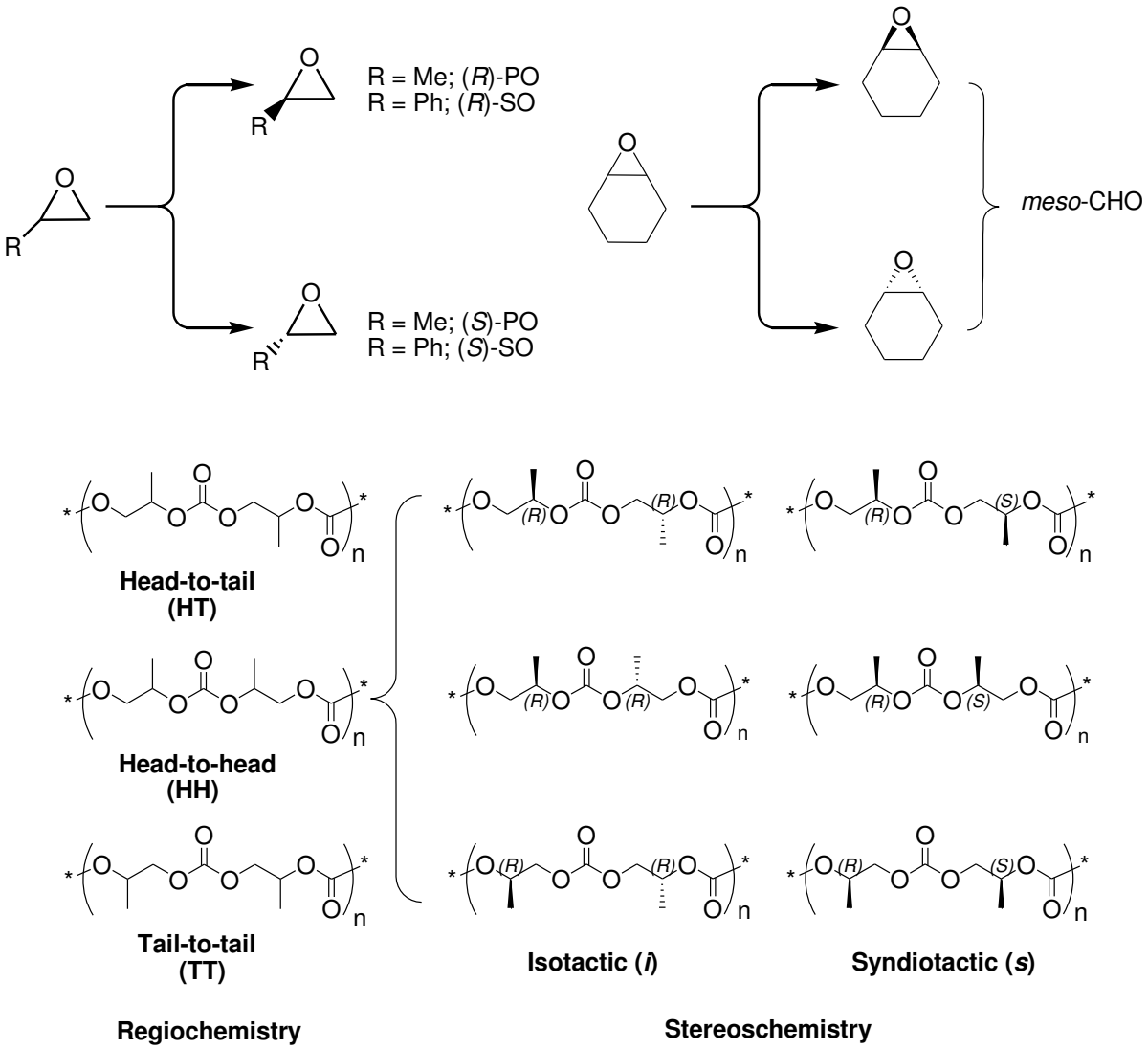

Scheme 1.3: Stereoconfiguration of epoxides monomers and their effect on the stereo- and regiostructure of poly(propylene carbonate).

1.4 Chiral Zn-based Catalysts

In 1999, Nozaki and co-workers reported the first example of asymmetric synthesis copolymerization of meso-CHO and CO_2, initiated by a chiral Zn catalyst using a 1:1 mixture of $ZnEt_2$ and (S)-α,α-diphenylpyrrolidine-2-yl-methanol.[39] Enantiomeric excess up to 70% has been achieved as determined by hydrolysis of the afforded copolymers with aqueous NaOH to obtain the corresponding diol. The molecular structure of this catalyst has been confirmed by X-ray single-crystal diffraction and revealed that the obtained zinc complex **12** formed a

dimeric structure in which two zinc centers were coordinated in a distorted tetrahedral geometry.[40] The copolymer end group was determined by MALDI-ToF spectrometer, which exhibited that the copolymerization was initiated by (S)-α,α-diphenylpyrrolidine-2-yl-methanol group. Accordingly, the asymmetric induction which achieved to give the optically active copolymer was explained by the participation of a dimeric zinc species in the copolymerization process (**Scheme 1.4**).[40]

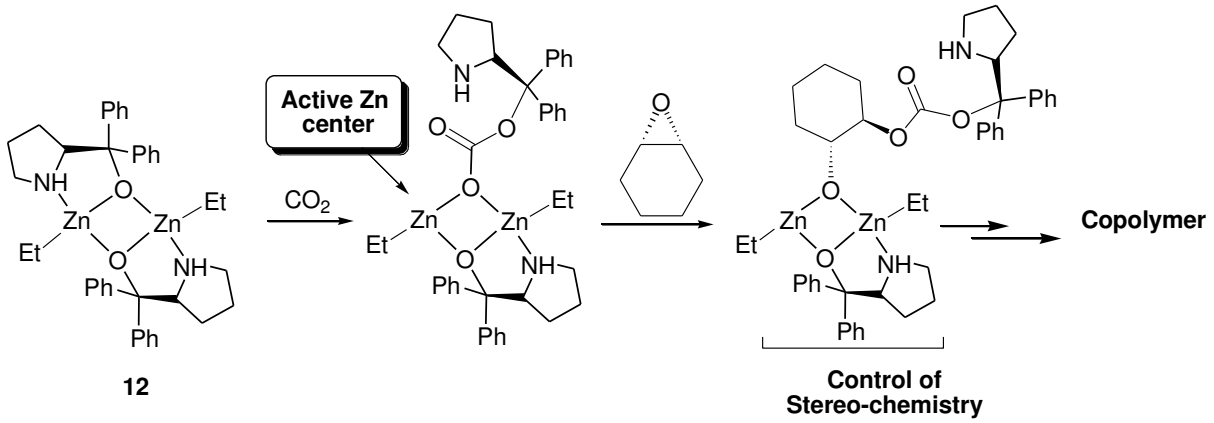

Scheme 1.4: proposed stereochemistry mechanism reaction of meso-CHO copolymerization and CO_2 using catalyst **12**.

The isolated dimeric zinc complex **12** showed lower enantioselectivity (ee = 50%) than those reported previously.[39] Upon addition of ethanol, the enantioselectivity increased to 80% ee, which demonstrated that the active species catalyst results from substituting of ethyl group by ethoxy group which was confirmed by MALDI-ToF MS.[40] Independently, Coates and co-workers were working in a parallel manner to design a hybrid imine–oxazoline ligands (**13**) to attempt stereochemical control.[41]

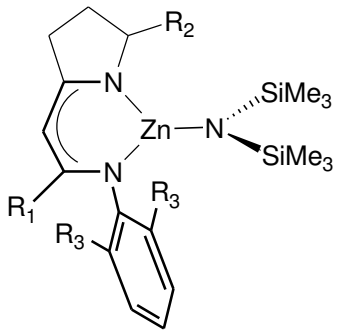

Cat.	R_1	R_2	R_3
13a	Me	(*R*)-Ph	^{i}Pr
13b	CF_3	(*R*)-Ph	^{i}Pr
13c	^{i}Pr	(*R*)-Ph	^{i}Pr
13d	^{i}Pr	(*S*)-^{i}Pr	^{i}Pr
13e	^{i}Pr	(*S*)-^{t}Bu	^{i}Pr
13f	^{i}Pr	(*S*)-^{t}Bu	Et
13g	CF_3	(*S*)-^{t}Bu	^{i}Pr
13e	^{i}Pr	(*S*)-^{t}Bu	^{i}Pr

Figure 1.5: Structure of zinc complexes of chiral imine-oxazoline ligands.

Interestingly, complex **13e** exhibits both the highest activity and stereoselectivity, producing a quantitative yield of poly(cyclohexene carbonate) from meso-CHO and CO_2 with an RR:SS ratio of 86:14. This was the first example of catalysts used to produce crystalline PCC with T_m equal 220 °C. On the other hand, **13e** was also investigated for the copolymerization of cyclopentene oxide (CPO) and CO_2, the copolymer formed contained 88% RR-units in the main chain.

1.5 Chiral Salen Ligand Complexes

Although cobalt catalysts have essentially no precedent in CO_2/epoxide polymerization,[42] The discovery of hydrolytic kinetic resolution (HKR) by Jacobsen and co-workers using chiral chromium[43] or cobalt[44,45] salen and salan ligands complexes to access the enantiomerically pure epoxides by ring-opening had inspired the investigation of chiral salen-type complexes for the synthesis of optically active polycarbonates.[46-54] Major research has been devoted to the synthesis of new catalysts to study their chemical activity and selectivity, as well as the mechanism and stereochemistry of the copolymerization.[14,55] In 2003 Coates and co-workers explored the application of [(salen)$Co^{(III)}$] complexes in selective preparation of poly(propylene carbonate) from the copolymerization of CO_2 and propylene oxide.[56] They focused their efforts on [Co(Salen)OAc] (**14a**-**14c**) (**Figure 1.6**) combinations known to affect both of the productive steps of polycarbonate formation.[53]

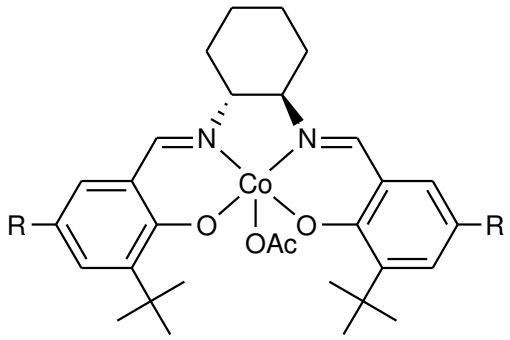

14a; R = Br
14b; R = H
14c; R = ^{t}Bu

Figure 1.6: Structure of [Co(Salen)OAc] (**14a**-**14c**).

All the complexes (**14a**-**14c**) are enantiomerically pure (R,R)-stereochemistry, thus enabling the stereoselectivity of epoxide enchainment to be measured. All the catalysts require high pressure (55 bar) for the most favorable activity, but with much higher selectivity for copolymer formation with alternating 95% carbonate linkages and narrow molecular weight distribution. Regarding the regioselectivity of PO enchainment, **14c** is highly selective with 80% head-to-tail linkages. Copolymerization of (S)-propylene oxide with enantiomerically-pure **14c** yields an isotactic (S)-copolymer with an unprecedented head-to-tail content of 93%, catalyst **14c** preferentially consumes (S)-propylene oxide over (R)-propylene oxide with a K_{rel} of 2.8. The stereo- and regiochemistry of the copolymers have been improved by addition of the cocatalyst, based on the fact that chiral [(salen)$Co^{(III)}$] complexes (Jacobsen catalyst) are highly efficient and enantioselective catalysts for the hydrolytic kinetic resolution of terminal epoxides.[43-45] Accordingly, Lu and co-workers designed a binary nucleophile–electrophile catalyst system consisting of chiral [(salen)$Co^{(III)}$] (**15**) complexes and quaternary ammonium salts (**Figure 1.7**) for the direct synthesis of optically active PPC from rac-epoxides.[46] In this system, the chiral [(salen)$Co^{(III)}$] complex was proposed to serve as an electrophile for selectively complexing one enantiomer of the rac-epoxides, and the anion of the quaternary ammonium salt serves as a nucleophile.

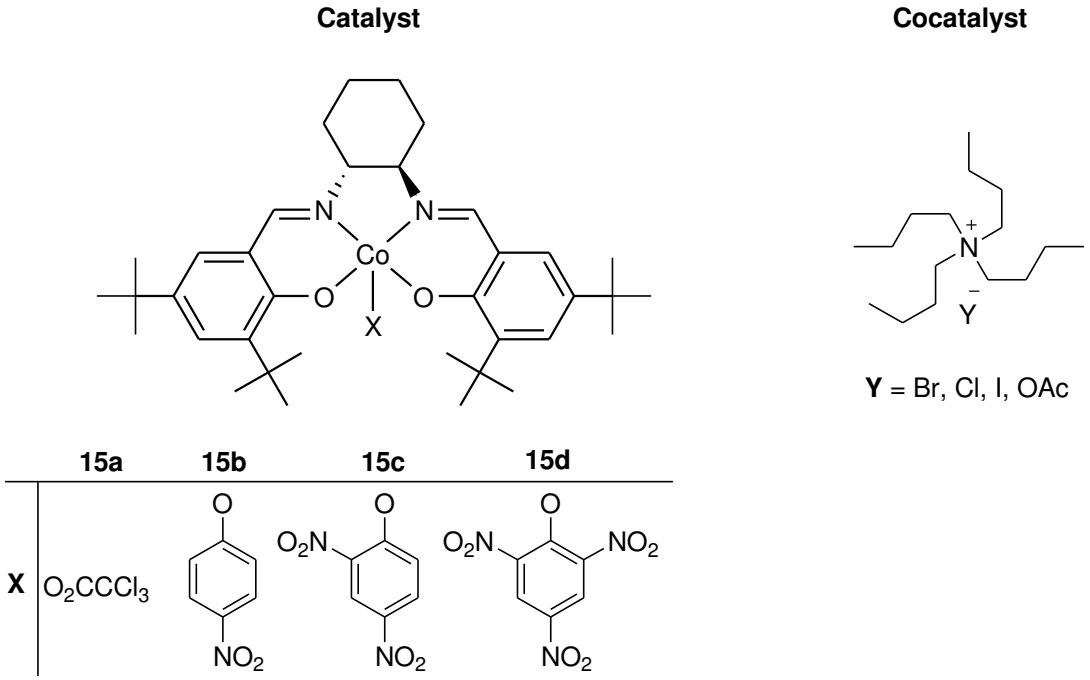

Figure 1.7: Binary cobalt-salen catalytic system for PO copolymerization with CO_2.

The regioselective attack of a nucleophile or activated CO_2 at the coordinated epoxide on the less substituted carbon atom leads to enantioselective ring-opening of the epoxide with subsequent formation of the chiral cyclic carbonates through intermolecular cyclic elimination (**Scheme 1.5**). It seems that the use of a cobalt complex with an electron-withdrawing axial group X and a quaternary ammonium salt, whose anion exhibits poor leaving ability, increases the selectivity for PPC. Notably, these binary catalyst systems based on chiral catalysts (**14c**, **15a**-**15d**) preferentially consume (S)-PO over (R)-PO (K_{rel} up to 3.5). In comparison to Coates catalytic system,[53] the binary catalytic system requires mild temperature (25 °C) and CO_2 pressure (20 bar) to afford the corresponding alternating copolymer with more than 95% head-to-tail regioregularity. Notably, these cobalt complexes or quaternary ammonium salts by themselves show no catalytic activity under the conditions employed, even for long reaction time. All the isolated polymers have narrow molecular-weight distributions consistent with a controlled polymerization.

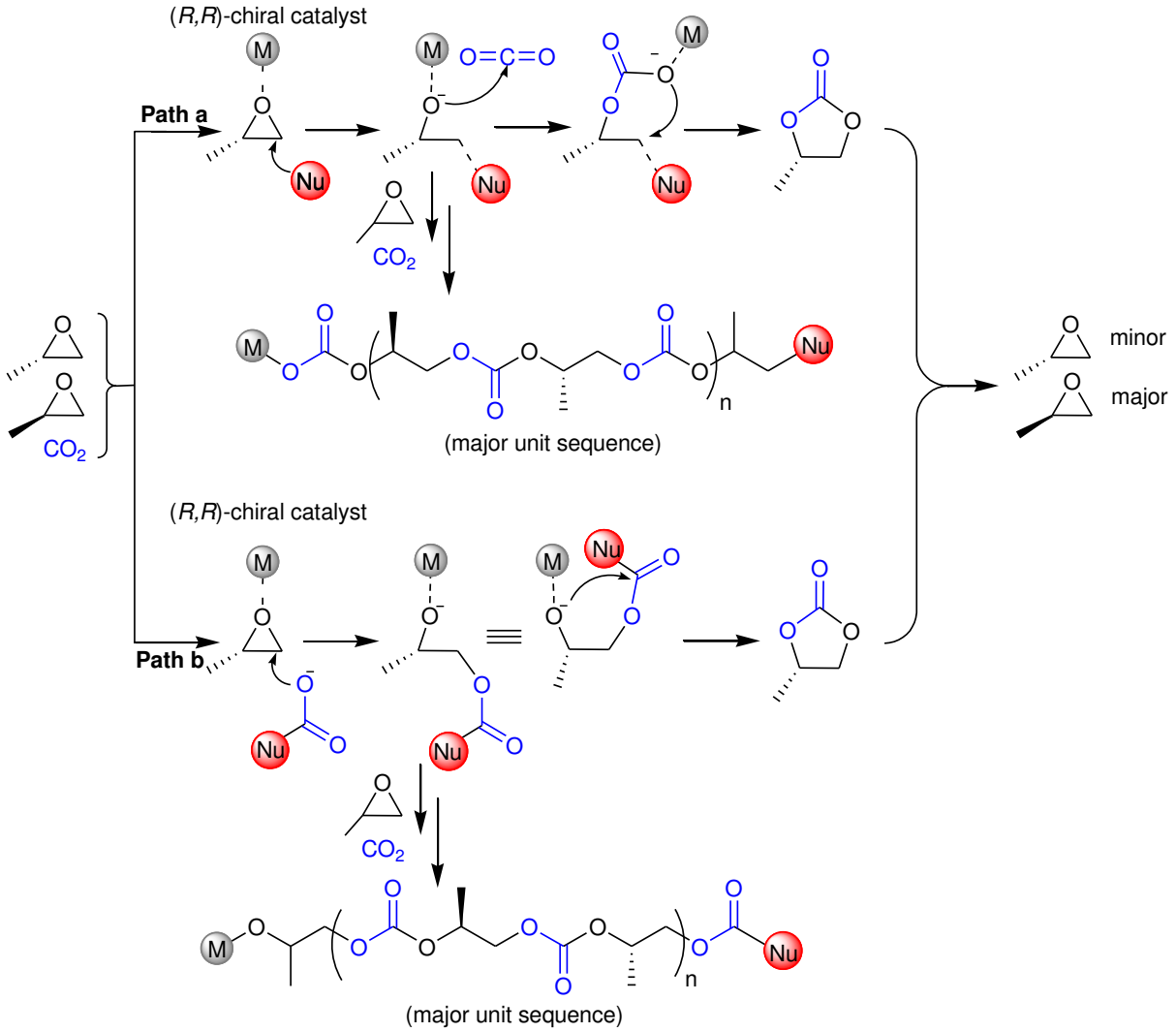

Scheme 1.5: Direct synthesis of optically active cPC or PPC from rac-PO and CO_2 using cocatalyst/enantiomeric pure chiral catalyst systems.

However, the M_n values are not close to the expected values which indicate the existence of chain transfer during the reaction. The ^1H NMR spectra of all produced PPCs show >99% carbonate linkages, and the $^{13}C\{^1H\}$ NMR spectra show that these polymers have an unprecedented head-to-tail content of 95%. Lu et al. work led Coates and co-workers to further catalyst optimization by employing organic salt cocatalysts.[54] Accordingly, Coates continued the studies concerning the PO/CO_2 copolymerization using complexes **16a-16d** (**Figure 1.8**) and **14c** as well.

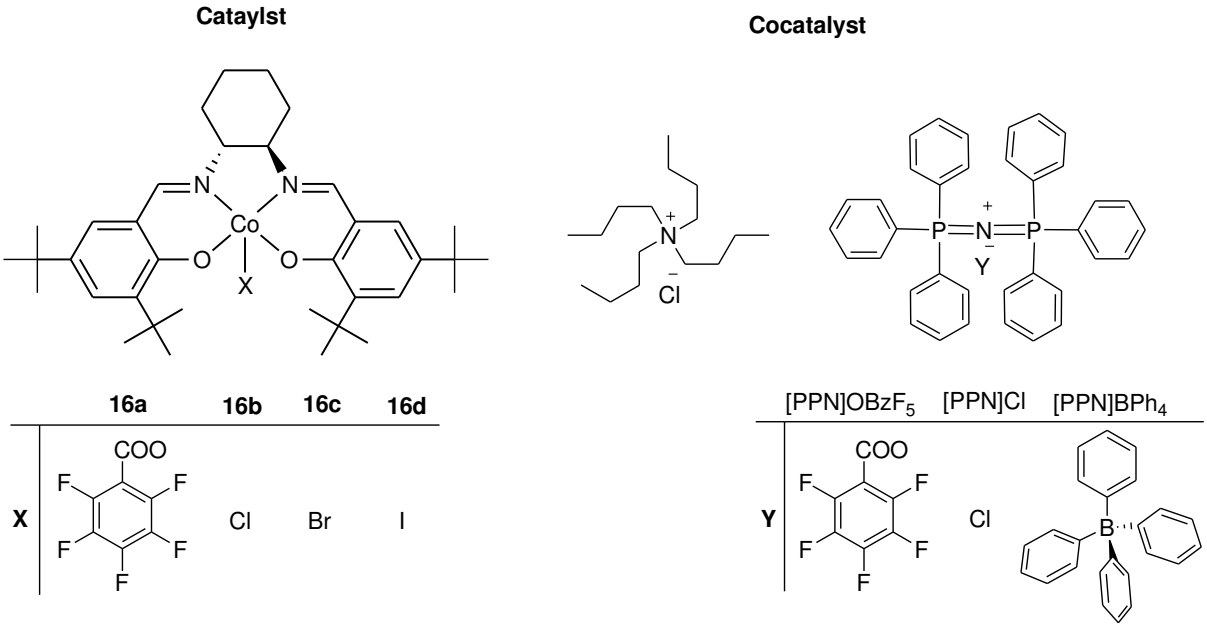

Figure 1.8: Chemical structures of complexes **16a-d** and the organic salts cocatalysts.

The influence of the catalyst initiator on overall performance and investigate the effects of $[PPN]^+$-based ionic cocatalysts (bis(triphenylphosphine)iminium) on catalyst activity, product selectivity, stereoselectivity and regioselectivity has been explored. The order of increasing activity for copolymerization with (R,R)-(salen)CoX complexes is **16d < 16b < 14c ≈ 16a < 16c**, with catalyst **16c**, producing PPC with a TOF = 90 h^{-1}. However, copolymerization of rac-PO and CO_2 by catalysts **16a-d** and **14**c using [PPN]Cl showed remarkable improvement in catalyst activities (TOF up to 520 h^{-1} using **16a**) , as well as increased stereo- and regioselectivites. The product PPC is nearly completely alternating, with >90% head-to-tail connectivity and is iso-enriched with high M_n and narrow molecular weight distribution (MWD). However, copolymerization of PO and CO_2 with different catalyst/cocatalyst combination, namely **16a/**[PPN]Cl and **16b/**[PPN]$OBzF_5$ has been investigated. The isolated copolymers from each system showed a UV activity whereas the ^{19}F NMR spectrum of each copolymer revealed that $OBzF_5$ end groups were present in both samples. Consequently, it

was hypothesized that each cobalt center propagates two polymer chains, whereas the initiation can occur from the catalyst precursor as well as salt cocatalyst (**Scheme 1.6**).

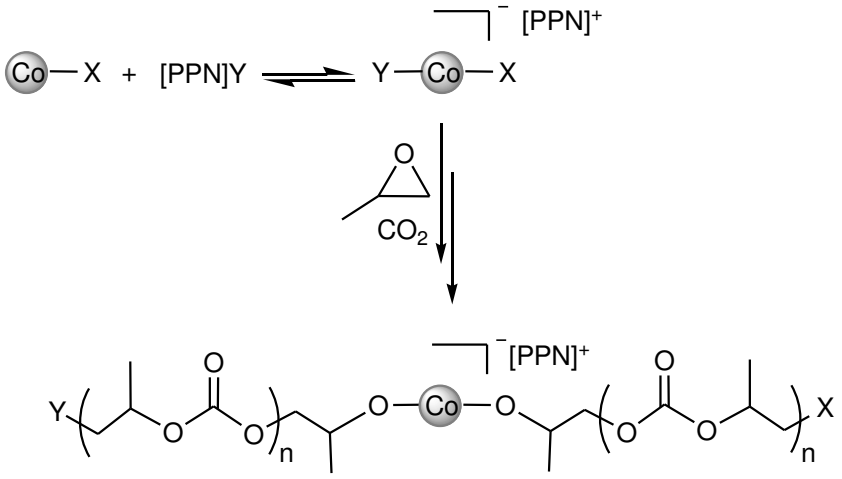

Scheme 1.6: Proposed dual side mechanism for copolymerization of PO and CO_2 by $Co^{(III)}$-salen catalysts and cocatalysts.

On the other hand, Coates and co-workers have applied the catalytic system (**14c**,**16a-d**) for copolymerization of CHO and CO_2.[57] Continuing to his previous work,[53] Coates et al. studied the effect of different catalytic systems on the copolymer stereochemistry. Accordingly, different copolymer microstructures have been synthesized based on the catalytic systems and the stereoconfiguration of the PO monomer. Specifically, based on the total reaction systems, regioregular atactic, regioregular isotactic, regioirrigular heterotactic and regioregular syndio-endriched copolymers have been synthesized.[54] Enantiomerically pure (R,R)-$Co^{(III)}$(salen) complexes **14c**, **16b**, **16d** and **17a-f** in conjunction with N,N-dimethylaminoquinoline (DMAQ) were investigated as catalytic systems for the copolymerization of PO and CO_2 over a wide range of CO_2 pressures.[58] These catalytic systems were active at low CO_2 pressures with optimal activity achieved in the range 15-35 bar of CO_2. Increasing the pressure above this range resulted in a significant reduction in reaction rate.

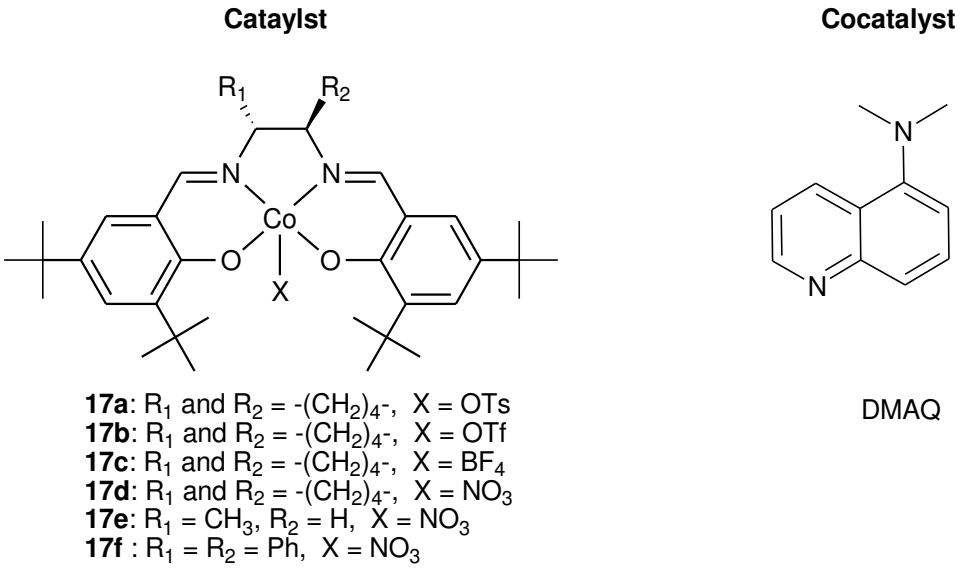

Figure 1.9: Chemical structures of complexes **17a-f** and organic base cocatalyst.

The ratio of catalyst/DMAQ was also found to influence the TOF. Optimal activity occurred when 2 equivalents of DMAQ were employed. Using only 1 equivalent of DMAQ decreased the activity by over 50%, whereas an increase beyond 2 equiv lead to a slight decrease in activity along with a slight increase in the polymer MWD. The nature of the catalyst's counter anion and ligand structure were found to influence both the activity and stereoselectivity of the copolymerization. The TOF changes with the identity of the counter anion with the NO_3^- anion providing the most active catalyst **17d**. However, there is no obvious trend between counter anion and catalyst activity. For the same counter anion, changing the salen ligand framework to incorporate non cyclic backbones resulted in a slight improvement in TOF as well as a significant drop-off in stereoselectivity as determined by the enantiomeric excess (ee) of the remaining PO. A K_{rel} of 5.1 is obtained with the (R,R)-cyclohexyl backbone, whereas the (R)-propyl and (R,R)-diphenyl backbones of catalyst **17e** and **17f** gave a K_{rel} of only 2.0 and 1.2, respectively. It has been postulated that the improvement in enantioselectivity observed with the addition of the DMAQ cocatalyst may be a result of the steric interactions between the coordinated amine and the salen ligand framework. These interactions may lead to improved ligand geometry about the active metal center that is better

able to induce enantioselectivity during the reaction. In addition, the utilization of the DMAQ cocatalyst also lead to a considerable improvement in regioselectivity in regards to PO enchainment. Examination of the carbonate region of the $^{13}C\{^{1}H\}$ NMR spectra of the polycarbonate product resulting from the copolymerization of rac-PO and CO_2 shows that **17a**/DMAQ is highly regioselective, as the polycarbonate product exhibits a microstructure with a head-to-tail content of 96%. Moreover, Lu and co-workers[47] have investigated the regio- and stereoselective alternating copolymerization of CO_2 and reacemic aliphatic epoxides by using binary catalyst system of a chiral Schiff base cobalt complexes **18a-c** (**Figure 1.10**) as well as complexes **15a** (**Figure 1.7**), **16b-c** (**Figure 1.8**) and **17d** (**Figure 1.9**) as catalysts in conjunction with an ionic organic ammonium salts or sterically hindered strong organic base as cocatalysts. With ionic ammonium salts as the cocatalyst, both the anion and cation of the ionic salt influence the rac-PO and CO_2 copolymerization. Anions with higher nucleophilicity and better leaving ability, such as I^-, Br^-, and N_3^-, are beneficial for improving the activity of the binary catalyst system, but have a negative effect on the selectivity for PPC. The use of a nucleophilic anion with poor leaving ability, such as Cl^- and F^-, can effectively suppress cyclic PC formation and increase the selectivity for the polymer as well as the enantioselectivity of the resulting PPC, while decreasing the catalytic activity to a certain extent.

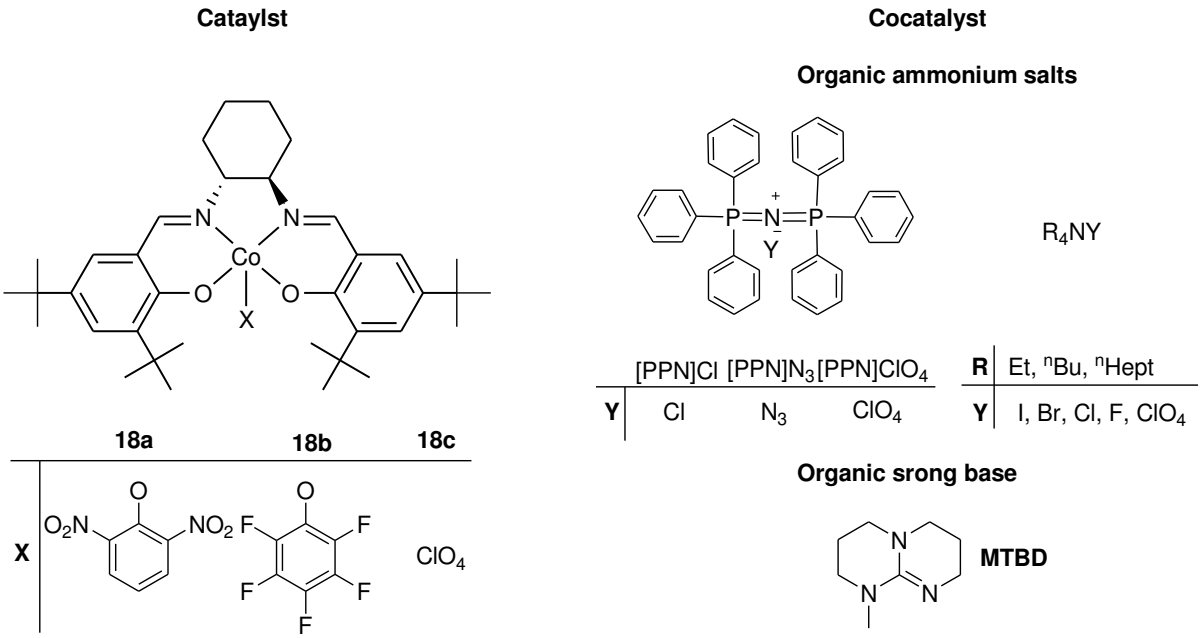

Figure 1.10: Binary catalytic systems for rac-PO and CO_2 copolymerization.

In contrast, if the anion of the used ionic ammonium salt has no nucleophilicity (ClO_4), the binary catalyst system is found to be ineffective for this reaction. However, the effects of the cation of the ionic organic salt have been found significant on reaction rate and PPC enantioselectivity. For example, $^{n}Hept_4NBr$ substituted for Et_4NBr with complex **18a** results in an increase of TOF from 156 h^{-1} to 314 h^{-1} and a K_{rel} from 3.2 to 4.4. Similar increases in activity and enantioselectivity also occur in the substitution of [PPN]Cl for $^{n}Bu_4NCl$ or $^{n}Bu_4NI$ as the cocatalyst. In general, an ionic ammonium salt consisting of a bulky cation and a nucleophilic anion with poor leaving ability as the cocatalyst is more beneficial for improving the activity, polymer selectivity, and enantioselectivity. On the other hand, sterically hindered strong organic bases, such as 7-methyl-1,5,7-triazabicyclo[4.4.0]dec-5-ene (MTBD) (**Figure 1.10**), combined with complex **18a** also effectively catalyzed the rac-PO/CO_2 copolymerization to selectively form PPC with improved enantioselectivity (TOF ≈ 77h^{-1} and K_{rel} ≈ 5.7). Also, the resulting PPC has a narrow MWD and a high head-to-tail content of up to 96%. A prolonged reaction time resulted in a linear increase in the polymer molecular weight, consistent with a controlled polymerization, and M_n close to the expected

values, which indicate a living polymerization nature. The results are different from those of the binary system with an ionic ammonium salt as the cocatalyst, in which unexpected chain transfer appears during the reaction. It is interesting that the molar ratio of MTBD with respect to **18a** in the binary catalyst system significantly affects the reaction rate and polymer molecular weight, rather than the polymer selectivity and molecular weight distribution, enantioselectivity, and stereochemistry of the resulting polymer. Increasing the MTBD molar ratio up to four equivalents results in a significant decrease in the polymer molecular weight. For the binary [PPN]Cl/**18a** system, increasing the ratio of the ionic ammonium salt with respect to **18a** also increases the rate, but causes a substantial decrease in the polymer molecular weight and the concomitant formation of cyclic propylene carbonate (cPC). It has been found that the binary **18a**/MTBD system can operate very efficiently at 0 °C and 6 bar of CO_2 or 25 °C and atmospheric pressure of CO_2 with TOF = 22 h^{-1}, 77 h^{-1} and K_{rel} = 6.2, 5.1, respectively. It represents the first example of rac-PO/CO_2 copolymerization under an atmospheric pressure of CO_2 with excellent activity, high polymer selectivity, > 99% carbonate linkages, and > 95% head-to-tail linkages. For binary catalyst systems of a chiral tetradentate Schiff base cobalt complex as the electrophile in conjunction with an ionic organic salt or a sterically hindered strong base as the nucleophile, the substituent groups on the aromatic rings, chiral diamine backbone, and axial X group of the electrophile, as well as the nucleophilicity, leaving ability, and coordination ability of the nucleophile all significantly affect the catalyst activity, polymer selectivity, enantioselectivity, and stereochemistry. Generally, a bulky chiral SalenCo$^{(III)}$X with an axial X group of poor leaving ability, in conjunction with a bulky ionic ammonium salt consisting of a bulky cation and a nucleophilic anion with poor leaving ability as the nucleophile, compose the ideal binary catalyst system for CO_2/rac-PO copolymerization to selectively produce PPC with excellent activity, relatively high enantioselectivity, >95% head-to-tail connectivity, and >99% carbonate linkages. A sterically hindered strong organic base with a low coordination ability (also a

bulky nucleophile) and a bulky electrophile of chiral SalenCo$^{(III)}$X compose the ideal binary catalyst system for CO_2/rac-PO asymmetric living copolymerization with improved enantioselectivity (**Scheme 1.7**).

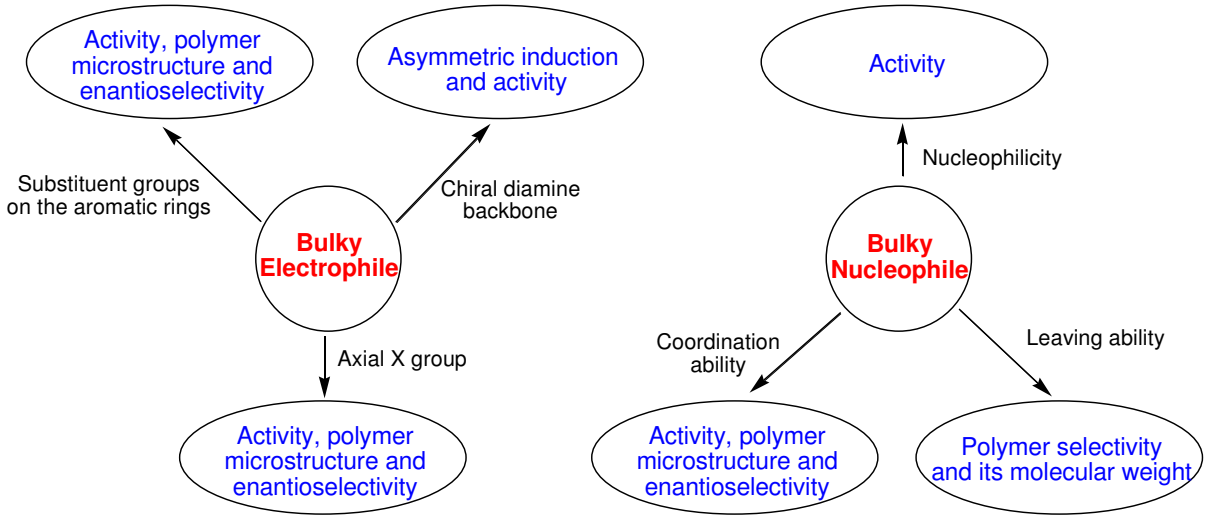

Scheme 1.7: Effects of the electrophile and nucleophile of the binary catalyst system on the rac-PO and CO_2 copolymerization.

Moreover Lu and co-workers[59] have applied the **15a**/[PPN]Cl catalytic systems for the asymmetric alternating copolymerization of alicyclic CHO and CO_2. This combined binary catalytic system has been found very active at ambient temperature and 6, 15 and 52 bar CO_2 pressure for meso-CHO/CO_2 copolymerization to provide (S,S)-enriched poly(cyclohexene carbonate) (RR:SS = 31:69, 31:69 and 36:64, respectively) with narrow MWD but with pronounced decrease in the catalytic activity at high CO_2 pressure. The enantioselectivity of the resulting PCHC was evaluated from the hydrolysis of PCHC with aqueous NaOH affording cyclohexene carbonate (cHC). However, the enantioselectivity value of this system is less than of PCHC obtained by Nozaki and Coates.[39-41] Moreover, Lu and co-workers studied the stereoselectivity of some SalenCr$^{(III)}$X complexes (**19**) for CO_2/epoxides copolymerization.[60]

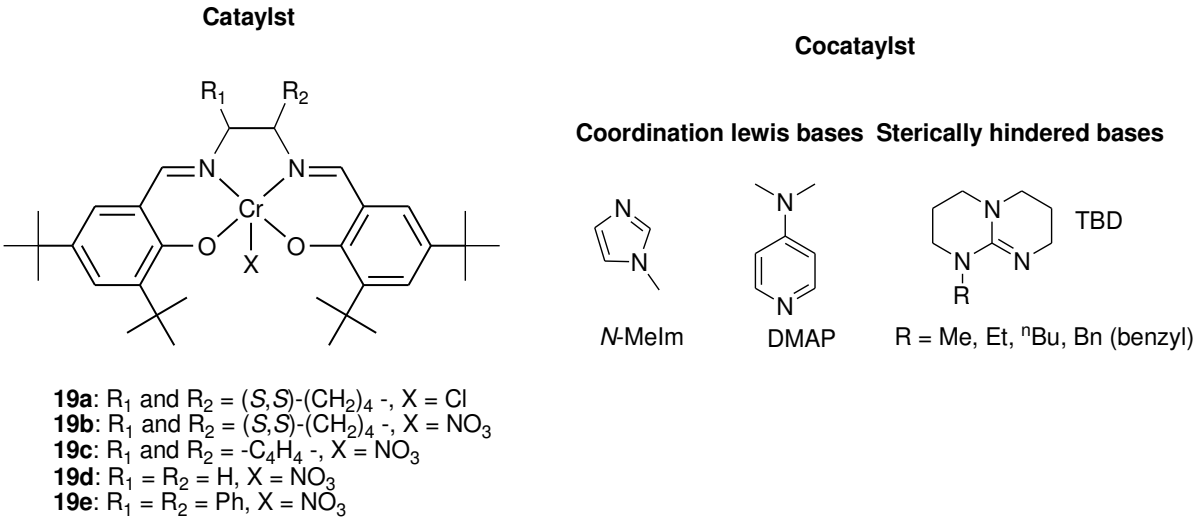

Figure 1.11: General structure of SalenCr(^{III})X complexes and organic bases utilized for CO_2 and PO copolymerization.

The polycarbonate produced is regioirregular with head-to-tail linkages range 64 to 92%. Copolymerization reaction of CO_2 and PO using catalysts **19a** and **19b** without cocatalyst, resulted in regioirregular PPC with head-to-tail linkages of 64% and 73%, respectively. The regioregularity of obtained PPC using **19b** in presence of cocatalysts was improved with head-to-tail connectivity up to 93% using ^{n}BuTBD as cocatalyst. The influence of the "polymer chain-end control" on polycarbonates stereochemistry control was also investigated. Because the ring-opening of a meso-epoxide proceeds with inversion at one of the two chiral centers, a successful asymmetric ring-opening by a chiral catalyst can give optically active polycarbonates with an (R,R)- or (S,S)- trans-1,2-diol unit. The binary system of the complex (1S,2S)-**19b** in conjunction with MTBD could operate efficiently for CHO and CO_2 copolymerization to selectively provide the corresponding polycarbonates, but the ee of the cyclohexane-1,2-diol produced from the hydrolysis of the resulting poly(cyclohexene carbonate) (PCHC) is only 14.5% with an R,R configuration. When a mixture epoxide of CHO and (R)-PO (1:1, molar ratio) was used for copolymerization with CO_2, the ee of the cyclohexane-1,2-diol produced from the hydrolysis of the resulting terpolymer increased to

26.6%. Further increase in the molar ratio of (R)-PO to CHO from 1:1 to 4:1 resulted in notable increase of ee up to 37.1%. Substituting (S)-PO for (R)-PO with the complex (1S,2S)-**19b** led to significant decrease in the propylene carbonate linkages in the resulted polymers. Interestingly, the ee of the corresponding cyclic propylene carbonate is only 72.5% with an (S)-configuration indicating a stereochemistry inversion occurring in ring-opening of (S)-PO during the polymerization. Furthermore, rac-SalenCr$^{(III)}$X complexes in conjunction with MTBD were tested for terpolymerization of CHO and chiral PO with CO_2, with the resulting polymers exhibiting certain enantioselectivity. The results clearly indicate that a "polymer chain end control" mechanism originating from the chiral propylene carbonate unit significantly affects the stereoselective opening of inserted CHO and thus further controls the stereochemistry of the resulting polycarbonates to a certain extent. However, due the low catalytic activity of SalenCr$^{(III)}$ complexes with respect to their analogous cobalt because of the higher electrophilicity of the central chromium ion of the SalenCr$^{(III)}$. Consequently, Lu and co-workers, have investigated decreasing the electrophilicity of the central metal ion of chiral chromium complexes by the assumption that SalanCr$^{(III)}$X complexes possess a lower electrophilicity which control the copolymer stereochemistry and enantioselectivity.[48] (**Figure 1.12**).

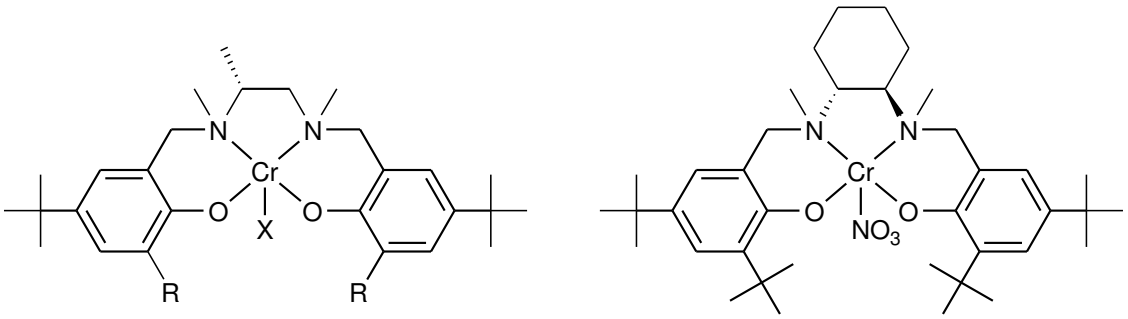

20a: R = ^{t}Bu, X = Cl
20b: R = ^{t}Bu, X = NO_3
20c: R = adamantyl, X = NO_3

20d

adamantyl :

Figure 1.12: Structures of SalanCr$^{(III)}$X complexes.

The catalysts **20a-d** preferentially consume (S)-PO over (R)-PO. The enantioselectivity of the binary catalytic systems of **20a**, **20b** and **20c** with different organic ionic salts showed K_{rel} up to 3.9. By using **20c/**$^{n}Bu_4NNO_3$ binary system, the K_{rel} has increased to 7.1 with 94% regioregular head-to tail connectivity, but with low relative catalytic activity (TOF = 14 h^{-1}) and low M_n (7.8 kg/mol). The influence of the copolymerization reaction temperature on PPC microstructure using **20b/**$^{n}Bu_4NNO_3$ binary catalytic system exhibited an increase in the regioirregularity of PPC microstructure and a decrease of the enantioselectivity of the catalyst with increasing the reaction temperature. The stereochemical studies of PPCs derived from the copolymerization of CO_2 with chiral PO at various conditions reveal that the polymer enantioselectivity is directly proportional to its head-to-tail linkages with regard to regioselective ring-opening of the epoxide. On the other hand, Nozaki and co-workers have studied the stereoselective copolymerization of meso-CHO and CO_2 using (R,R)-SalalenCr$^{(III)}$Cl as catalysts (**21**).[61]

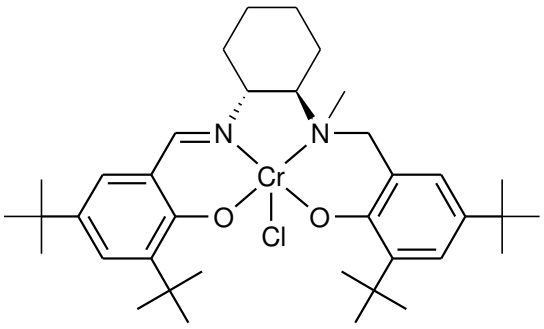

21

Figure 1.13: (R,R)-SalalenCr$^{(III)}$Cl as catalysts (**21**) for copolymerization of CHO and CO_2.

The optimum Copolymerization reaction condition of meso-CHC and CO_2 using the binary catalytic system **21**/[PPN]Cl was found to be at 70 °C and 3.4 MPa of CO_2 affording alternating PCHC with (TOF = 230 h^{-1} , M_n = 9.1 kg/mol. The NMR spectrum revealed that afforded PCHC is almost atactic copolymer. The alkali treatment of the copolymer gave

trans-cyclohexene-1,2-diol in a very low degree of desymmetrization with enantiomeric excess of 11% (R,R).

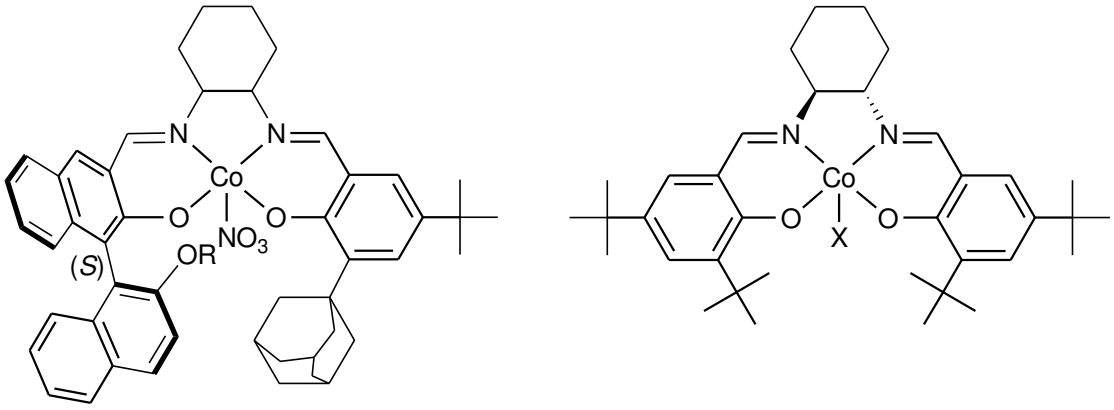

22a: (*S*,*S*)-,R = Me
22b: (*S*,*S*)-,R = ^{n}Bu
22c: (*S*,*S*)-,R = ^{i}Pr
22d: (*R*,*R*)-,R = ^{i}Pr

22e: X = NO_3
22f: X = 2,4-dinitrophenoxy

Figure 1.14: Structure of cobalt complexes **22a-22f**.

In comparison with the previously reported systems based on **22e** or **22f**,[62] the enhanced K_{rel} observed in the present catalyst systems is probably ascribed to the cooperative chiral induction of the S configuration of 2′-alkyloxy-1,1′-binaphthyl in complexes **22a**–**c**. In order to clarify it, they also prepared cobalt-salen complex **22d** with a (R,R,S) configuration, originating from (R,R)-1,2- diaminocyclohexane backbone and S-configured 2′-isopropyloxy-1,1′-binaphthyl. Although complex **22d** exhibited an excellent activity similar to complex **22c** and the resulting polycarbonate had a high head-to-tail content up to 98%, the K_{rel} of 1.1 led to very low copolymer enantioselectivity. This result demonstrates that the S configuration of 2′-alkyloxy-1,1′-binaphthyl in complexes **22a**–**c** plays a significant role in the chiral induction during asymmetric copolymerization of CO_2 and rac-PO. As anticipated, MTBD is an excellent cocatalyst which, in combination with complex **22c,** is also efficient in catalyzing this copolymerization to selectively provide the corresponding polycarbonates with more than 99% carbonate linkages and 98% head-to-tail connectivity. Substituting $^{n}Bu_4NCl$ for [PPN]Cl with complex **22c** resulted in decreasing K_{rel} from 12.4 to 9.1, as well as an apparent decrease

in catalyst activity. On the other hand, the catalytic activity and enantioselectivity enhanced by using bulky cations, which ascribed to the existence of a coulombic interaction between the quaternary ammonium cation and the chain- growing carbonate anion. The influence of reaction temperature on polymer microstructure and K_{rel} has been investigated. The decrease in reaction temperature from 25 to 0 °C resulted in a significant increase of K_{rel} from 12.4 to 18.1. Further decrease in reaction temperature led to slight increase in K_{rel}, while the resulting polymers also had more than 99% head-to-tail connectivity. On the other hand, Lu and co-workers have investigated multichiral catalyst systems,[52] which contain a derived chiral BINOL and a 1,5,7-triazabicyclo[4.4.0]dec-5-ene (TBD, a sterically hindered organic base) unit anchored on the ligand framework for asymmetric, regioselective and stereoselective alternating copolymerization of CO_2 with rac-aliphatic terminal epoxides (**23a-d**).

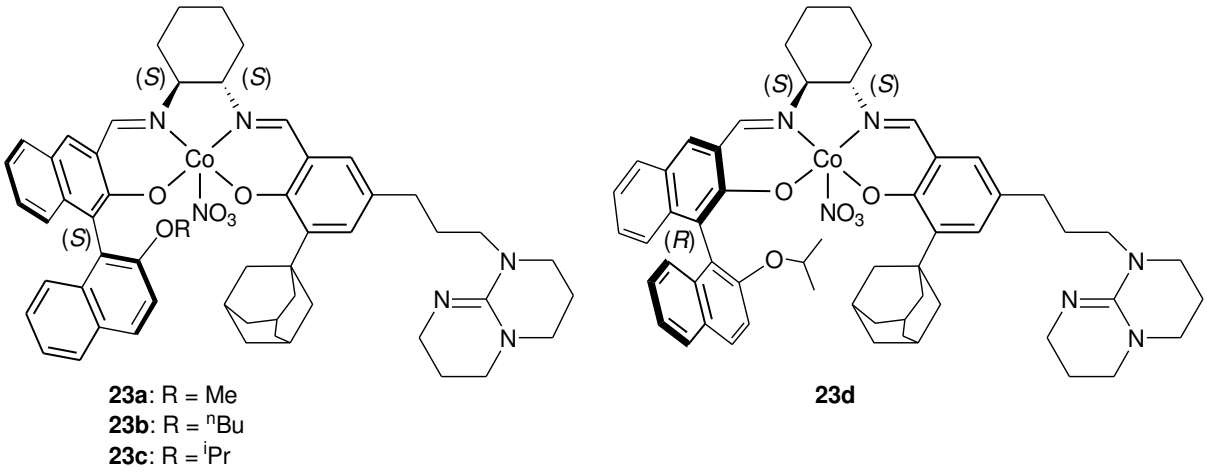

Figure 1.15: structure of single site cobalt salen complexes with chiral BINOL ligand (**23a-23d**).

The initial studies show that complexes **23a-c** could efficiently catalyze copolymerization of CO_2 and rac-PO to selectively afford PPCs with more than 99% carbonate linkages at a [PO]/[catalyst] ratio of 5000 at 20 °C and under 1.0 MPa CO_2 pressure. The steric hindrance of 2´-alkyloxy group in the chiral BINOL has an important influence on kinetic resolution of the rac-epoxide during the copolymerization with CO_2. Among these catalysts, complex **23c** with isopropoxy as substituent group proved to be more efficient in consuming (R)-epoxide

over (S)-epoxide with a K_{rel} of 12.9. On the contrary, complex **23a** with methoxy as substituent group shows less efficient kinetic resolution of rac-PO, indicating that highly steric hindrance helps to promote the competition coordination of (R)-epoxide over (S)-epoxide to the central metal ion. The higher K_{rel} observed is probably ascribed to the enhanced chiral induction in the presence of derived (S)-BINOL in complexes **23a–c**. Moreover, the reaction temperature has a significant influence on kinetic resolution of the rac-epoxide during the copolymerization with CO_2. A decrease in reaction temperature from 20 to 0 °C results in a K_{rel} increase from 12.9 to 19.0. Furthermore, when the reaction was performed at −20 °C, a K_{rel} of 24.3 was achieved, the highest record in this asymmetric copolymerization. Comparing the catalytic activity of **23d** and **23c** shows same catalytic activity and copolymer regiostructure, but discrete enantioselectivity (K_{rel} = 1.4 and 12.9, respectively). It exhibits the influence of the BINOL configuration on the enantioselectivity which affects the copolymer microstructure, with respect to the configuration of cyclohexene backbone. The resultant polycarbonates, however, have more than 99% head-to-tail linkages. The (S,S,S)-cobalt-based complex **23c** is also a highly efficient catalyst system for the copolymerization of CO_2 and various terminal epoxides with a long aliphatic chain to provide corresponding optically active polycarbonates under solvent free condition.[52] The stereochemistry of salen ligands significantly impacts the catalytic activity and enantioselectivity of their complexes.[54] Accordingly, Nozaki and co-worker synthesized binuclear cobalt complexes consisting of two identical (**24a-d**) or opposite (**25a-d**) enantiomers of a cobalt–salen unit.[50] In general, The (R,R)-(R,R)- complexes showed much lower activity than (R,R)-(S,S)-analogs. The length of carbon backbone linker also significantly influenced the catalytic activity of copolymerization reaction of PO and CO_2. The catalyst **25c** with hexanedioate linker demonstrated the highest activity and can keep its catalytic activity even under diluted condition ([PO]/[Co] = 10,000, TOF = 120 h^{-1}). Increase in reaction temperature to 40 °C improved the catalytic activity (TOF up to 430 h^{-1}).

However, a further increase in polymerization temperature (60 °C) diminished the catalytic activity. The regioselectivity of PO ring-opening ratio could be calculated by $^{13}C\{^{1}H\}$ NMR spectra of the copolymers.

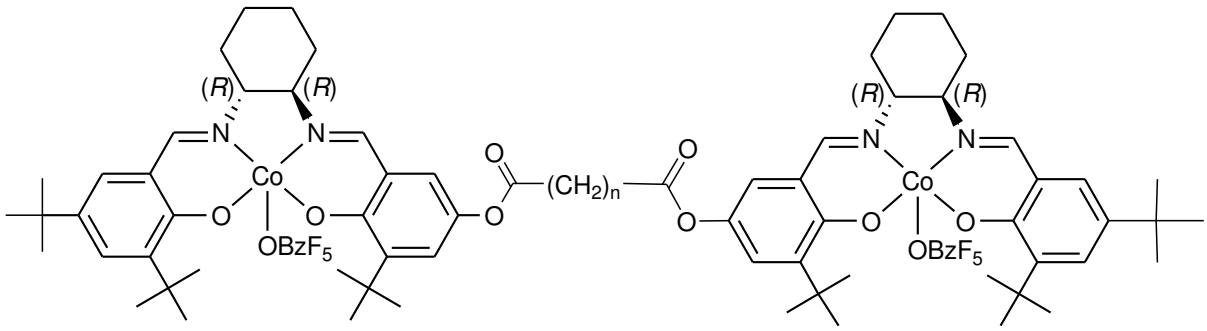

24a, n = 10
24b, n = 7
24c, n = 4
24d, n = 3

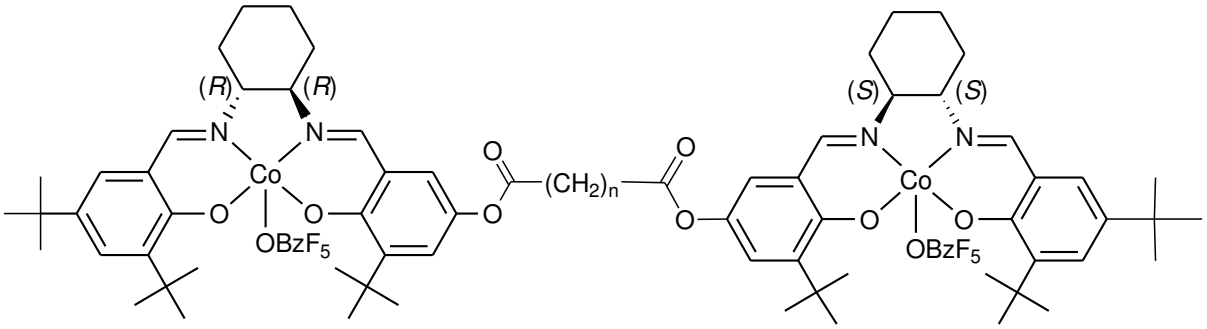

25a, n = 10
25b, n = 7
25c, n = 4
25d, n = 3

Figure 1.16: Structure of dinuclear Co-Salen complexes with aliphatic backbone bridge.

The meso and racemo microstructures existing in the HT regiostructure depend on the asymmetric center in the main chain. Although complete peak separation for each of the triad structure **ii**, **is**, **si**, and **ss** was unsuccessful, Nozaki et al. measured the ratio of [**ss**]/[**ii**] ratio which essentially represents the s/i ratio. The HT stereostructure based on [**ss**]/[**ii**] ratios using **25a-c** were found 3.4, 3.5, and 2.0 respectively indicating the bimetallic propagation mechanism. The head-to-tail selectivity was all around 80% with the binuclear complexes

25a-c. It is notable that the [**ss**]/[**ii**] ratio was affected by the length of the linker between the two salen ligands.

1.6 Microstructure analysis of polycarbonates

1.6.1 Poly(propylene carbonate) microstructure

The PPC copolymer obtained from copolymerization of PO and CO_2 was first analyzed by Inoue and co-workers.[12,13] PPC copolymer was characterized using elemental analysis data and ^{1}H NMR spectroscopy using $ZnEt_2/H_2O$ catalytic at atmospheric CO_2 pressure.[13] The elemental analysis measurements showed existence of 88% carbonates linkages, which is consistent with the value calculated from ^{1}H NMR spectrum (**Figure 1.17**).[13] On contrary, the elemental analysis of PPC copolymer obtained using $ZnEt_2/H_2O$ at high CO_2 pressure showed almost completely alternating copolymer.[12]

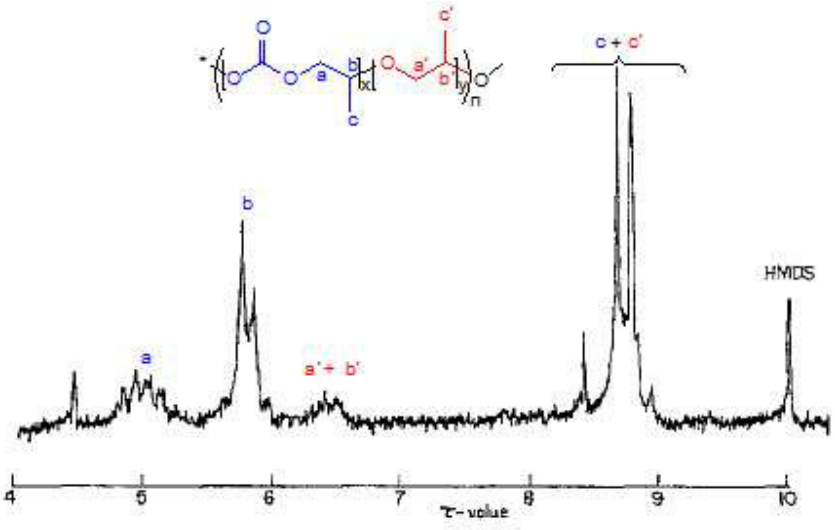

Figure 1.17: ^{1}H NMR spectrum ($CDCl_3$, 100 MHz) of poly(propylene carbonate).[13]

The ^{1}H NMR spectrum of polyether-polycarbonate block copolymer from CO_2 and PO was also reported and analyzed by NMR spectroscopy.[63] Moreover, PO in the copolymerization reaction with CO_2 has two different centers to be attacked (i.e., methylene carbon center and

methine carbon center). The mode of the ring-opening of PO reflects the nature of the reaction, under basic conditions the methylene carbon-oxygen linkage is predominantly cleaved whereas under acidic conditions ring-opening of methine carbon-oxygen linkage takes place.[64] The mode of ring-opening of enantiomerically pure PO was first studied by Inoue and co-workers using $ZnEt_2/H_2O$ catalytic system by investigation the optical purity of hydrolysis product of PPC to propylene glycol.[64] The racemization was found 9.6% where each ring-opening of methine-oxygen bond accompanied by inversion of the configuration of the carbon atom. Consequently, racemization of 9.6% corresponds to 4.8% ring-opening of methine-oxygen bond with predominant 95.2% methylene-oxygen bond ring-opening of PO. This analysis reveals that the obtained PPC from copolymerization of enantiomeric pure PO and CO_2 is almost isotactic stereostructure. However, the $^{13}C\{^1H\}$ NMR spectra in 1977 by Inoue and co-workers of the copolymer obtained either by copolymerization of rac-PO and CO_2 or (R)-PO and CO_2 by using $ZnEt_2/H_2O$ catalytic system exhibit no differences.[65] Therefore Inoue et al. believed that the spectral information does not necessarily reflect the microstructure of the copolymers, and the tacticity of PPC.[65] In 1985, Lednor and co-worker have assigned the $^{13}C\{^1H\}$ NMR spectra of the carbonate carbon region for different PPC based on the regiostructure of different copolymer samples.[66] The observed carbonate carbon atom resonances could be described as three main groups of peaks, (HT, HH, and TT) and an additional minor peak labelled HT´ (**Figure 1.18**).

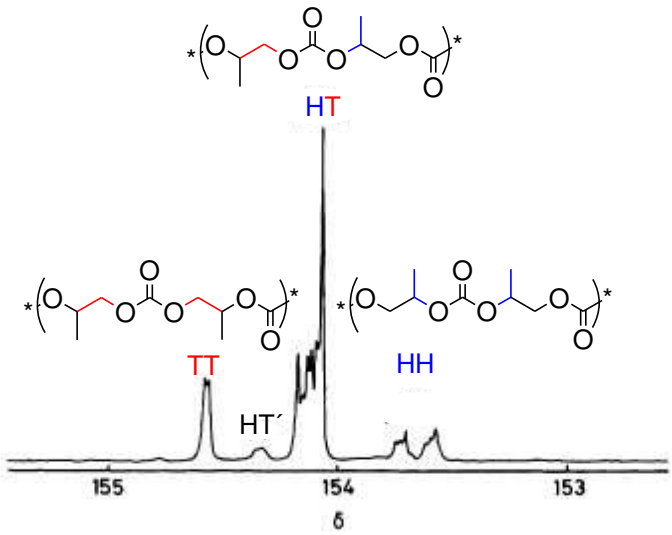

Figure 1.18: $^{13}C\{^{1}H\}$ NMR spectrum ($CDCl_3$, 100 MHz) of poly(propylene carbonate).[66]

The main groups of peaks arise from the mode of ring-opening (RO) of PO. The basis of this assignment is perceived by number of carbon atoms around the central carbonate carbon atom, being respectively 2,3, and 4 for the **TT**, **HT**, and **HH** units. On the other hand, for randomly occurring inversions of PO units in a chain, the amounts of head-to-head and tail-to-tail units are statistically equal to each other. The fact that, in the three cases examined, the intensities of the peaks assigned to **HH** and **TT** units are indeed equal to each other is taken as evidence in support of the assignment. However, tacticity of the copolymer was yet undefined, as the peak assigned as **HH** shows a greater splitting than that assigned as **TT**. The tacticity effect will be the most pronounced in the **HH** case. The minor peak labeled **HT'** is believed to be due to a carbonate carbon atom flanked by ether linkages. In 2002, Chisholm and co-workers have assigned the $^{13}C\{^{1}H\}$ NMR spectra for different PPC copolymer based on statistical approach.[67] First, the $^{13}C\{^{1}H\}$ NMR spectrum of (S)-PPC obtained from copolymerization of (S)-PO and CO_2 using zinc glutarate catalyst has been studied. The carbonate carbon region showed more than one resonance providing information concerning the possible regiosequences that occur at the tetrad level. Consequently, Chisholm et al. proposed four regiosequences with central **HT** junctions that are distinguishable by NMR for

the carbonate carbons (**Figure 1.19**). Accordingly, the predominant carbonate carbon signal of PPC obtained from copolymerization of (S)-PO and CO_2 has been assigned to the **iii** tetrad of the (**HT**)(**HT**).(**HT**)(**HT**) sequence, which must, by accidental degeneracy, occur with one of the other less abundant regiosequences (**HT**)(**HT**).(**HT**)(**TH**) or (**TH**)(**HT**).(**HT**)(**HT**). The minor signal is assigned to one of the latter and the least favored (**TH**)(**HT**).(**HT**)(**TH**) sequence. However, a statistical probability calculation for copolymerization, a mixture of (S)-PO:rac-PO with a ratio of 1:1 and CO_2 will favor the eight stereosequences of the (HT)(HT).(HT)(HT) tetrad as follows: **iii** (0.320), **iis** (0.117), **sii** (0.117), **iss** (0.117), **ssi** (0.117), **isi** (0.070), **sis** (0.070), and **sss** (0.070).

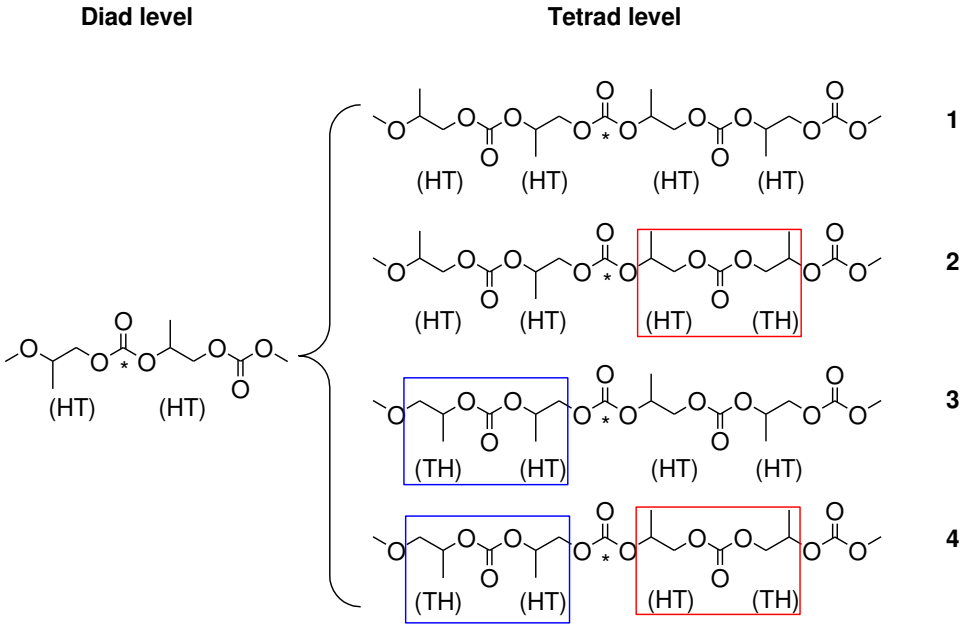

Figure 1.19: proposed four regiosequences with central HT junctions.

The other carbonate carbon signals arising from **TT** and **HH** junctions at the diad level were assigned as **s**. Because other regiosequences are in combination roughly equally probable to the major (**HT**)(**HT**).(**HT**)(**HT**) tetrad, Chisholm and co-workers were unable to make any further unequivocal assignments. Moreover, they have applied the same statistical approach for aliphatic carbon in PPC but at triad level,[67] and later on, they have tried to analyze the structure of oligoether carbonates.[68] The compounds $R(PO)_nOCO_2(PO)_nR$, where R = Me, Et,

or H, and n = 1, 2, 3, 4, ~10 and ~30, were synthesized and have been examined as potential models for PPC microstructural assignments in NMR studies. The $^{13}C\{^{1}H\}$ NMR investigations of those compounds showed that the carbonate carbon signals have both regio- and stereosensitivity at the diad and the tetrad levels to its adjacent ether units.[68] However, as an aid to the interpretation of the NMR data, calculations based on density functional theory (DFT) and the Gaussian 98 suite of programs have been applied to examine the energies of various conformers. The calculations on the model compounds indicated that the carbonate groups exist predominantly at cis-cis geometries with more than one stable conformation for each molecule. In addition, the $^{13}C\{^{1}H\}$ chemical shifts predicted in the calculations were sensitive to the conformations of the molecules and the configurations of the stereocenters in PO ring-opened units. On the other hand, Coates and co-workers have assigned the $^{13}C\{^{1}H\}$ NMR spectra for different PPC microstructure according to the stereochemistry around the carbonate carbon.[54] Initially, Coates et al. assigned the most upfield **HT** shift in (S)-PPC spectrum as the **ii** triad which aligns with the most upfield **HT** resonance of atactic PPC. Furthermore, the **is** and **si HT** linkages should integrate equally yet show different resonances due to the directionality in the PPC. Therefore, central **HT** resonances have been assigned to the **is/si** triads and the remaining **ss** triad to the most downfield **HT** resonance. Based on this scheme, the most downfield and upfield resonances in both the **TT** and **HH** portions of the spectrum were assigned to **s** and **i** diads, respectively. **Figure 1.20** is a simplification of the complex triad sequences from the many possible combinations of neighboring stereo- and regiosequences.

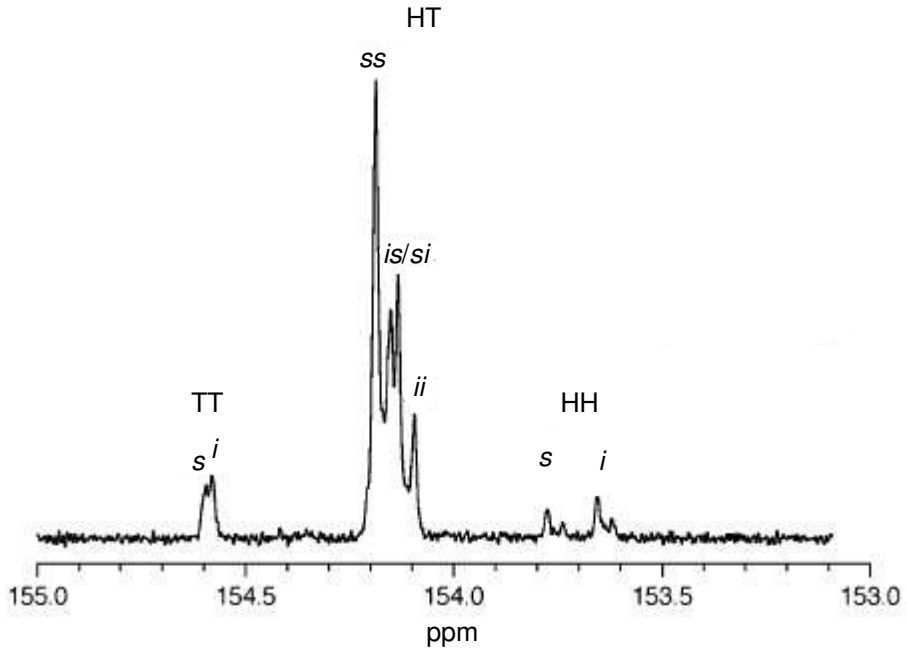

Figure 1.20: Stereostructure assignment of Carbonate carbon region of the $^{13}C\{^1H\}$ NMR spectrum of poly(propylene carbonate).[54]

1.6.2 Poly(cyclohexene carbonate) microstructure

Cyclohexene oxide (CHO) exists only as cis (meso)-isomer. According to the mode of ring-opening during CHO and CO_2 copolymerization reaction, the monomer units in the copolymer can be in cis or trans form.[69] Alkaline hydrolysis of PCHC obtained from copolymerization of cis-CHO and CO_2 using $ZnEt_2/H_2O$ catalytic system, was found to contain monomeric units of trans-form, therefore, ring-opening of CHO occurred with inversion of configuration. Enantiomeric excess of hydrolyzed PCHC obtained from copolymerization reactions of meso-CHO and CO_2 using chiral zinc-based catalyst to diols showed up to 70% (R,R)-cyclohexane-1,2-diol ee.[39] However, (R,S)-cyclohexane-1,2-diol was not obtained,[39] which confirms the completely S_N2-type ring-opening as predicted by Inoue et al.[69] The $^{13}C\{^1H\}$ NMR spectra of PCHC with different (R,R):(S,S) ratio raises a question regarding the syndiotactic and isotactic diads. Corresponding to a (R,R):(S,S) ratio of 80:20, if all the (S,S)-diol unit is involved in syndiotactic diads, the possible maximum content of the

syndiotactic diad would be 40%, and the possible minimum content of the isotactic diad would be 60%. However, the 83:17 ratio of peaks at δ_C 153.7 and 153.1 (**Figure 1.21**) would be interpreted as isotactic and syndiotactic, respectively.[39] This signal assignment contradicts reported assignments by Kuran and co-worker.[70] Coates and co-workers have studied the chemical structure and physical properties of the CHO/CO_2 polymer derived using chiral bis(oxazoline) derived zinc catalysts in detail.[41] The carbonate region (δ_C 152–154) of the $^{13}C\{^1H\}$ NMR spectrum of the polymer appears to exhibit partial tetrad resolution based on comparison of experimental and predicted intensities assuming an enantiomorphic-site control mechanism. The large peak at δ_C 153.8 is assigned to the chemical shift equivalent i-centered tetrads (**iii**, **iis** and **sis**), while the small shifts at δ_C 153.3 and 153.2 are assigned to the **isi** and **sss** tetrads (they cannot be unambiguously determined due to their statistical equivalence in the polymer).

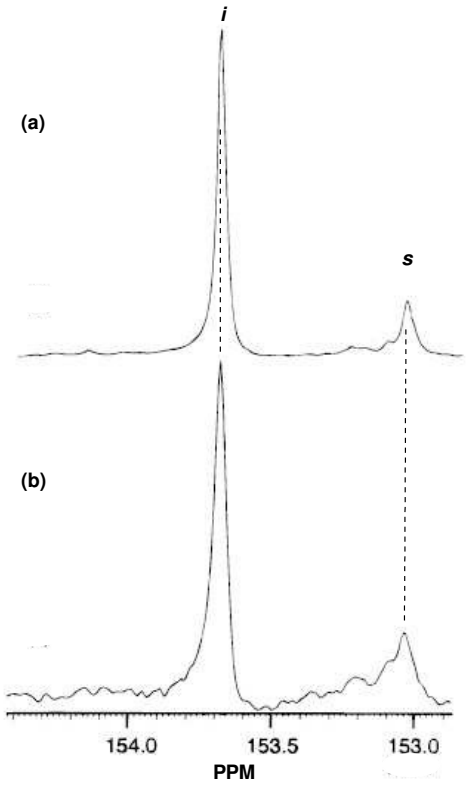

Figure 1.21: Stereostructure assignment of Carbonate carbon region of the $^{13}C\{^1H\}$ NMR spectrum of poly(cyclohexene carbonate).[39]

Finally, the peak at δ_C 153.1 is assigned to the **iss** tetrad. In 2001, Nozaki and co-worker reexamined the $^{13}C\{^1H\}$ NMR spectra assignment of the carbonate carbon of PCHC based on synthesis of appropriate dimers and tetramers of syndiotactic and isotactic structure models (**Figure 1.22**). Because both syndio-**1** and iso-**1** dimers have hydroxyl groups that do not exist in the main chain of the copolymer, they are not proper model compounds. Thus, the hydroxyl groups were protected with a methoxycarbonyl group to obtain syndio-**2** and iso-**2**, respectively, which more resembles the main chain structure of the copolymer.

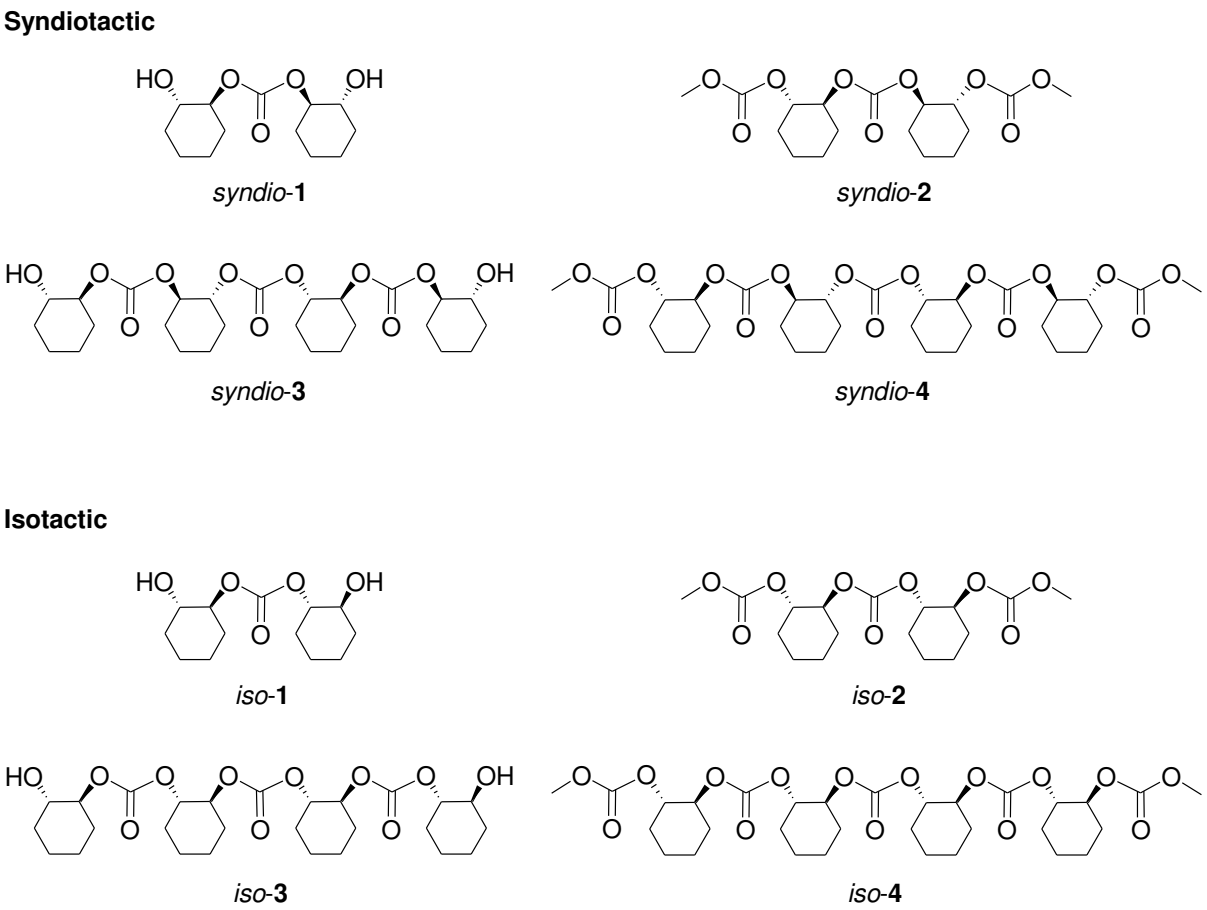

Figure 1.22: syndio- and isotactic diad and tetrad models of cyclohexene carbonate.[71]

The $^{13}C\{^1H\}$ NMR spectrum of iso-**2** showed a signal (153.8 ppm) which appears at a slightly lower field than that of syndio-**2** (153.7 ppm). As the chemical shift difference between syndio-**2** and iso-**2** is much smaller (0.1 ppm) than the one (0.6 ppm) between the two signals (153.7 and 153.1 ppm) of the copolymer, it seems that the dimers are too short to mimic the

diads in the copolymer. In addition, a few more signals observed at 153.3 and 153.2 ppm in the copolymer indicates a possible signal splitting which reflects longer configurational sequences. To further clarify the influence of the longer sequence, syndiotactic and isotactic tetramers (syndio-**4** and iso-**4)** were synthesized and $^{13}C\{^{1}H\}$ NMR was measured focusing on the central carbonate carbon signals. $^{13}C\{^{1}H\}$ NMR Spectra of syndio-**4** and iso-**4** were examined. Chemical shift of iso-**4** (153.7 ppm) is almost identical with that of dimer iso-**2**, whereas the central carbonate carbon signal of syndio-**4** appeared at 153.1 ppm, 0.6 ppm higher field than that of syndio-**2** (153.7 ppm). These results indicate that the copolymer shows a down-field peak corresponding to **i**-diad and an **s**-diad peak at a higher field than the **i**-diad peak. It was concluded that the signal at 153.7 ppm of the copolymer corresponds to signals of central carbonate carbons of **i**-centered tetrads, and the signals of the central carbonate carbons of **s**-tetrads are located outside the signal in the region of 153.7 ppm, probably at a higher field.[71] On the other hand, Coates and co-workers[57] have applied Bernoullian statistical methods to support the proposed $^{13}C\{^{1}H\}$ NMR assignments of PCHC and compared them with the observed concentration of each tetrad with its corresponding calculated amount. In each case, both [**iii**] and [**iis**] tetrads were correlated to one central resonance at 153.7 ppm and the remaining **s**-centered tetrads resided in the 153.3–153.1 ppm range. The $^{13}C\{^{1}H\}$ NMR spectrum of less syndiotactic PCHC, shows the [**sss**] and [**ssi**] tetrad resonances approach each other in magnitude with a more significant contribution from the [**iii**] and [**iis**] tetrads, relative tetrad occurrences of [**iii**] + [**iis**] = 15%, [**sis**] = 15%, [**sss**] = 35%, [**ssi**] = 29% and [**isi**] = 6% were calculated. Furthermore, the $^{13}C\{^{1}H\}$ NMR spectrum of the same PCHC sample using a lower resolution spectrometer showed only the five resonances at 152.95, 153.06, 153.12, 153.17 and 153.70 ppm. The iso-enriched PCHC, has a $^{13}C\{^{1}H\}$ NMR spectrum similar to that of previously reported isotactic PCHC.[39,41] In this case a large resonance was observed correlating to the combined [**iii**] + [**iis**] tetrads at 153.70 ppm and additional resonances representing the [**ssi**] and [**isi**] stereoerrors with no detectable [**sss**]

or [**sis**] tetrads. The methylene regions in the $^{13}C\{^{1}H\}$ NMR spectra of PCHC also vary with PCHC stereochemistry. In the case of syndiotactic PCHC, two series of two adjacent resonances are observed which [**ss**] and [**is**] that can be assigned as triads corresponding to the nonequivalent methylene carbons in the PCHC backbone. In each case, the [**is**] and [**si**] triad resonances cannot be distinguished. The $^{13}C\{^{1}H\}$ NMR spectrum of less syndiotactic PCHC shows [**ss**] triads of decreased intensity relative to the [**is**] triad resonances and additional downfield resonances were detected which is assigned to the [**ii**] triads. Alternatively, the $^{13}C\{^{1}H\}$ NMR spectrum of atactic PCHC reveals more intense [**ii**] triad resonances compared to the syndiotactic PCHC samples with the [**is**] and [**ss**] triad resonances. In this case, some tetrad resolution was observed where the [**ss**] triad resonances are split into their [**ssi**] and [**sss**] components and the [**is**] triad resonances are broadened. Finally, the $^{13}C\{1H\}$ NMR spectrum of iso-enriched PCHC shows that the downfield [**ii**] triad resonances in the methylene region have the greatest intensities relative to the [**is**] and [**ss**] triad signals.

2. Aims of Research

Based on previous research, the validity of the reactivity of chiral-Salen $M^{(III)}X$ (M = Co, Cr; X = Cl, OH) towards copolymerization of propylene oxide and CO_2 will be investigated. In this work, the commercially used and well-known Chromium and Cobalt-containing salen complexes as catalysts for polycarbonate (PC) formation utilizing CO_2 and epoxides as feedstock chemicals will be tested.

The main part of this work concerns studying the microstructure of the obtained poly(propylene carbonate) (PPC) using a combination of chiral GC and high resolution NMR spectroscopy. Accordingly, the microstructure of the obtained PPC will give important information on the stereo- and enantioselectivity of epoxide ring-opening.

In the second part of this work, we study the copolymerization reaction mechanism by applying a kinetic study. To investigate the epoxide ring-opening mechanism for different catalytic systems, an in situ ART-IR instrument will be used. On the other hand, a propagation process mechanism study will be concluded from the PPC microstructure at different reaction time. This study will pave the way to make a correlation between the microstructure and the reaction mechanism, which sheds light on the design of new salen-type catalysts to control the stereo- and enantioselectivity of the epoxide as well as the copolymer microstructure.

Due to the utilization of PPC in the industry, we focus the third part of the study on the correlation between the physical properties of the obtained PPCs and their microstructures. In this part of the work, we focused on the dynamic and folding behavior of the PPC chains in THF solution by using labeled polymers and applying the FRET technique.

All the results of each subject handled in this work are summarized and discussed in subchapters under results and discussion. A complete conclusion, summarizing the most important results of all three parts, is given at the end of this work.

3. Results and discussion

3.1 Synthesis of Salen ligands and corresponding metal complexes

Previous work in the literature has indicated that so-called Salen catalysts have great potential to produce high molecular weight poly(propylene carbonate) with high activity while retaining control over polymer microstructures and thus over the physical and chemical properties of the resulting polymer. The significant effect of the catalysts synthesis in enantiomerically pure configuration was the resolution of 1,2-diaminocyclohexane.[72] The monotartrate salt was obtained in high diastereomeric purity from the commercial mixture of trans- and cis-isomers. The precipitation of the monotartrate salt from aqueous acetic acid and recrystalization from hot water results in colorless crystals. Initial investigations have centered on traditional ligand structures comprising tert-butyl substituents at the aromatic moieties (**Scheme 3.1**).

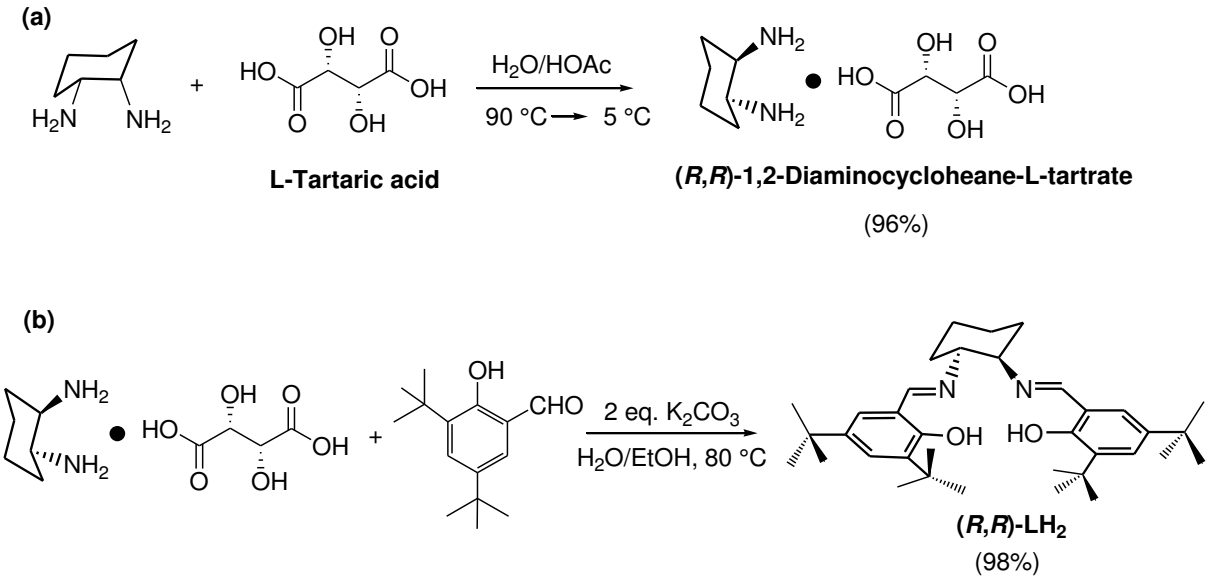

Scheme 3.1: a) Resolution of cis/trans 1,2-Diaminocyclohexane. b) Synthesis of (R,R)- Salen parent ligand.

The purity and the chemical structure of **(R,R)-LH_2** Salen ligand was confirmed by different modern analytical characterization methods; namely NMR spectrometer, elemental analysis

and ESI-MS. All of the analytical results integrate well with the calculated percentage of each atom in **(R,R)-LH$_2$**. To this end, a series of Jacobsen-type catalysts have been synthesized and complexed. Complexation of the salen ligand with Cr and Co metal centers was undertaken (**Scheme 3.2**). The complexation of the salen ligand to Cr was found to proceed best in two steps; namely first by reaction of the ligand with $CrCl_2$ under anhydrous conditions, followed by slow aerobic oxidation of the complex to form the required $Cr^{(III)}$ complex (**19a`**) as a brown compound after recrystalization from CH_3CN.[43]

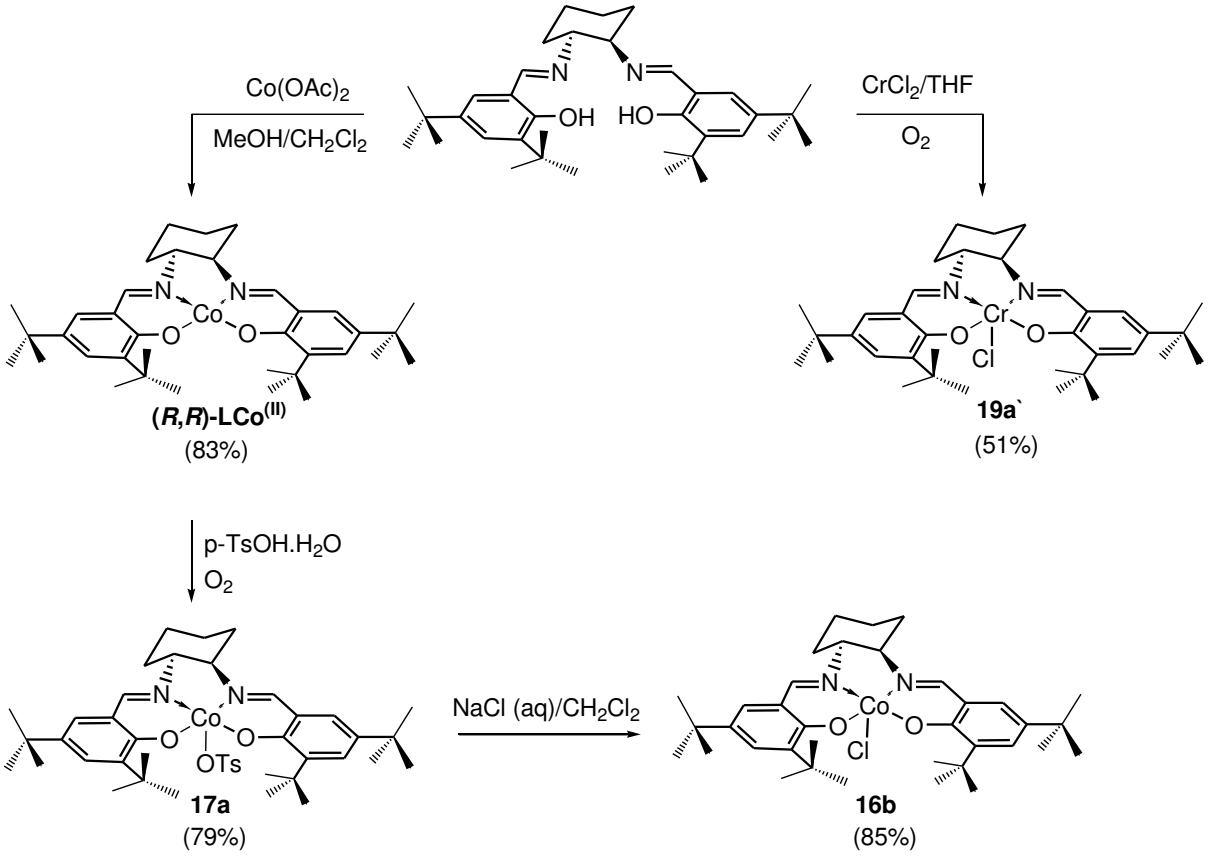

Scheme 3.2: Synthesis of (R,R)-Salen $M^{(III)}$ (M = Co, Cr)catalysts.

On the other hand, the cobalt-based catalyst (**16b**) was performed in three steps. Complexation of the Salen ligand with Co in an anaerobic atmosphere in a mixture of CH_2Cl_2/MeOH solution results in the (R,R-Salen)$Co^{(II)}$ precursor as red powder. The reaction of **(R,R)-LCo$^{(II)}$** precursor with an equimolar ratio of p-tolouensulfonic acid monohydrate (p-

TsOH.H_2O) in an inert atmosphere then under dry oxygen system results in **17a** a green solid. The tosylate co-ligand has been then substituted by Cl co-ligand by simple extraction of the tosylate group from **17a** in CH_2Cl_2 solution by a saturated brine solution to produce the required **16b** as dark brown complex. Due to the paramagnetic properties of the $Cr^{(III)}$ complexes the chemical structure of **19a`** was confirmed by elemental analysis and ESI-MS technique. The elemental analysis data were found to fit well with **19a`** with coordinated solvents. On the other hand, the ESI-MS spectrum showed a signal at 596.0 m/z which corresponds to [**19a`-Cl**]$^+$ and the existence of dimer complex with oxo-bridged at 1209.2 m/z which are formed under ESI-MS condition (**Figure 3.1**).

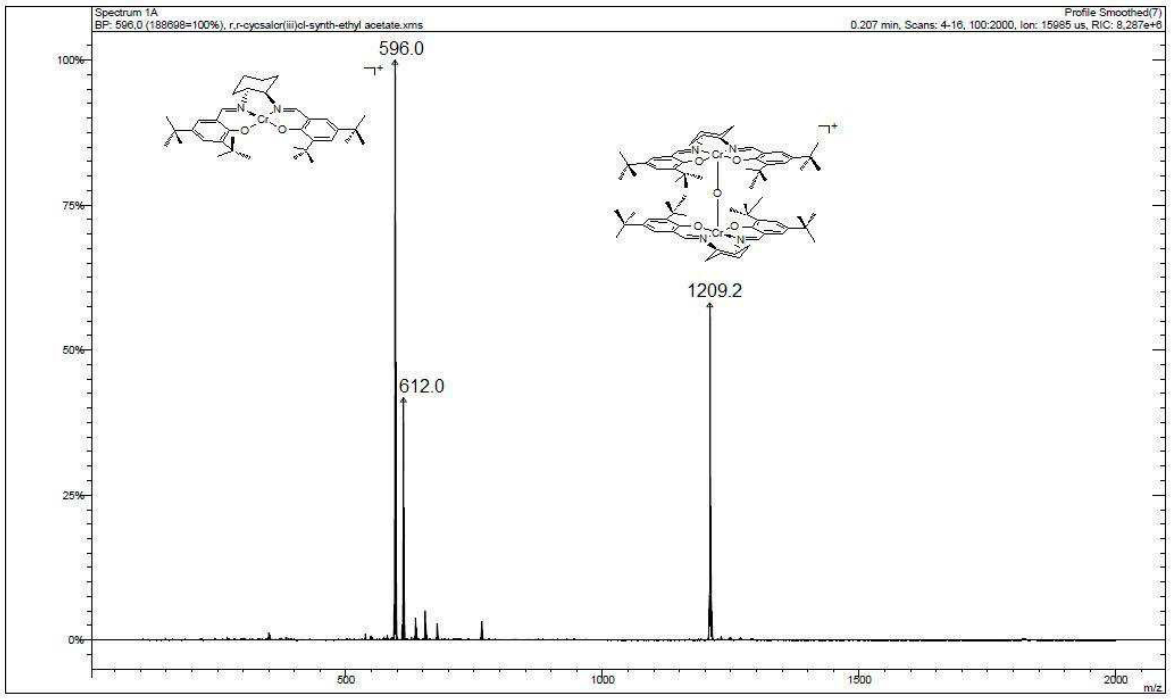

Figure 3.1: ESI-MS spectrum of Chromium complex **19a`**.

The diamagnetic properties of $Co^{(III)}$ complexes allowed in addition to elemental analysis and ESI-MS measurements to imply NMR spectrometer. In spite of that all the analytical results fit with the chemical structure of **16b**, the ESI-MS spectrum showed two significant signals at

m/z 603.2 and 626.1 which are attributed to [**16b-Cl**]$^+$ and [**16b-Cl+Na**]$^+$, respectively, which are formed under ESI-MS condition (**Figure 3.2**).

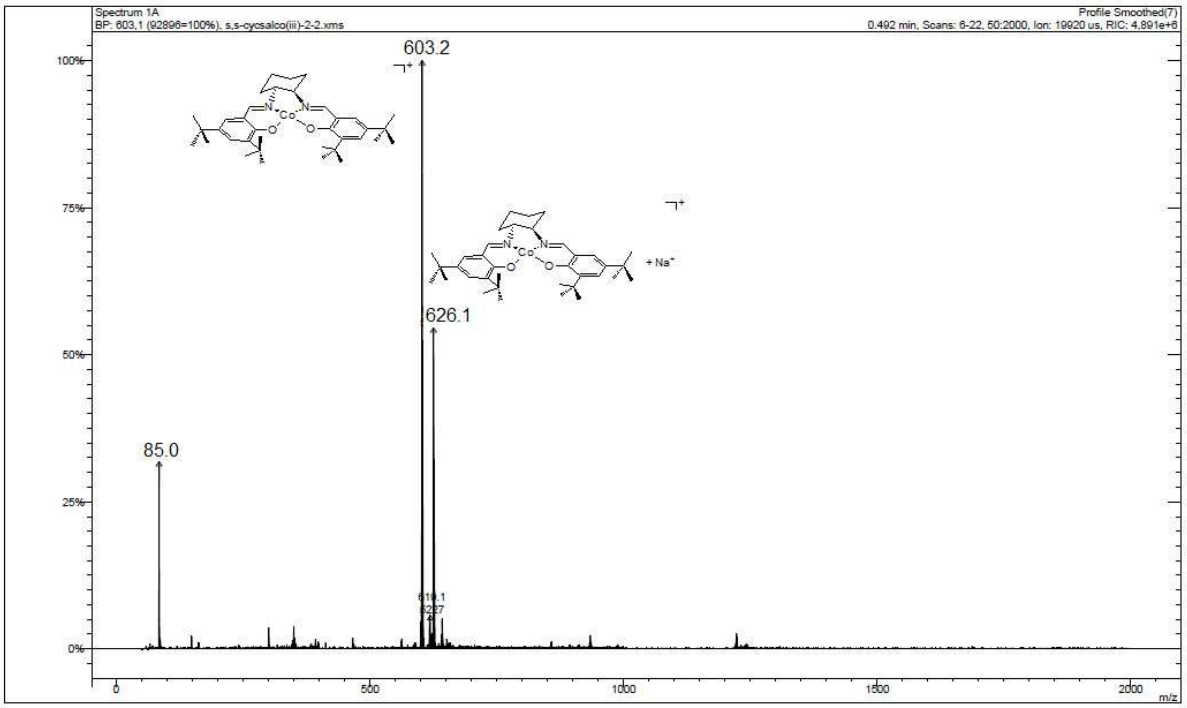

Figure 3.2: ESI-MS spectrum of Cobalt complex **16b**.

Moreover, the "mirror stereochemistry" of the above ligand and complexes have been synthesized (**Scheme 3.3**). Although the ligand **(S,S)-LH$_2$** was synthesized by a direct condensation reaction of enantiomeric pure (S,S)-1,2-diaminocyclohexane and 3,5-di-tert-butylsalicylaldehyde, the syntheses procedures and the analytical methods which were used for (R,R-Salen) metal complexes have been applied to synthesize and characterize the corresponding (S,S-Salen) metal complexes. As expected, the analytical results of all the products from both (R,R-Salen) and (S,S-Salen) isomers are identical. Due to formation of μ-oxo Cr$^{(III)}$ dimer under ESI-MS condition, the Cr$^{(III)}$ complex with OH co-ligand has been synthesized. Treatment of complex **19a** with KOH solution produces the chloride-free complex **26**, whereas the Cl co-ligand was exchanged by an OH co-ligand (**Scheme 3.3**). The

complex **26** was further used in a copolymerization reaction to investigate the effect of the co-ligand´s nature on the catalysts' activity and the copolymer properties.

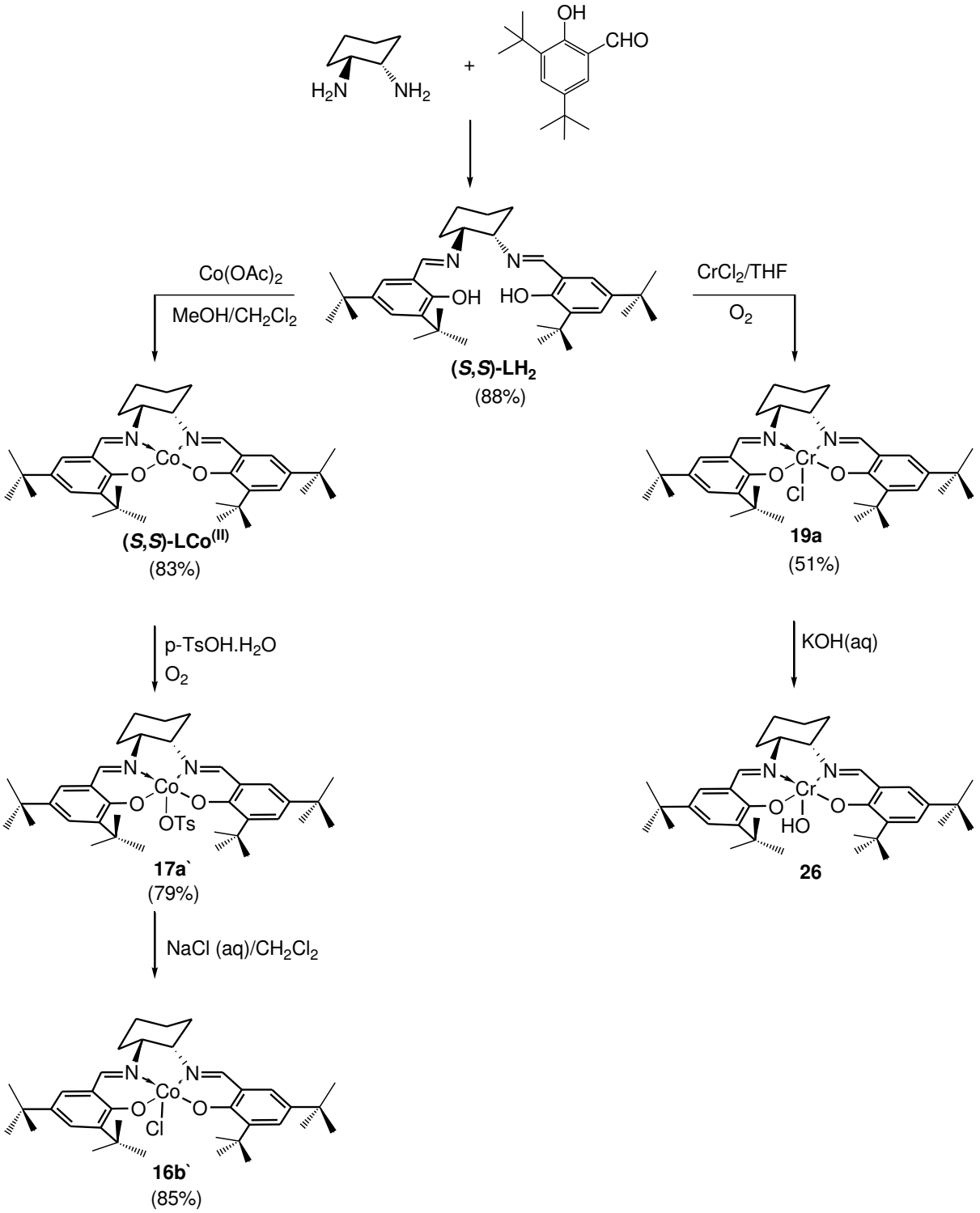

Scheme 3.3: Synthesis of (S,S)-Salen $M^{(III)}$ (M = Co, Cr)catalysts.

3.2 The Catalytic Activity of (R,R-Salen)$Cr^{(III)}Cl$ (19a`)

Polymerization testing has been undertaken with (R,R-Salen)$Cr^{(III)}Cl$ complex. Two cocatalysts were principally employed in these tests with the majority of work being focused on the use of 4-(dimethylamino)pyridine (DMAP) and bis(triphenylphosphine)iminium chloride ([PPN]Cl) (in appropriate variations of previous work, **Table 3.1**).[48,73]

Table 3.1: Copolymerization of CO_2 and rac-PO using **19a`** For 20 h.

entry	Cocat.:cat.:PO	Temp °C	Pressure (bar)	Conv (%)[a]	TOF[b]	PPC (%)[a]	Carbonate linkages (%)[a]	HT (%)[d]	M_n[e]	PDI[e]
DMAP as cocatalyst										
1	1:1:500	30	25	33	8	≥99	≥97	76	8.2	1.3
2	1:1:1000	30	25	14	7	≥99	≥97	87	5.9	1.3
3	0.5:1:500	30	25	39	10	≥99	≥97	81	ND	---
4	0.5:1:500	30	50	20	5	≥99	≥97	83	6.6	1.2
5	0.5:1:500	50	50	58	15	≥99	≥97	80	7.4	1.3
6	0.25:1:500	50	50	59	15	≥99	≥96	78	12.6	2.1
7*	0.5:1:500	30	25	69	5	≥99	≥99	85	11.0	1.3
[PPN]Cl as cocatalyst										
8	1:1:1000	30	25	43	11	40	≥95	86	----	----
9	1:1:1000	50	25	85	43	71	≥95	92	8.8	1.2
10	1:1:1000	25	50	34	17	traces	----	----	----	----
11	0.5:1:1000	40	50	34	17	91	≥99	88	7.1	1.3
12	1:1:1000	70	25	99	50	55	ND	ND	ND	ND

[a]Determined by ^1H NMR spectroscopy (300 MHz). [b]TOF = Conv (%) X 0.0715/moles of the catalyst/time (h). [d]Determind by $^{13}C\{^1H\}$ NMR spectroscopy (75 MHz). [e]Determined by GPC in $CHCl_3$ (kg/mol), calibrated with polystyrene standard. *The reaction time is 72 h.

In general, the microstructures of the alternating polymers have been investigated. By using **19a`** with [PPN]Cl as an initiator at low CO_2 pressure (25 bar) and increasing the reaction temperature an increase in the overall conversion was shown, but with decreasing the copolymer (PPC) selectivity over cyclic carbonate (CPC), with the optimum conditions at 25 bar and 50 °C (conv = 85% and PPC = 71%). With increasing CO_2 pressure (50 bar), the PPC selectivity was enhanced to 91% but the PPC conversion decreased to 34%. On the contrary,

when DMAP was used as an initiator the optimum copolymerization conditions were found to be 50 bar pressure and 50 °C (conv = 58% and PPC ≥99%).

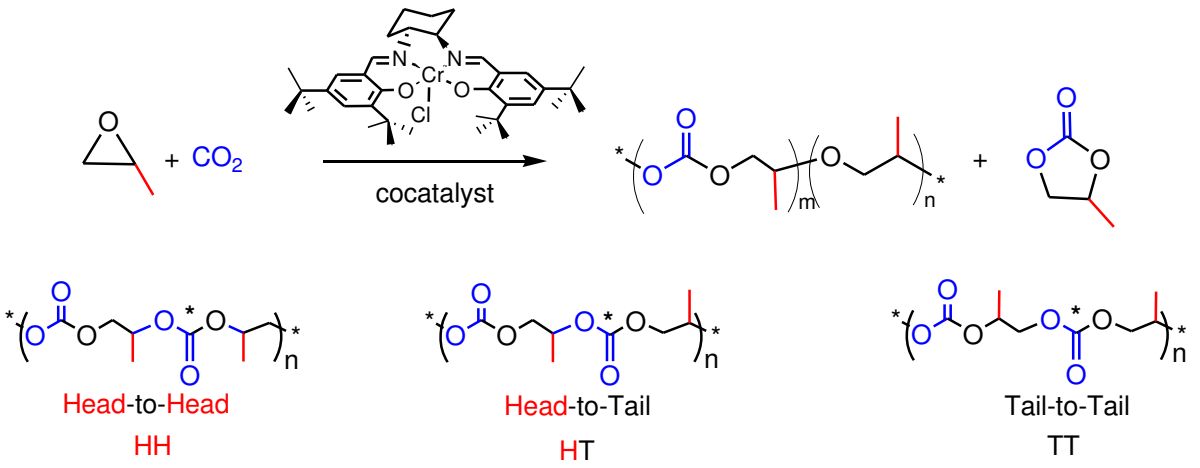

Scheme 3.4: Copolymerization reaction of PO and CO_2 and regiostructure of the resulting PPC.

The microstructure of the copolymer was characterized by using MALDI-ToF mass spectrometer and NMR spectroscopy, with the majority of the work being focused upon the use of DMAP (in appropriate variations of previous work). In general, the microstructures of the alternating polymers have been investigated, with high levels of regioselectivity (up to 88 % head-to-tail linkages) **(Scheme 3.4)**.

3.2.1 MALDI-ToF MS analysis

The polymeric materials were analyzed by MALDI-ToF MS to determine the PPC end groups, at least for those chains that are volatilized. In the mass spectrum of the low molecular weight copolymer, two set of masses were found. Although only one combination of the end groups can be expected, the MALDI-ToF MS spectrum showed bimodal molecular weight distribution. The lower M_n series (**Figure 3.3**) shows perfect alternative polycarbonate chains units with –Cl and –H end-groups. The expected chain ends originate from ionization by Na^+ of a PPC of repeating propylene carbonate units resulting from the catalyst-Cl co-

ligand initiating moiety and a proton on the other side originating from hydrolysis of the carbonato-catalyst bond during the workup process. The higher M_n series (**Figure 3.3**) show the existence of polymer chain units in different structures regarding the formation of ether linkages range from 3-11% maximum per chain. It could be seen around 3% ether linkages by ^{1}H NMR for the corresponding PPC, with the –H and –allylic end-groups.

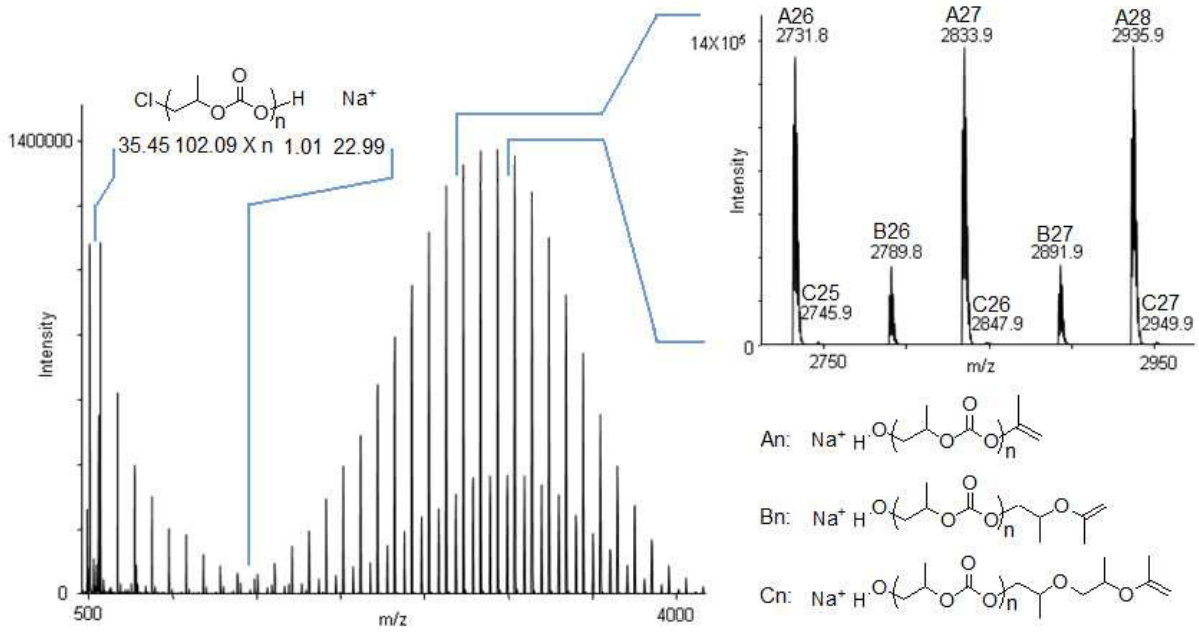

Figure 3.3: MALDI-ToF mass spectrum of PPC prepared with **19a`** and the series assignments.

However, the presence of allylic end groups is attributed to various side reactions including *β*-H transfer and oxiranes rearrangement, which may be explained by the presence of a propenyl end group. A further possible explanation could be the base-mediated isomerization of oxiranes into ketones and allylic alcohol. Epoxides can react with strong, non-nucleophilic bases by deprotonation in either α- hydrogen to produce allylic alcohols and/or ketones or *β*-position which exclusively forms allylic alcohol.[74] Oppenauer oxidation/Meerwein-Ponndorf-Verley reductions (MPVO) are two well-known synthetic transformations by zinc catalysts. However, MPVO is also reported by Williams and co-workers using di-cobalt[75] and di-

magnesium[76] catalysts coordinated by a macrocyclic ancillary ligand for CHO and CO_2 copolymerization reaction. Accordingly, the possibility of chain scission during MALDI-ToF MS experiments should be examined, since these peaks were not observed in the MALDI-ToF MS spectra of PPC samples prepared by zinc glutarate catalyst.[67] The existence of the terminal double bond in PPC copolymers, was investigated by bromination reaction using UV-Vis spectrometer. A λ_{max} at 413 nm was observed for Br_2 stock solution in $CHCl_3$. A slight addition of PPC amounts to the Br_2 solution did not show an absorption decrease at corresponding wave length and a new peak at λ = 271 nm which attributed to an n→π* transition state of the carbonate carbon group which appeared. However, addition of 100 mg of PPC to the Br_2 solution showed a slight decrease of the absorption at 413 nm over 1, 12 and 24 h. On the contrary, the UV-Vis spectrum of the stock solution showed a dramatic decrease of the solution absorption to half after 24 h, which raises the question of stability of the stock solution and the nature of UV-Vis spectra of PPC and Br_2 mixture in $CHCl_3$. The PPC was then recovered from the bromine solution, dried up and subjected to MALDI-ToF mass spectroscopy, whereas two different PPC molecular weights were found.

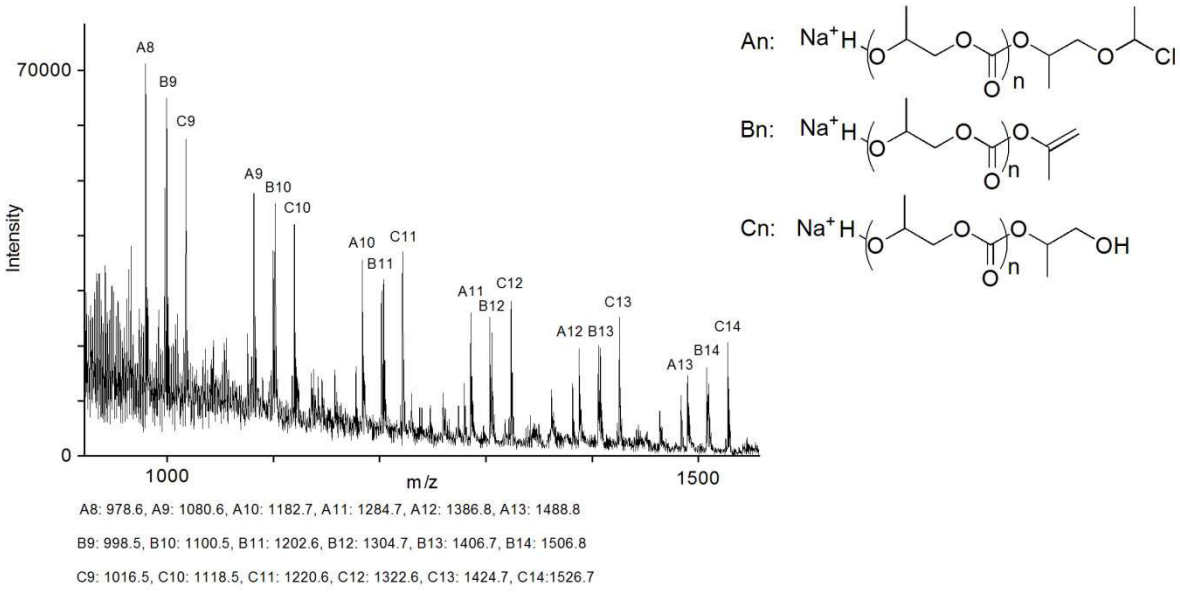

Figure 3.4: MALDI-ToF mass spectrum of low M_n PPC series prepared with catalyst **19a`** and the series assignments.

The lower M_n (**Figure 3.4**) and high M_n (**Figure 3.5**) series show same polycarbonate chains units, as shown previously for the same sample before bromination in **Figure 3.3**.

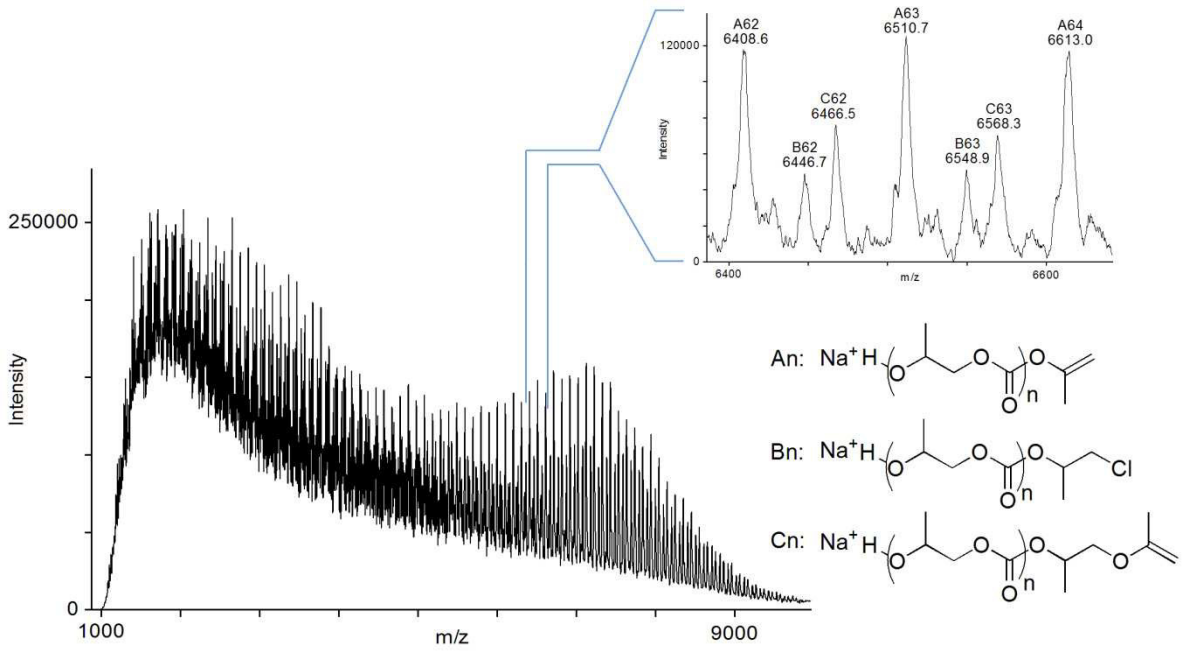

Figure 3.5: MALDI-ToF mass spectrum of high M_n series PPC prepared with **19a`** catalyst and the series assignments.

The MALDI-ToF MS spectra (**Figure 3.4** and **Figure 3.5**) show polycarbonate chain units, with –Cl end group resulting from the catalyst-Cl co-ligand initiating moiety. Since polycarbonate chains units with –Br end-groups have not been observed, the observed allylic end group in the resulting spectra can be attributed to the possibility of chain scission during MALDI-ToF MS experiments or dehydration of –OH chain unit end-groups which are attributed to chain transfer reaction by contaminated water. [61,67,75,77] In order to examine the chain transfer reaction effect due to trace contamination of water, two different copolymerization reactions have been performed using freshly distilled and ambient PO (**Figure 3.6** and **Figure 3.7**), respectively.

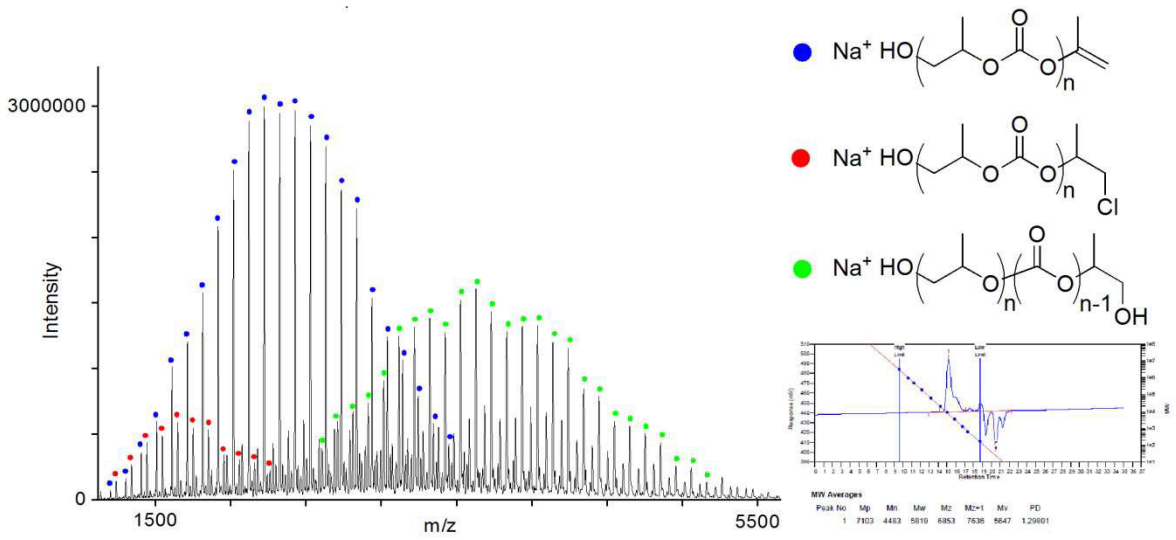

Figure 3.6 : MALDI-ToF mass spectrum of PPC series prepared from copolymerization of CO_2 and freshly distilled PO using Salen-$Cr^{(III)}$Cl catalyst ,and the series assignments.

Figure 3.6 clearly shows that using freshly distilled PO in the copolymerization reaction of CO_2 and PO involving the Cl-co-ligand in the PO ring-opening. However, the influence of a trace amount of water in the copolymerization reaction system is significantly pronounced as illustrated by the signal intensity corresponding to the chain units with –OH end groups in the MALDI-ToF MS spectrum as well as the bimodality of the corresponding GPC elugram. On the contrary, using ambient PO in the copolymerization reaction with CO_2 and in spite of a chain-transfer reaction due to water contaminants, the average molecular weight distribution was relatively narrow and a monomodal GPC elugram was observed (**Figure 3.7**), indicating that the copolymerization proceeded mainly via an immortal mechanism with reversible and rapid chain-transfer reactions

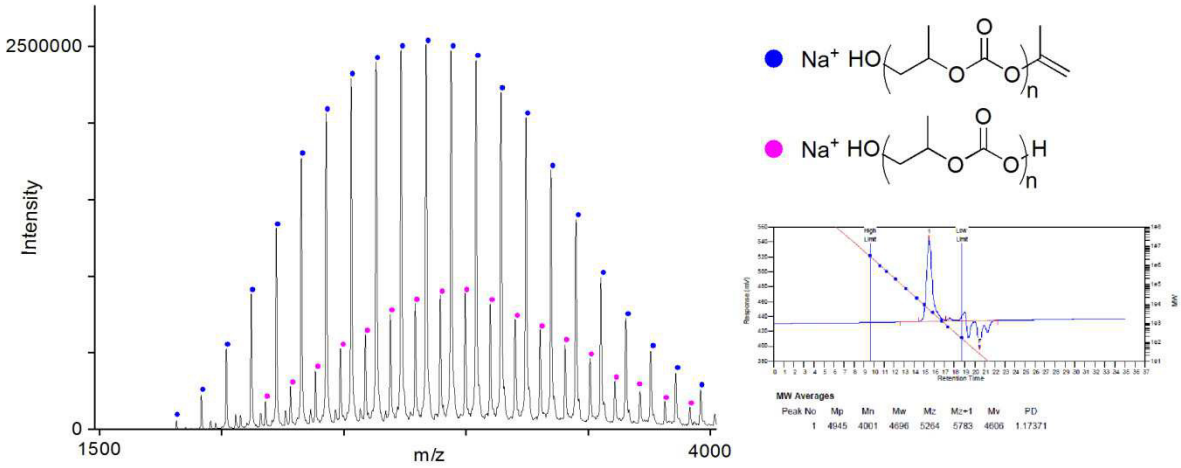

Figure 3.7: MALDI-ToF mass spectrum of PPC series prepared from copolymerization of CO_2 and ambient PO using Salen-$Cr^{(III)}$Cl catalyst ,and the series assignments.

Indeed, the MALDI-ToF MS spectra did not show any DMAP end group. It is expected that the polymer-DMAP bond could be readily hydrolyzed, either because of the work up procedure or due to chain transfer reactions with trace amounts of water in the copolymerization reaction. However, by using various workup procedures no changes were observed in either GPC[78] or MALDI-ToF MS spectra,[74] indicating that the various end groups were formed during the copolymerization reaction.

3.2.2 Molecular Weight Analysis

The polymers obtained using catalyst **19a`** in neat PO show bimodality in their molecular mass distribution in GPC elugrams. Such a bimodal distribution is often observed with similar catalysts in this reaction. The observed peak molecular mass of low-M_n fractions corresponds approximately to half of that of the high-M_n fractions of the polymer batch. MALDI-ToF MS series assignments fit well with the bimodality of a representative GPC trace (**Figure 3.8**) with $m \geq 2n$.

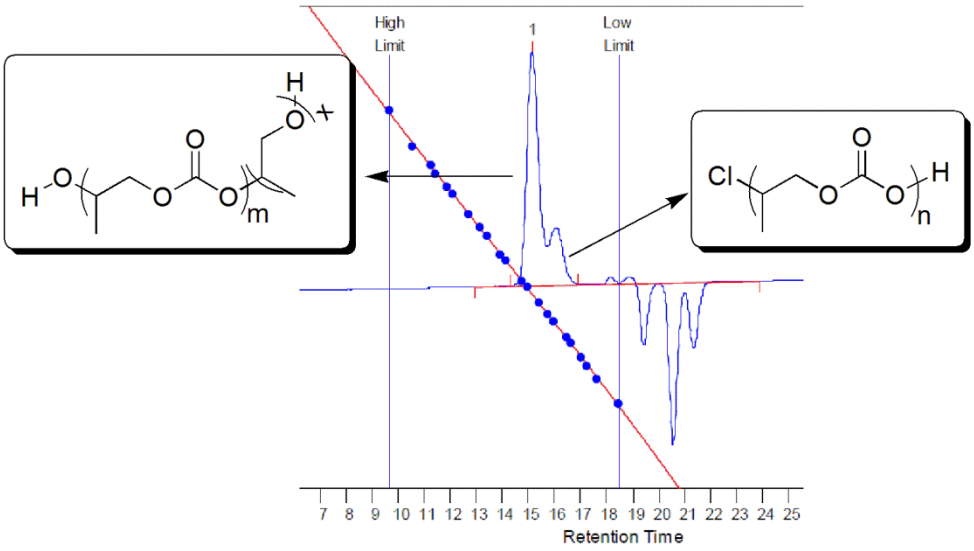

Figure 3.8: representative GPC traces of PPC synthesized from rac-PO/CO_2 copolymerization using **19a`**and cat:cocat ratio 0.5:1 and 500 equivalent PO for 20 h, with assignment of bimodal trace.

3.2.3 Binding Mode of 19a` and Cocatalysts

Further experiments were done to understand the reaction mechanism by studying the binding of N,N`-dimethyl aminopyridine (DMAP) to **19a`** in a solution prepared in CH_2Cl_2. The positive ion electrospray ionization spectroscopies (ESI-MS) of DMAP: **19a`** mixtures in 1:1 and 1:2 molar ratios have been studied. In both solutions the spectrum mainly contains the species m/z 123.1, 596.1, 718.0 and 1209.4 corresponding to $[DMAP]^+$, $[\mathbf{19a`}\text{-}Cl]^+$, $[\mathbf{19a`}+DMAP]^+$ and [2 X (**19a`**) + O]. These results indicate the preference of **19a`**to bind with one molecule of DMAP to form the initiation species (**Figure 3.9**) This result contradicts Lu and co-workers report.[79] In their work, the authors reported binding two equivalents of DMAP on the chromium metal center when the chromium complex is mixed with DMAP in a 2: 1 molar ratio. However, Lu et al. also reported that the Salalan chromium analogue showed 30 times higher activity. The ESI-MS spectrum of the Salalan Cr complex and DMAP mixture of different molar ratios showed a dominant signal corresponding to 1 equivalent DMAP

coordinated to the metal center. The effect of DMAP/catalyst molar ratios on CO_2 and PO copolymerization reaction has been studied by Rieger and co-workers.[73] Rieger et al. found that the PPC formation is optimized when a mixture of DMAP to the catalyst in 1:2 molar ratios is used. Accordingly, the active initiating species is proposed to be binding only 1 equivalent DMAP with the Cr catalyst.[73,79]

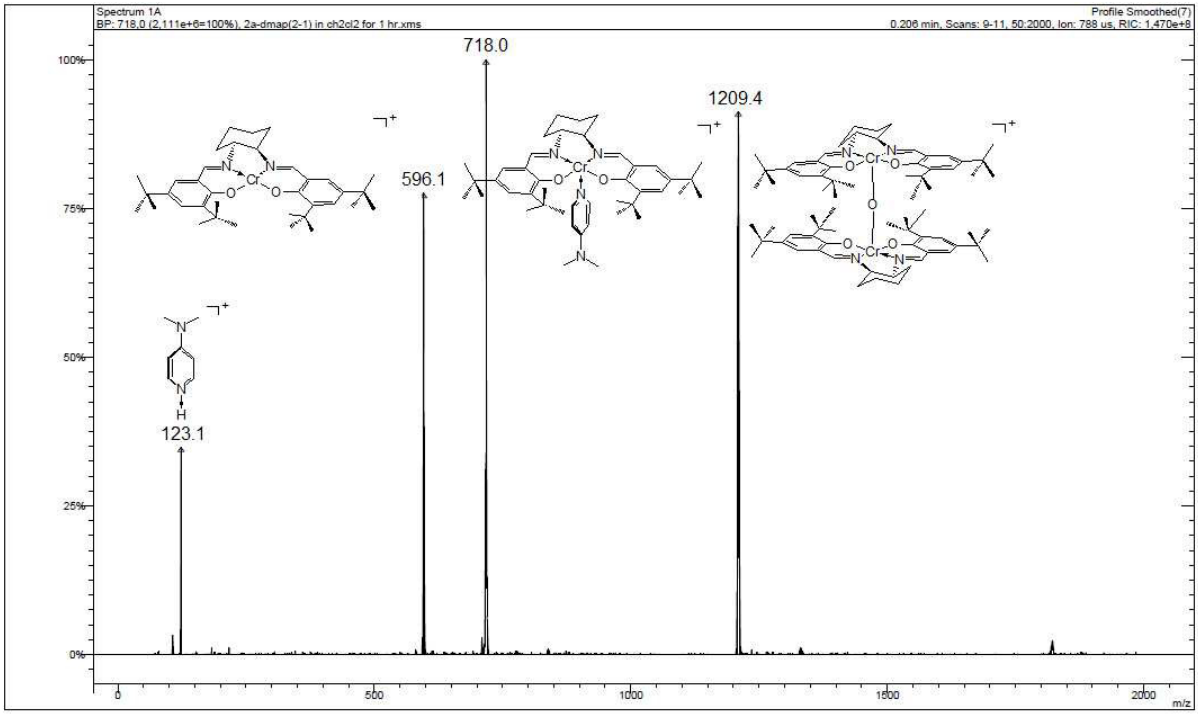

Figure 3.9: Binding of DMAP to $Cr^{(III)}$ Sal Cl (1:0.5) molar ratio shown by ESI-MS.

On the other hand, copolymerization of CO_2 and PO in presence of DBU as cocatalyst did not show any activity. ESI-MS spectrum of catalyst and DBU solution in CH_2Cl_2 in 1:0.5 molar ratios did not show any indication of the DBU binding to the catalyst (**Figure 3.10**). It could be attributed to the strong affinity of DBU to form $[DBU\text{-}H]^+$ species which prohibits its binding ability to the metal center.

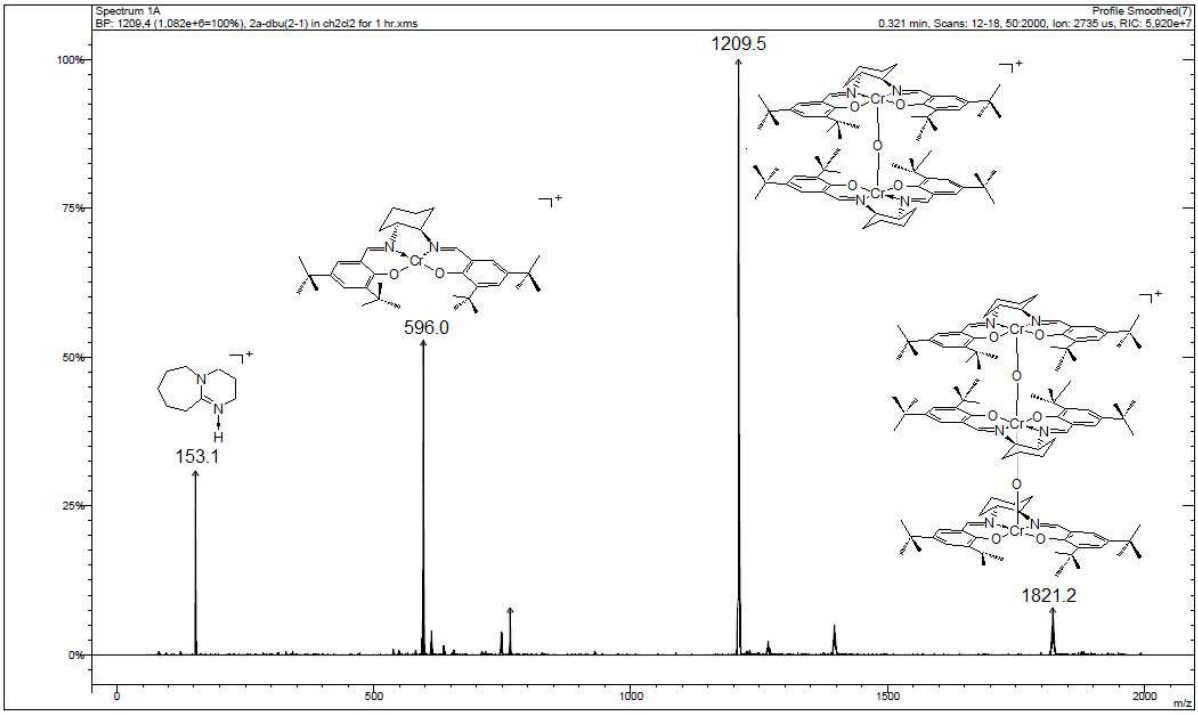

Figure 3.9: Binding of DBU to $Cr^{(III)}$ Sal Cl (1:0.5) molar ratio shown by ESI-MS.

3.2.4 Microstructure Identification Attempt

Different PPC copolymers have been produced from S-PO, R-PO, 25% S-PO/75% R-PO, rac-PO and 75% S-PO/25% R-PO (Figure 2), by employing **19a`** and DMAP as initiators and by using the optimum conditions determined in previous studies ([PO]: [DMAP]: [catalyst]; 1:0.5:500, at 50 °C and 50 CO_2 bar). The simplest $^{13}C\{^1H\}$ NMR spectra were demonstrated from the S-PO and R-PO with **HT** preferable regiosequence over **HH** or **TT**. From these two spectra the predominant peak as triad level can be assigned as **ii**. Taking into consideration that **HH** or **TT** regiosequence represents only diad level; which means by using pure enantiomeric propylene oxide ((R)-PO and/or (S)-PO) the only peak which appeared in **TT** or **HH** region can be assigned as **i**. After using mixed isomers or rac-PO, a new peak in the **TT** region appeared downfield to that of the original peak and was assigned as **s**. Consequently, the small downfield shifted peak appeared in the **TT** and **HH** regions even when enantiopure PO was used. This is indicative of a small percentage of the more disfavored "abnormal" ring-

opening of PO during the polymerization resulting in a small degree of inversion of epoxide stereochemistry (**Figure 3.11**).

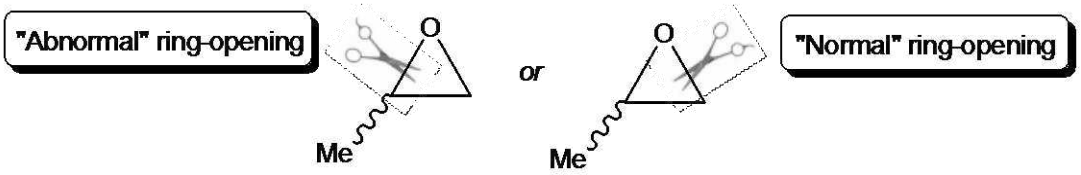

Figure 3.11: alternative PO ring-opening.

From this, we can conclude that any additional downfield peaks which appeared when we used the mixed isomers or rac-PO represent the least tacticity regiosequence. However, more investigation of the PPC microstructure has been performed using Salen-$Co^{(III)}$ catalysts compared to that which was synthesized using the Cr-analogous.

3.3 The Catalytic Activity of (R,R-Salen)$Co^{(III)}$Cl (16b)

According to the literature,[46,54] the activity of cobalt salen complexes towards CO_2 and epoxide copolymerization can be increased using binary catalyst systems. Consequently, the (R,R-Salen)$Co^{(III)}$Cl (**16b**) and [PPN]Cl binary system was initially chosen for our studies (**Table 3.2**).

Table 3.2: Copolymerization of CO_2/rac-PO using complex **16b** and [PPN]Cl as cocatalyst and 1000 PO equivalents with respect to the catalyst at 30 °C and 30 bar CO_2.

entry	Cocat./cat. (equivalent)	Time (min)	Selectivity (% PPC)[a]	Yield (% PPC)[b]	Carbonate Linkages (%)[a]	M_n (kg/mol)[c]	PDI (M_w/M_n)[c]
1	1	30	64	12	≥98	14	1.3
2	1	60	90	27	≥99	16	1.4
3	1	90	96	40	≥99	22	1.4
4	1	120	98	51	≥99	29	1.2
5	1	180	99	53	≥98	29	1.5
6	1	240	99	65	≥99	28	1.5
7	0.5	30	88	9	≥99	10	1.2
8	0.5	60	96	15	≥99	18	1.2
9	0.5	90	97	21	≥99	19	1.2
10	0.5	120	97	28	≥99	27	1.3
11	0.5	180	98	41	≥99	33	1.2
12	0.5	240	98	50	≥99	38	1.2
13	0.5	360	99	65	≥99	45	1.2
14	0.25	60	98	15	≥99	14	1.2
15	0.25	120	98	20	≥99	22	1.3
16	0.25	180	99	32	≥99	26	1.4
17	0.25	240	99	49	≥99	30	1.5

[a]Determined by ^{1}H NMR spectroscopy (500 MHz). [b]based on the isolated PPC. [c]Determined by GPC in THF, against polystyrene standard.

Variation of cocatalyst loading was shown to have a significant impact on PPC selectivity in the beginning of the copolymerization reaction. This effect was most pronounced when equimolar quantities of [PPN]Cl cocatalyst with respect to **16b** were employed (**Table 3.2**, **entry 1**). In all cases, the PPC selectivity was observed to be independent of cocatalyst loading at longer reaction times with highly alternating polycarbonate structures obtained in all cases.

3.3.1 Copolymer Microstructure

Since the pioneering discovery of a catalytic system for alternating copolymerization of CO_2 and epoxides,[12,13,15,64,69] the utilization of CO_2 as a renewable C_1 feedstock for polymer synthesis has attracted great attention. In particular, extensive research has been dedicated to CO_2/epoxide copolymerization.[7,14,42,80-86] Understanding the mode of the ring-opening of propylene oxide (PO)[64] or styrene oxide (SO)[65,87] was initially studied by Inoue and co-workers, with the CO_2/(R)-PO copolymerization reaction showing a partial racemization of around 95% predominant ring-opening (RO) at the methylene group ("Normal" RO). In contrast, in the CO_2 and (R)-SO copolymerization reaction the methine group is attacked ("Abnormal" RO) with around 96% predominant inversion (**Scheme 3.5**).[88]

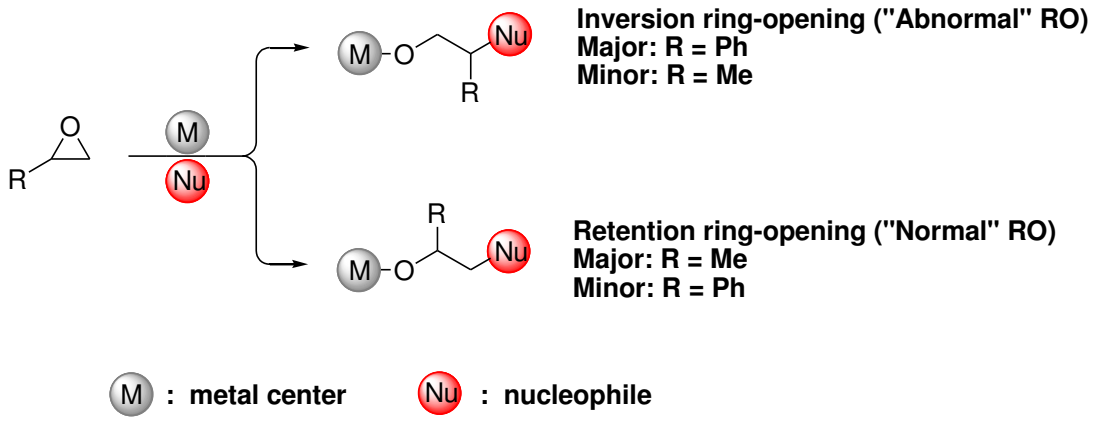

Scheme 3.5: Difference of the ring-opening between styrene oxide and propylene oxide.

Early reports on $^{13}C\{^1H\}$ NMR spectra of the CO_2 and epoxide copolymers[65,87,89] have been followed by more detailed interpretation of the signals in the carbonate carbon region[66] with respect to the regiostructure of the poly(propylene carbonate)s (PPC) (**Figure 3.12**). Based on both the aliphatic and carbonate carbon signals, Chisholm and co-workers investigated the regularity of alternating[67] and non-alternating PPC. [68]

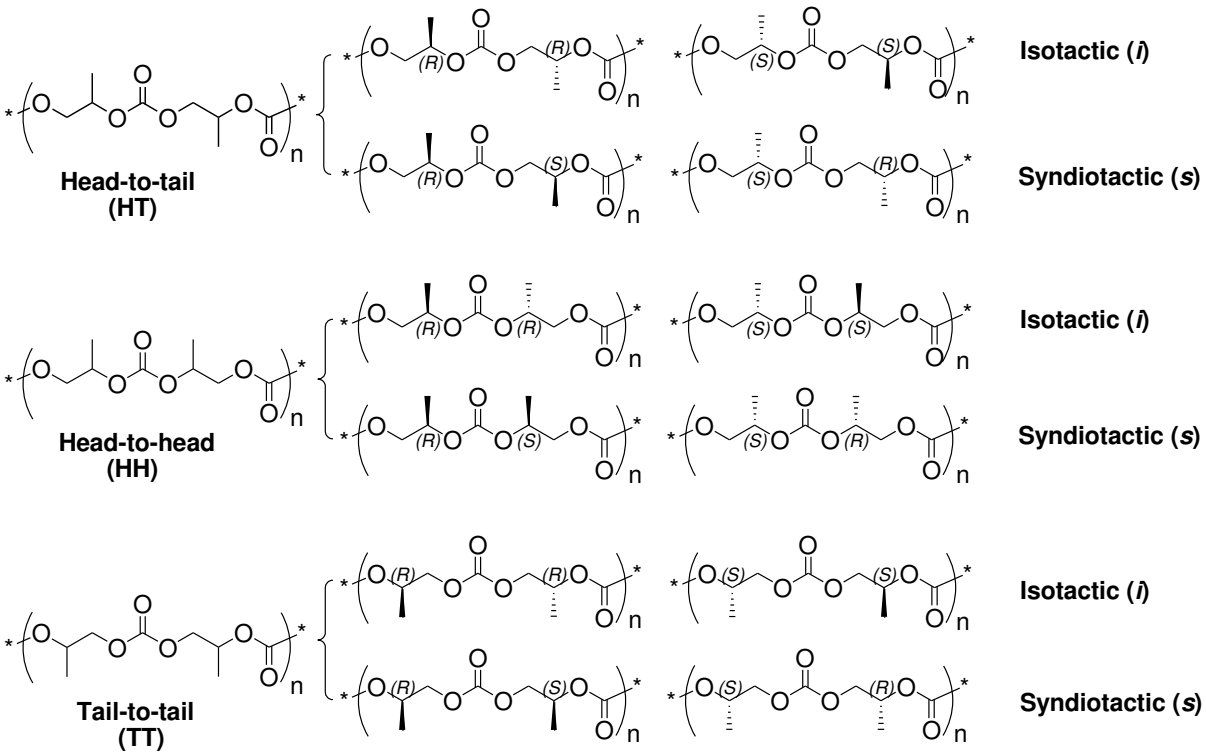

Figure 3.12: Regio- and stereochemistry around the carbonate carbons of PPC.

The development of hydrolytic kinetic resolution (HKR) by Jacobsen and co-workers using chiral chromium[43] or cobalt[44,45] salen complexes to access the enantiomerically pure epoxides by ring-opening has inspired the investigation of chiral salen-type complexes for the synthesis of optically active polycarbonates.[46-54] Research has mainly been devoted to the synthesis of new catalysts to study their chemical activity and selectivity, as well as the mechanism and the stereochemistry of the copolymerization.[14] Consequently, new catalytic systems have been developed for propylene oxide,[52,90] cyclohexene oxide,[51,91,92] styrene oxide,[93] epichlorohydrin[94] and indene oxide[95] copolymerization reactions with CO_2. In addition, studies of CO_2/epoxide copolymer microstructures have attracted much attention. Stereoblock and stereogradient PPCs have been reported from CO_2/PO copolymerization reactions, which showed different thermal stabilities.[90] Poly(styrene carbonate) (PSC)[96] has also been thoroughly studied showing major "abnormal" ring-opening with predominant stereocenter inversion upon copolymerization of SO/CO_2, which is consistent with Inoue´s earlier study.[87]

Moreover, we reported an exploration of PPC microstructure using a combination of GC and high resolution NMR spectroscopy.[97] Our study concerns the regio- and stereostructure of PPC connected with the enantioselectivity of the epoxide ring-opening during the copolymerization reaction as a function of reaction time and of increase in the number average molecular weight of the copolymer (M_n). The effect of cocatalysts and the nature of the catalytically active metal (**Figure 3.14**) on these parameters is described.

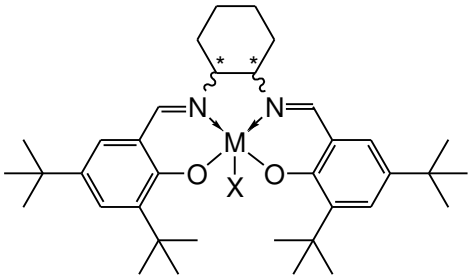

16b: (*R*,*R*), M = Co; X = Cl
16b`: (*S*,*S*), M = Co; X = Cl
19a`: (*R*,*R*), M = Cr; X = Cl
19a: (*S*,*S*), M = Cr; X = Cl
26: (*S*,*S*), M = Cr; X = OH
27: *rac*, M = Co; X = Cl

Figure 3.14: Structures of the applied catalyst complexes used in this study.

It is known that the PO ring-opening usually occurs at the epoxide methylene group via an S_N^2 type mechanism ("normal" RO),[88] leading to a predominant **HT** regiostructure of the CO_2 and PO copolymer. By contrast, tail-to-tail (**TT**) or head-to-head (**HH**) connectivities arise from the less favored PO ring-opening at the methine carbon ("abnormal" RO). If enantiomerically pure (R)-PO is copolymerized with CO_2 using catalyst **16b** (**Table 13.3**, **entry 1**), the resulting copolymer exhibits 88% **HT** connectivity with the remaining 12% equally distributed between **HH** and **TT** contributions (~ 6% each), as was found by $^{13}C\{^1H\}$ NMR spectral analysis of the carbonate region (**Figure 3.15a**). After the degradation of this copolymer, 5% (S)-cPC and 95% (R)-cPC were detected by GC measurements, which show that 95% of PO was incorporated into the copolymer with retention of configuration.

Table 3.3: Copolymerization of CO_2 and PO using [PPN]Cl as cocatalyst and 1000 PO equivalents with respect to catalyst at 30 °C and 30 bar CO_2 for 20 h.

Entry	Catalyst	PO	Cocat./cat. (equivalent)	Carbonate linkage (%)[a]	HT (%)[b]	Enantiopurity (%)[c]
1	**16b**	R-	1	≥ 99	88	95.0 (R)
2	**16b`**	R-	1	≥ 99	94	99.0 (R)
3	**16b**	S-	1	≥ 99	96	n.d
4	**16b`**	S-	1	≥ 99	87	n.d

[a]Determined by ^{1}H NMR spectroscopy (500 MHz). [b]Determined by ^{13}C{^{1}H} NMR spectroscopy (125 MHz). [c]Determined by GC. n.d: not determined.

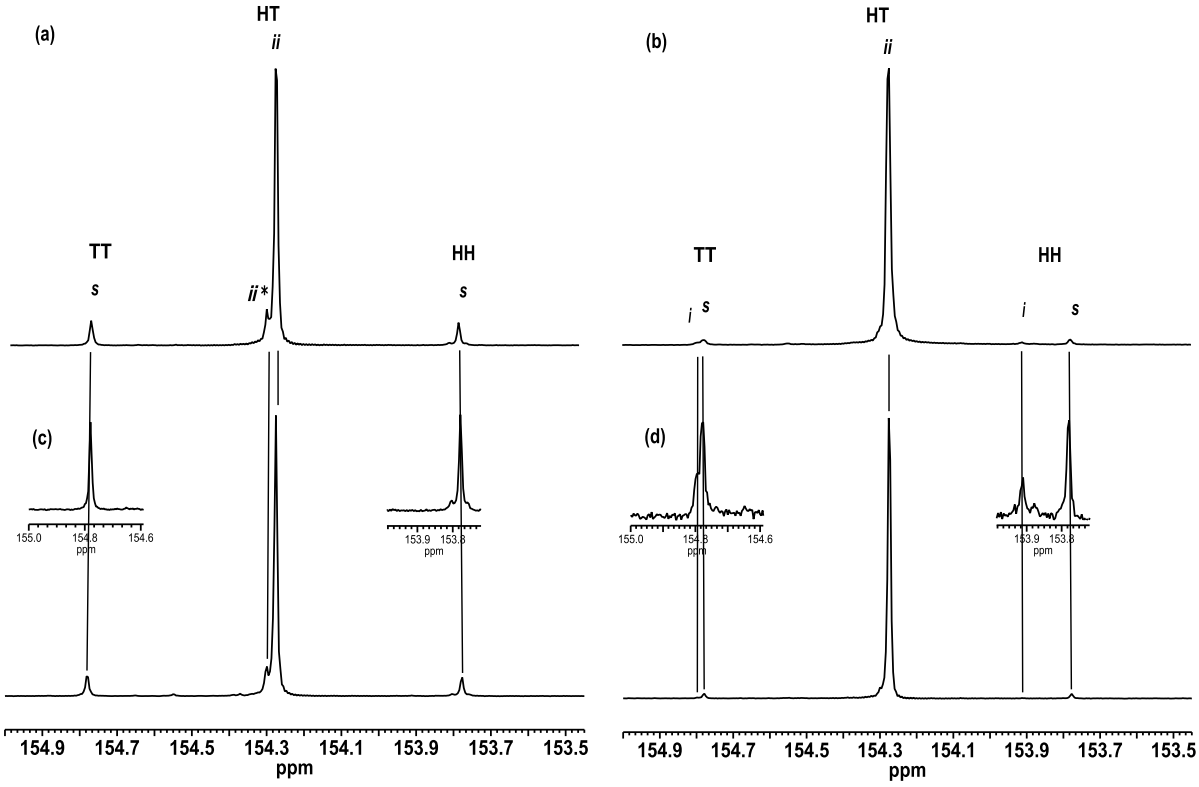

Figure 3.15: ^{13}C{^{1}H} NMR spectra (125 MHz, $CDCl_3$) of the carbonate carbon region for (a) (R)-PPC copolymer synthesized using **16b**, (b) (R)-PPC copolymer synthesized using **16b`**, (c) (S)-PPC copolymer synthesized using **16b`**, (d) (S)-PPC copolymer synthesized using **16b**, with 1 equivalent [PPN]Cl and 1000 equivalent PO at 30 °C and 30 bar CO_2 for 20 h.

The value of 5% for cPC with inverted configuration compares well with the amount of **HH** or **TT** junctions, respectively, as was found by NMR spectroscopic analysis. This observation

can be reasonably explained by an isolated regioerror model of the copolymer microstructure, according to which the less favored ("abnormal") PO ring-opening at the methine carbon (associated with inversion of configuration) is immediately followed by ring-opening at the methylene center. The assignment of carbonate carbon signals at δ_C 153.8 and 154.8 ppm to **HH** and **TT** syndiotactic diads, respectively (**Figure 3.16**) is consistent with the previous work of Chisholm and co-workers.[98]

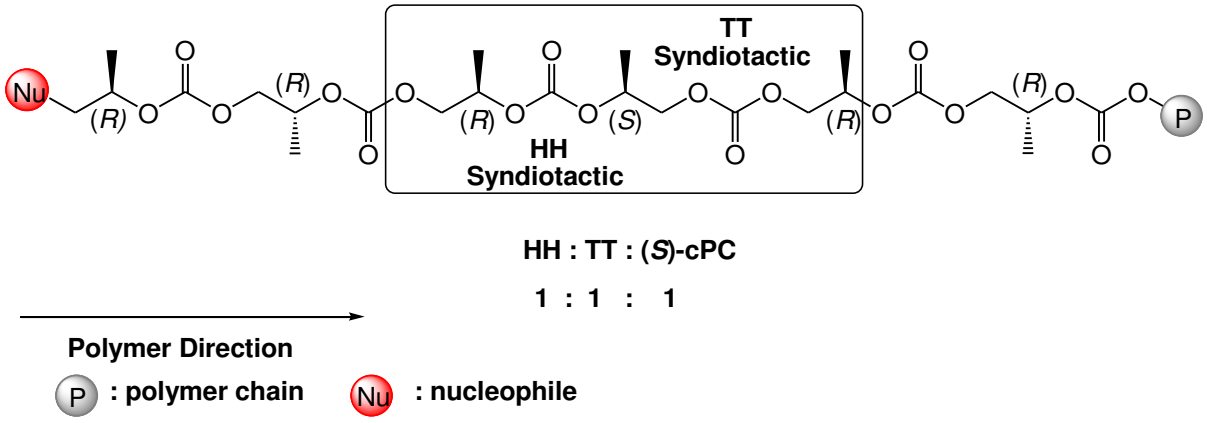

Figure 3.16: Syndiotactic HH and TT in (R)-PPC synthesized using **16b**, 6bresulting from methine ring-opening inversion.

Copolymerization of enantiomerically pure (R)-PO with **16b`** (**Table 13.3**, **entry 2**) showed a lower degree of regioerrors in the $^{13}C\{^1H\}$ NMR spectra of the copolymer (**Figure 3.15b**). The $^{13}C\{^1H\}$ NMR spectrum of this copolymer shows 94% **HT** contribution with each **HH** and **TT** contribution of around 3%. The **HH** region is represented by two peaks at δ_C 153.8 and 153.9 ppm. In the TT region, a shoulder of the peak at δ_C 154.8 ppm appears at the low-field side. GC analysis of the degraded copolymer showed 99% (R)-cPC (**Table 3.13**, **entry 2**) with 1% inversion, which indicates that the ring-opening at methine-center leading to regioerror occurred both with inversion and retention of the stereocenter configuration. Consequently the additional **HH** and **TT** peaks are assigned as an isotactic diad structure (**i**) (**Figure 3.15b** and **3.15d**).[98] Comparison of $^{13}C\{^1H\}$ NMR spectra (**Figure 3.15**) reveals that

the signal of the PPC **HT** backbone prepared from (R)-PO or (S)-PO appears at the same chemical shift (δ_C 154.28 ppm), typical for strictly alternating regio-regular isotactic structure. Remarkably, in the **HT** region of (R)-PPC prepared with catalyst **16b**, there is a small but clearly expressed downfield-shifted peak at ~ δ_C 154.3 ppm, the intensity of which seems to depend on the intensity of the **HH** (or **TT**) signal. That is, in case of (S)-PPC prepared with catalyst **16b**, the intensity of the **HH** (or **TT**) signal is much lower and the minor peak in the **HT** region appears only as a small shoulder (**Figure 3.15**). Although, the integration of this peak is not very legible, its intensity is approximately equal to that of the **TT** signal, allowing to its assignment to the isotactic sequence adjacent to the regioerror, namely either **ii**$*$ or $*$**ii** (the asterisk refers to a regioerror). Copolymerization of 25% (R)-PO:75% (S)-PO and CO_2 for 1h using catalyst **16b** or **16b`** results in two significantly different copolymer microstructures. In case of catalyst **16b**, an iso-enriched copolymer with a low degree of regioerror is formed. Indeed, the peak corresponding to an isotactic sequence at δ_C 154.27 ppm is noticeably higher than all other signals. In addition, three low intensity signals in the **HT** region are observed at δ_C 154.32, 154.34 and 154.39 ppm, respectively. Their intensity becomes comparable with that of the isotactic sequence peak if the catalyst **16b`** is applied (**Figure 3.17**). Moreover, the conversion of the copolymer prepared with catalyst **16b`** is noticeably lower, which is a consequence of the reduced copolymerization rate. Simultaneously, this results in a higher ratio of regioerror (**Table 3.4**) and is associated with the selectivity of the chiral catalyst. Thus, the rate of (S)-PO copolymerization with (R,R)-configuration catalyst **16b** is fast, whereas the (S,S)-configured catalyst **16b`** prefers (R)-PO and produces more regioerrors upon copolymerization of (S)-PO.

Table 3.4: Different copolymerization reaction of CO_2 using 1000 equivalents of PO and 1 equivalent PPNCl with respect to the catalyst at 30 °C and 30 bar CO_2.

Entry	Catalyst	PO (S)-PO:(R)-PO	Time (h)	Selectivity (% PPC)[a]	Conv (% PPC)[a]	Carbonate linkages (%)[a]	HT (%)[b]
1	**16b**	75:25	1	93	40	≥ 99	96
2	**16b`**	75:25	1	65	9	≥ 97	93

[a]Determined by ^{1}H NMR spectroscopy (300 MHz). [b]Determined by $^{13}C\{^1H\}$ NMR spectroscopy (125 MHz).

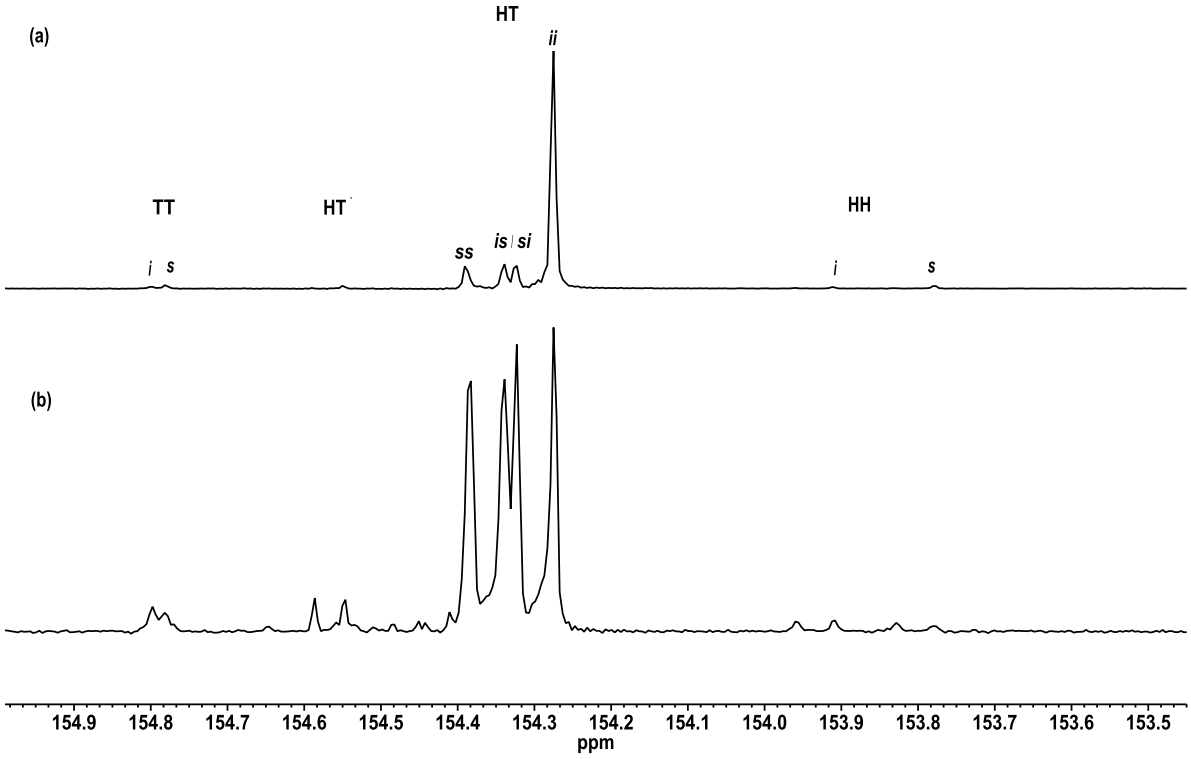

Figure 3.17: $^{13}C\{^1H\}$ NMR spectrum (125 MHz) of the carbonate carbons of the PPC copolymer synthesized with 1 equivalent [PPN]Cl , (a) using 75% (S)-PO and 25% (R)-PO and catalyst **16b**, (b) using 75% (S)-PO and 25% (R)-PO and catalyst **16b`** (**Table 3.4**).

The observed $^{13}C\{^1H\}$ NMR spectra in carbonate carbon region are best explained in terms of a model based on triad stereosequences,[54] taking into account the direction of the copolymer chain. That is, four signals of triads ($2^{(n-1)} = 2^2 = 4$),[99] namely **ii**, **is**, **si** and **ss** are expected, whereas the direction of chain causes the non-equivalence of the chemical shift for **is** and **si**

triads. The choice of chain direction is arbitrary; however we would prefer here to associate it with chain direction of the copolymer growth (**Figure 3.18**). As each triad structure contains three carbonate carbon atoms, the one in the middle is assigned as the atom producing the signal of this particular triad (marked with an asterisk).

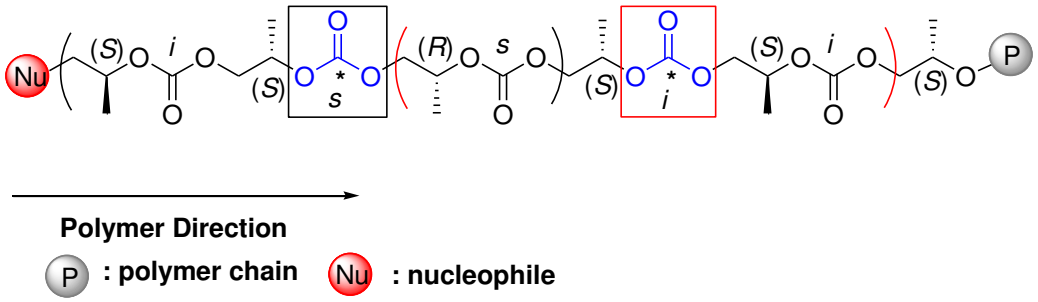

Figure 3.18: Effect of copolymer chain direction on **is** and **si** triads.

The asymmetry of the **is** and **si** triad is apparent from **Figure 3.18**. For the first triad, the corresponding carbonate carbon is surrounded by two stereocenters with the opposite configuration (R and S), whereas for the second triad, the corresponding carbonate carbon is surrounded by stereocenters with the same configuration (S and S). At the beginning of the copolymerization reaction with rac-PO and catalyst **16b**, mostly (S)-PO is incorporated into the copolymer with minimal insertion of (R)-PO. This leads to an iso-enriched copolymer with isolated stereoerrors, for which the intensity of is, si and ss sequences should be equal. A similar spectral pattern was also found in the experiment with 75% (S)-PO:25% (R)-PO ratio using catalyst **16b** (**Figure 3.17a**). For further studies, CO_2/rac-PO copolymerization reactions were performed for different reaction times. The regio- and enantioselectivity have been estimated for the isolated copolymers using NMR spectroscopy and chiral GC and analyzed statistically.

3.3.2 Statistical Modeling

Based on the triad structure inferred from the ^{13}C NMR spectra (**HT** carbonyl region), For more calculations based on the enantioselectivity data, a statistical model has been built to study the relationship between values of % S_{exp} (determined from GC measurements) and the values of **ii** %, **is** % and **ss** % (determined by NMR spectroscopy) are shown as a function of time (**Table 3.5**). However, close analysis of the spectral data reveals the presence of additional peaks at low intensity in the **HT** region. The relative intensity of these peaks increases with copolymerization time and is congruent with the growth of signals in the **TT** and **HH** region.

Table 3.5: Microstructure analysis data for copolymers from CO_2/rac-PO using 1000 equivalents of PO with respect to the catalyst at 30 °C and 30 bar CO_2.

entry	Catalyst	Cocat./cat. (equivalent)	Time (min)	TOF (h^{-1})[a]	HT (%)[b]	Enantioselectivity (%)[c]	K_{rel}[d]	ss (%)	is/si (%)	ii (%)
1	**16b**	1	30	242	96	81.4 (S)	4.8	15.2	35.8	49.0
2	**16b**	1	60	268	95	75.9 (S)	3.8	17.5	41.1	41.4
3	**16b**	1	90	270	95	70.6 (S)	3.1	18.1	42.4	42.3
4	**16b**	1	120	256	93	65.9 (S)	2.6	17.9	42.6	39.5
5	**16b**	1	180	177	93	66.0 (S)	2.7	17.9	42.7	39.4
6	**16b**	1	240	163	92	64.5 (S)	3.0	18.0	42.4	39.6
7	**16b**	0.5	30	178	98	81.0 (S)	4.6	14.0	34.2	51.7
8	**16b**	0.5	60	149	96	80.1 (S)	4.5	14.8	35.2	50.0
9	**16b**	0.5	90	141	95	77.4 (S)	4.0	15.6	37.1	47.3
10	**16b**	0.5	120	141	96	75.0 (S)	3.6	16.2	38.2	45.5
11	**16b**	0.5	180	138	95	71.1 (S)	3.3	17.8	42.1	40.1
12	**16b**	0.5	240	125	93	66.3 (S)	2.7	17.7	41.7	40.6
13	**16b**	0.5	360	108	93	65.7 (S)	3.2	17.8	41.8	40.4
14	**16b**	0.25	60	147	95	81.5 (S)	4.9	14.3	34.3	51.4
15	**16b**	0.25	120	162	95	79.6 (S)	4.5	15.3	36.4	48.4
16	**16b**	0.25	180	162	93	77.5 (S)	4.3	15.5	37.4	47.1
17	**16b**	0.25	240	121	93	73.8 (S)	4.3	16.8	40.6	42.6

[a]Moles of the PPC/moles catalyst per time(h), [b]Determined by $^{13}C\{^1H\}$ NMR spectroscopy (125 MHz). [c]Determined by GC. [d] $K_{rel} = \ln[1-c(1+ee)]/\ln[1-c(1-ee)]$; c = conversion, ee = enantiomeric excess in the polymer.

Upon the above results, an average microstructure for copolymer chains at different reactions time can be proposed based on the NMR and GC results. The proposed average

microstructure for the copolymers shows a gradient change of the copolymer sequences from iso-enriched to stereogradient microstructure due to the catalyst enantioselectivity (**Figure 3.19**).

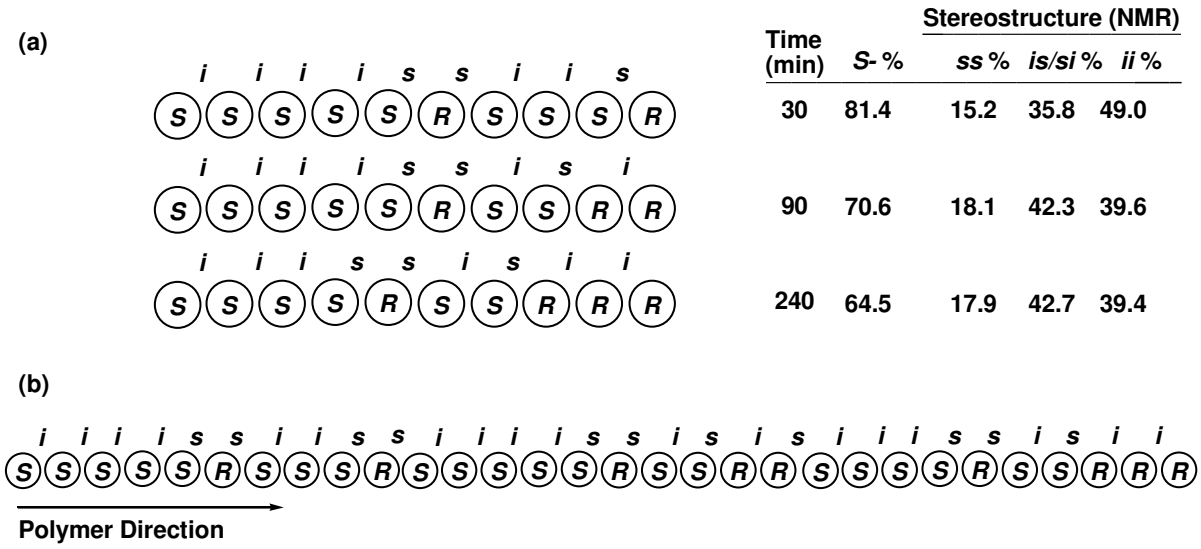

Time (min)	S- %	Stereostructure (NMR) ss %	is/si %	ii %
30	81.4	15.2	35.8	49.0
90	70.6	18.1	42.3	39.6
240	64.5	17.9	42.7	39.4

Figure 3.19: Stereomicrostructure of the copolymers (**HT**) obtained from CO_2 and rac-PO copolymerization reactions using catalyst **16b** with 1000 eqivalent neat rac-PO and 1 equivalent [PPN]Cl as cocatalyst at 30 °C and 30 bar CO_2 (**Table 3.4**).

The model which was presented in this study was based on triad structure obtained from the $^{13}C\{^1H\}$ NMR spectroscopy (**HT** carbonyl region). For more accurate calculations based on the enantioselectivity data (**Table 3.5**), a statistical model has been built to study the relationship between values of % S_{exp} (determined from GC measurements) and the values of **ii** %, **is** % and **ss** % as a function of time. The contributions of different stereosequence of SSS, RRR, SSR, RRS, SRS, and RSR to the polymer stereosequence will be estimated as triad structures for the HT region as a function of time. The model depends on the basic equation 1.

$$\%\ S_{calc} = C_1 \times \mathbf{ii}\ \% + C_2 \times \mathbf{is}\ \% + C_3 \times \mathbf{ss}\ \% \quad (1)$$

Minimization of the difference between the value % S_{calc} and % S_{exp} was done by means of the solver of Microsoft Excel software using the constrains; $C_1 \leq 1$, $0.333 \leq C_2, C_3 \leq 0.666$. Initial estimation of $C_1 = 1.0$, $C_2 = C_3 = 0.666$ values were used because of the large initial

percentage of S configuration in the copolymer samples. The values of coefficients which are preferring stereosequences of the stereosequences present in the polymer as shown in **Table 3.6**. The initial values of C_1 which are about 1 at 30 min are an indication of SSS stereosequence, the initial values of C_2 which are very close to 0.666 are an indication of SSR stereosequence and the values of C_3 which are very close to 0.666 are an indication of SRS stereosequence. Thus, the initial stereosequence of the copolymer can be readily determined using this model.

Table 3.6: The coefficients values perfairing to the stereosequence.

Coefficient	Value	Stereosequence	Stereostructure
C_1	1.0	SSS	**ii**
C_1	0.0	RRR	
C_2	0.666	SSR	**is**
C_2	0.333	RRS	
C_3	0.666	SRS	**ss**
C_3	0.333	RSR	

The change of C_1, C_2 and C_3 values with time are given in **Figures 3.20**, **3.21**, and **3.22** respectively, for the copolymers obtained using different catalyst to cocatalyst molar ratios.

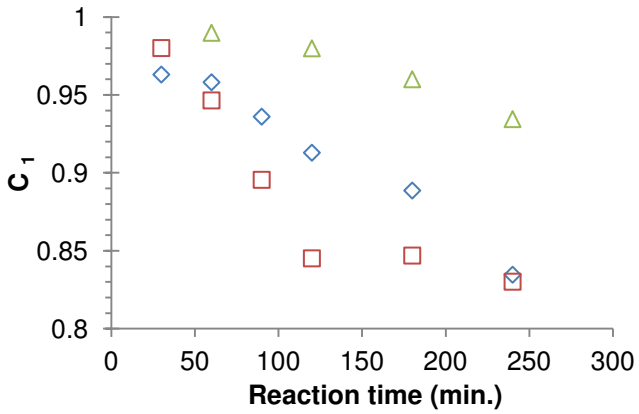

Figure 3.20: Change of C_1 values using different [PPN]Cl loading (0.25 equiv. (triangles), 0.5 equiv. (diamond) and 1 equiv. (squares)) and 45.7 mg of catalyst **16b** with 1000 equivalent rac-PO.

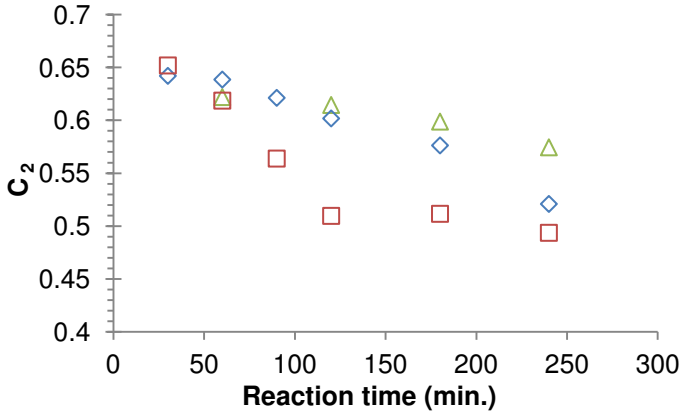

Figure 3.21: Change of C2 values using different [PPN]Cl loading (0.25 equiv. (triangles), 0.5 equiv. (diamond) and 1 equiv. (squares)) and 45.7 mg of catalyst **16b** with 1000 equivalent rac-PO.

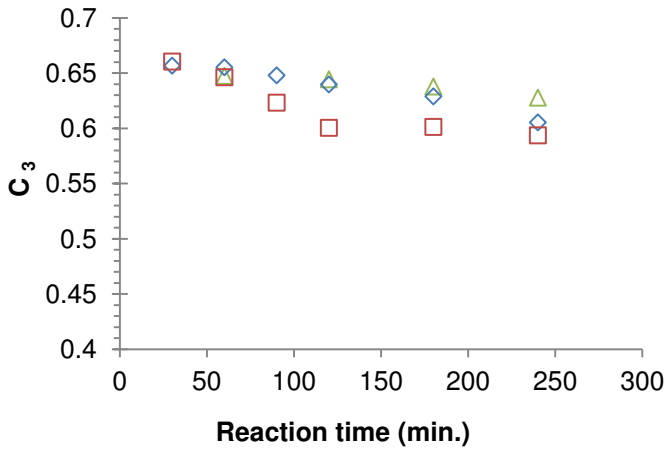

Figure 3.22: Change of C_3 values using different [PPN]Cl loading (0.25 equiv. (triangles), 0.5 equiv. (diamond) and 1 equiv. (squares)) and 45.7 mg of catalyst **16b** with 1000 equivalent rac-PO.

As shown in these Figures, the decrease of these coefficients with time is more dramatic for the catalyst:cocatalyst ratio of 1:1. Thus, the departure of the values of C_1, C_2, and C_3 from 1, 0.666, and 0.666 (SSS, SSR and SRS), respectively, increases with increasing the amount of the cocatalyst. Depending on the following equations, the coefficient C_1 can be fragmented into relative contributions of SSS and RRR, the coefficient C_2 into SSR and RRS and C_3 into SRS and RSR (**Table 3.7**).

$C_1 = 1 \times SSS + 0 \times RRR$ (2)

$C_2 = 0.666 \times SSR + 0.333 \times RRS$ (3)

$C_3 = 0.666 \times SRS + 0.333 \times RSR$ (4)

Table 3.7: Relative Contributions of the stereosequences in the polymer chains during the CO_2/PO copolymerization reactions using catalyst **1** with 1000 equivalent neat PO and [PPN]Cl as cocatalyst at 30 °C and 30 bar CO_2.

Cocatalyst/catalyst (equivalent)	Stereosequences	Relative contributions of stereosequence as a function of time					
		30 min	60 min	90 min	120 min	180 min	240 min
1	SSS	0.980	0.946	0.896	0.845	0.847	0.830
	RRR	0.020	0.054	0.104	0.155	0.153	0.17
	SSR	0.956	0.856	0.692	0.529	0.535	0.481
	RRS	0.044	0.144	0.308	0.471	0.465	0.519
	SRS	0.981	0.939	0.870	0.801	0.804	0.781
	RSR	0.019	0.061	0.130	0.199	0.196	0.219
0.5	SSS	0.963	0.958	0.936	0.913	0.889	0.835
	RRR	0.037	0.042	0.064	0.087	0.111	0.165
	SSR	0.927	0.916	0.864	0.806	0.729	0.563
	RRS	0.073	0.084	0.136	0.194	0.271	0.437
	SRS	0.970	0.966	0.944	0.919	0.887	0.816
	RSR	0.030	0.034	0.056	0.081	0.113	0.184
0.25	SSS	-----	0.990	-----	0.980	0.960	0.934
	RRR	-----	0.010	-----	0.020	0.040	0.066
	SSR	-----	0.867	-----	0.844	0.797	0.724
	RRS	-----	0.133	-----	0.156	0.203	0.276
	SRS	-----	0.942	-----	0.933	0.913	0.883
	RSR	-----	0.058	-----	0.067	0.087	0.117

As shown, the change of the stereosequence is significant up to 120 min for catalyst:cocatalyst molar ratio 1:1, and after this time the sequences reached plateau due to decreasing (S)-PO in the reaction feed, which may be decreases the copolymerization reaction rate regarding the unfavorable (R)-PO insertion. For catalyst:cocatalyst molar ratio 1:0.5 and 1:0.25, the changes of the stereosequence did not reach plateau and the sequences are continuously changing. Furthermore, the change of SSR and RRS stereosequences as a

function of time, were more dramatic than other stereosequences (**Figure 3.22**). The changes of the stereosequences are more significant when the catalyst:cocatalyst molar ratio is 1:1.Since the change of % conversion with time is not the same for the polymers obtained using different catalyst:cocatalyst molar ratios, it is clear from **Figure 3.22** that, during the polymer growth using rac-PO, the (S)-PO insertion is more favored than (R)-PO. This can be seen especially at the beginning of the CO_2/rac-PO copolymrization reaction since each (R)-PO insertion can be inverted to (S)-stereosequence by methine-oxygen bond ring-opening to form **HH** regiostructure which keeps the stereoregularity of the polymer chain, or it can be inserted by methylene-oxygen bond ring-opening which follows by (S)-PO insertion which forms isotactic-syndiotactic (**is**) stereosequence. It is shown (**Table 3.7**) that the copolymer stereosequence consists of 98% SSS, 96% SSR and 98% SRS for the copolymer which was formed using a catalyst:cocatalyst molar ratio of 1:1 for 30 minutes which clearly shows the enantiselectivity of the chiral catalyst for (S)-PO. Any (R)-PO insertion is followed immediately by (S)-PO insertion. The effect of cocatalyst ratio comparison on the changes of the stereosequences with % conversion (**Figure 3.23**) shows in all experiments that the changes of sequences for different cocatalyst loadings for each stereosequence behave same. This shows that the effect of the copolymer yield conversion is more significant than the reaction time which is related to the copolymer chain growth. The SSR stereosequence also shows significant change as a function of time.

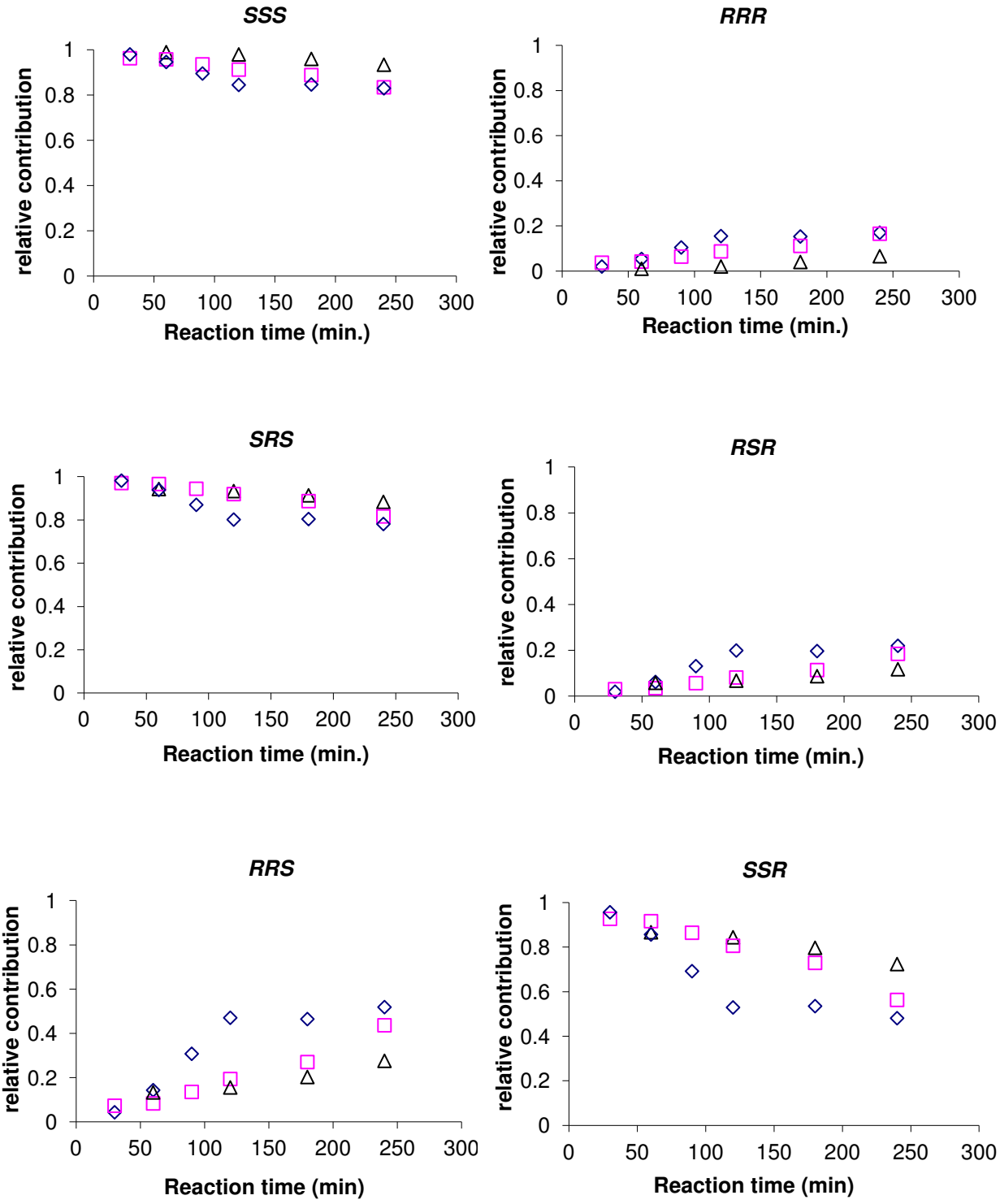

Figure 3.22: Relative contribution of the stereosequences in the polymer chain as a function of time using different [PPN]Cl loading (0.25 equiv. (triangles), 0.5 equiv. (squares) and 1 equiv. (diamonds)) and 45.7 mg of catalyst **16b** with 1000 equivalent rac-PO.

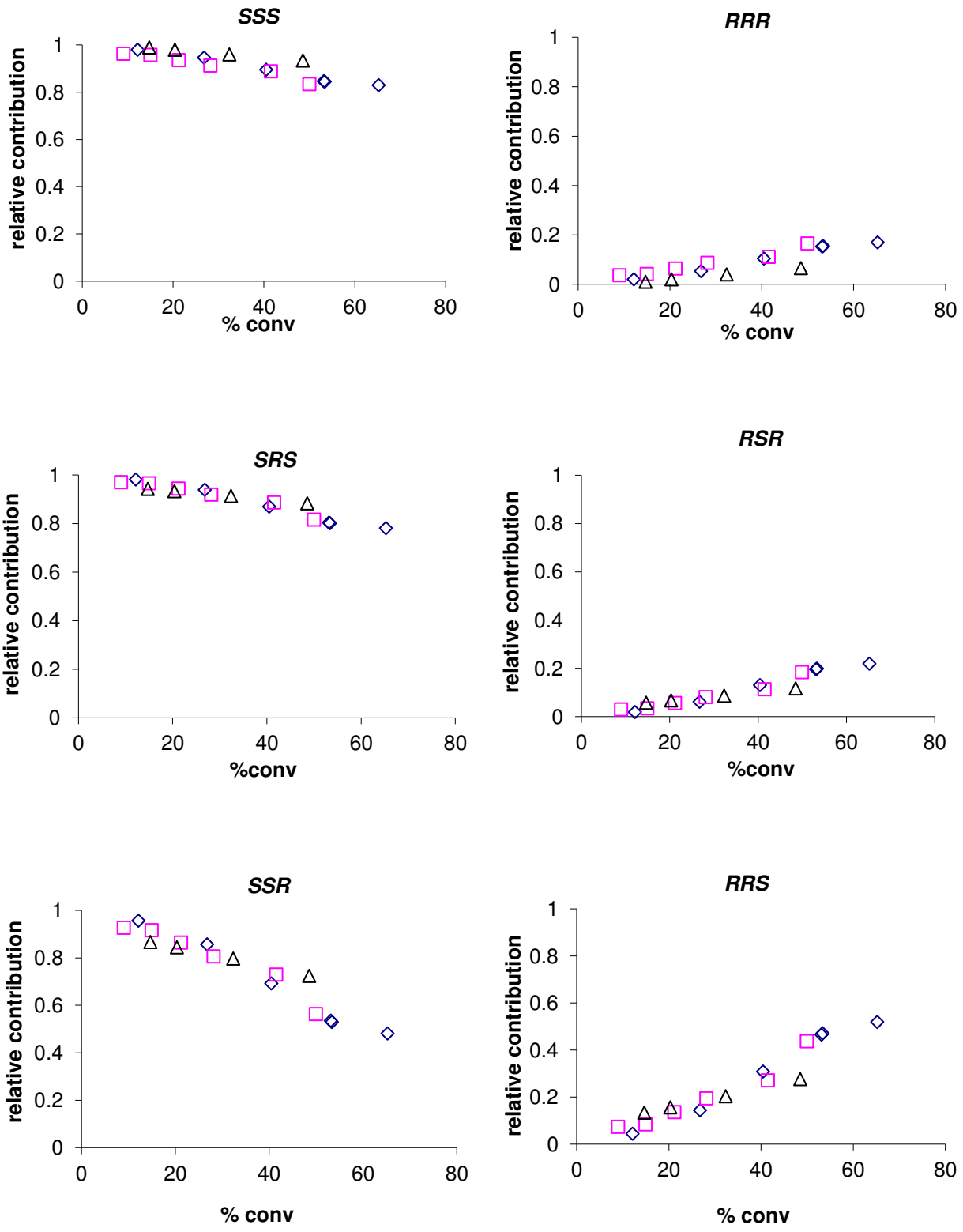

.**Figure 3.23:** Relative contribution of the stereosequences in the polymer chain as function of % conversion using different [PPN]Cl loading (0.25 equiv. (triangles), 0.5 equiv. (squares) and 1 equiv. (diamonds)) and 45.7 mg of catalyst **16b** with 1000 equivalent rac-PO.

It is clear that from **Figure 3.22** and **Figure 3.23** the change of % conversion with time is not the same for the polymers obtained using the different catalyst:cocatalyst molar ratios, it is necessary to study the changes of stereosequences with the % conversion (instead of time). Comparison of effects of cocatalyst ratio on the changes of the stereosequences with % conversion is shown in **Figure 3.23**. In the case of the three catalyst:cocatalyst molar ratios, the changes of stereosequences are most significant for SSR stereosequence. There are no significant differences between the polymers obtained using the three ratios of catalyst if the % conversion is used instead of time as the basis for comparison of changes of sequences copolymer which is obtained by chiral catalyst shifts from iso-enriched to stereogradient because of the non-alternating (S)-PO/(R)-PO insertion which is formed from the selectivity of the catalyst to one of the stereosequence than the other.

3.3.3 NMR assignment based on tetrad level

Unfortunately, the spectra recorded at 125 MHz $^{13}C\{^{1}H\}$ NMR spectroscopy are not sufficiently resolved for reliable integration. In this respect, higher frequency NMR spectroscopy was employed to obtain further information. Two different iso-enriched and syndio-enriched copolymers have been synthesized (**Table 3.8**). Both samples were analyzed using high resolution (both 500 and 900 MHz) NMR spectroscopy (**Figure 3.24**). The increase in the frequency clearly shows a higher resolution of the signals in both HT and TT region. For the iso-enriched copolymer (**Figure 3.24b**), the signal assigned as **ii** shows a downfield shoulder, whereas the **ss** signal splits into two signals.This therefore necessitates the consideration of the influence of the neighboring stereocenters and application of a tetrad model for the signals of various stereosequences, taking into account the direction of the copolymer according to the above-listed considerations. Interestingly, for the syndio-enriched copolymer, the splitting of the signal assigned as **is**-triad (**Figure 3.24c**) was observed as a shoulder, whereas the highest signal of the **ss**-triad was resolved as a single peak.

Table 3.8: Different copolymerization reaction of CO_2/rac-PO using 1000 equivalents of PO with respect to the catalyst at 30 °C and 30 bar CO_2 for 2h, without cocatalyst.

Entry	Catalyst	Conv (%)[a]	Selectivity (PPC %)[a]	Carbonate linkages (%)[a]	HT (%)[b]	M_n (kg/mol)[c]	PDI (M_w/M_n)[c]
1	**16b**	22	100	≥ 97	82	19.7	1.2
2	**27**[d]	27	97	≥ 98	83	17.7	1.3

[a]Determined by ^{1}H NMR spectroscopy (500 MHz). [b]Determined by $^{13}C\{^1H\}$ NMR spectroscopy (125 MHz). [c]Determined by GPC in THF, calibrated with polystyrene standard. [d]Prepared by equimolar mixing of catalysts **16b** and **16b`**.

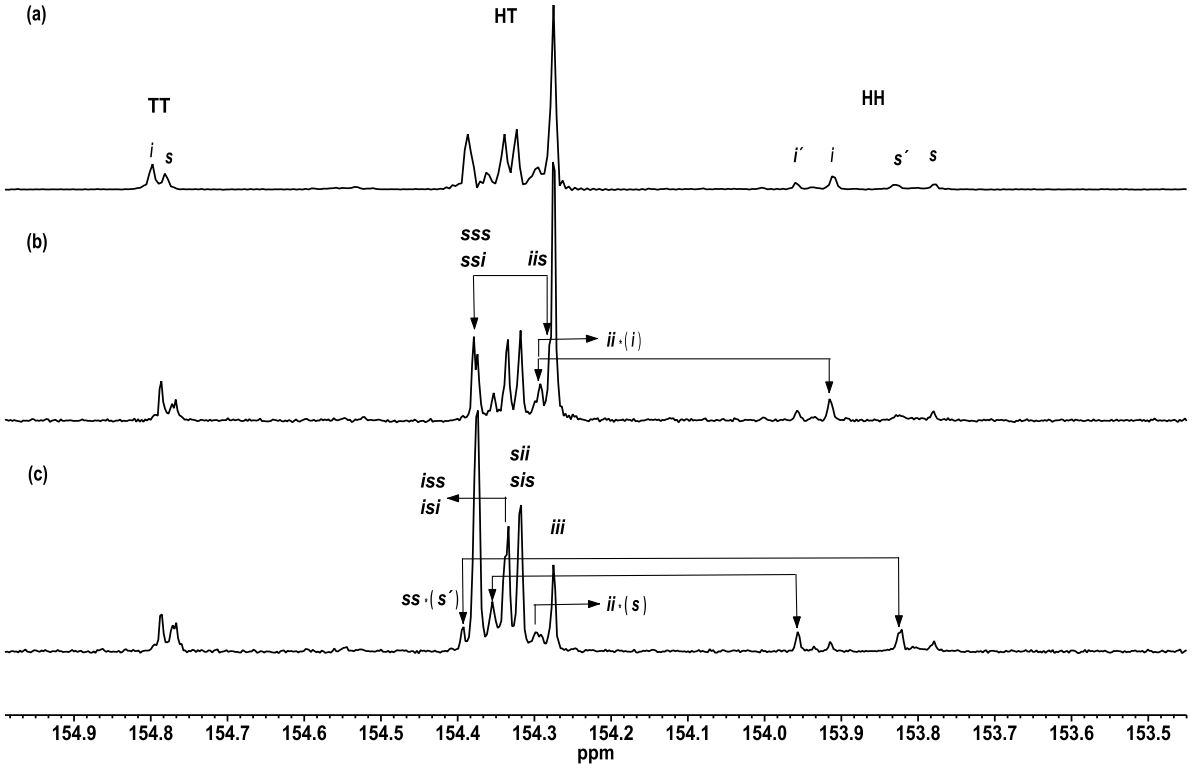

Figure 3.24: $^{13}C\{^1H\}$ NMR spectrum of a carbonate carbon region of a) iso-enriched PPC (125 MHz), b) iso-enriched PPC (225 MHz) and c) syndio-enriched PPC (225 MHz) and the proposed assignment of signals on the tetrad level.

However, a new low intensity peak in the vicinity of ss-signal in the lower field region was observed, which wasattributed to an effect of regioerror close to the syndiotactic triad. Accordingly, all observed low-intensity signals (~ δ_C 154.29, 154.30, 154.35 and 154.39 ppm)

correlate well with the signals in **HH** and **TT** region due to the regioerror (**Figure 3.24**). For comparison with the Co-based catalyst, the (R,R)-[(t-Bu)$_2$SalcyCr$^{(III)}$Cl] (**19a`**)/DMAP system was tested with two different (S)-PO:(R)-PO ratios (1:3 and 3:1, respectively) which showed the preference of this catalyst for (S)-PO, thus mirroring the case of the Co-analogue.

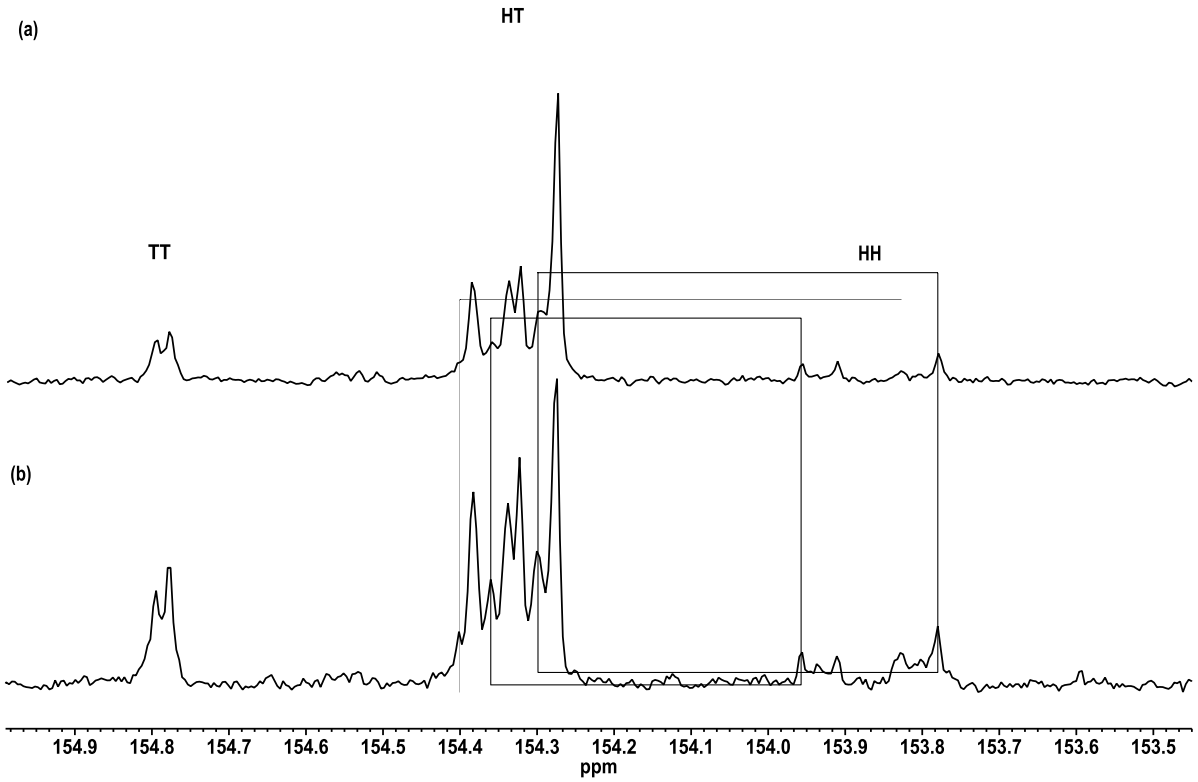

Figure 3.25: $^{13}C\{^1H\}$ NMR spectrum (75 MHz) for PPC copolymer synthesized using catalyst **19a`** with 0.5 equivalent DMAP, (a) using 75% (S)-PO and 25% (R)-PO, (b) using 25% (S)-PO and 75 % (R)-PO at 50 °C and 50 bar CO_2 for 20 h.

However, this Cr-based system leads to copolymers with a high regioerror ratio compared to the Co-based catalyst as can be seen from the intensity of the signals in the **HH** and **TT** regions (**Figure 3.25**). The higher intensity of the latter **TT** is accompanied by a higher intensity of the signals in **HT** region associated with regioerrors (**ii**$*$/$*$**ii**, **si**$*$/$*$**is**, **is**$*$/$*$**is** and **ss**$*$/$*$**ss**) which fits well with the proposed assignment model. Aside from the **HT** region, the splitting pattern of the signals in **HH** region of the spectrum is very informative with respect

to copolymer microstructure. The splitting pattern of the signals in **TT** region is not pronounced, which indicates a weak influence of the neighboring stereoconfiguration onto the chemical shift of this junction. Therefore, it is expected that the **TT**-junction does not strongly affect the chemical shifts of the neighboring stereosequences, but only the **HH** junction does. This has been verified from the ratio of **HH**:**TT**:**ii**$_*$ peaks area of the (R)-PPC (**Figure 3.15a**), since this was found to be approximately 1:1:1 and not 1:1:2. The assignment of **HH** signals to **i** or **s** diads has already been reported and was verified in our study using GC measurements. Based on this, we have proposed the assignment of four peaks in this region as shown in **Figure 3.24**. Importantly, a higher number of peaks in **HH** region can be observed for copolymers with high degree of regioerrors, for which the model of isolated regioerror is no longer valid. The origin of **i**-diads in **HH** region is referred to an "abnormal" PO-enchainment with retention of configuration of the stereocenters. This would imply either an S_N1-type ring-opening mechanism or S_N2-type with retention of configuration, both unusual for propylene oxide.[88] Chisholm and co-workers have reported that (R,R-Salen)Cr catalyst (**19a`**) prefers the "abnormal" ring-opening of (S)-PO in copolymerization with CO_2 to generate the primary alkoxide with (S)-configuration.[98] They have observed a high intensity of the **i**-diad signal in the **HH** region compared to **s**-diad. In order to verify whether this phenomenon could be connected with the nature of the initiating group of the catalyst, copolymers produced from (R)-PO/CO_2 copolymerization by two (S,S-Salen)Cr catalysts, namely **19a** and **26** were compared (**Table 3.9**).

Table 3.9: Different copolymerization reaction of CO_2 and (R)-PO using 1400 equivalents of PO with respect to the catalyst at ambient temperature and 50 bar CO_2 for 48h, without cocatalyst.

Entry	Catalyst	Yield. (%)[a]	Selectivity (%PPC)[b]	Carbonate linkages (%)[b]	HT (%)[c]	M_n (kg/mol)[d]	PDI (M_w/M_n)[d]
1	**19a**	5.2	≥99	≥92	79	8.0	1.4
2	**26**	5.5	≥99	≥89	80	7.0	1.4

[a]Based on isolated yield of the copolymer. [b]Determined by ^{1}H NMR spectroscopy (500 MHz). [c]Determined by $^{13}C\{^1H\}$ NMR spectroscopy (125 MHz). [d]Determined by GPC in THF, against polystyrene standard.

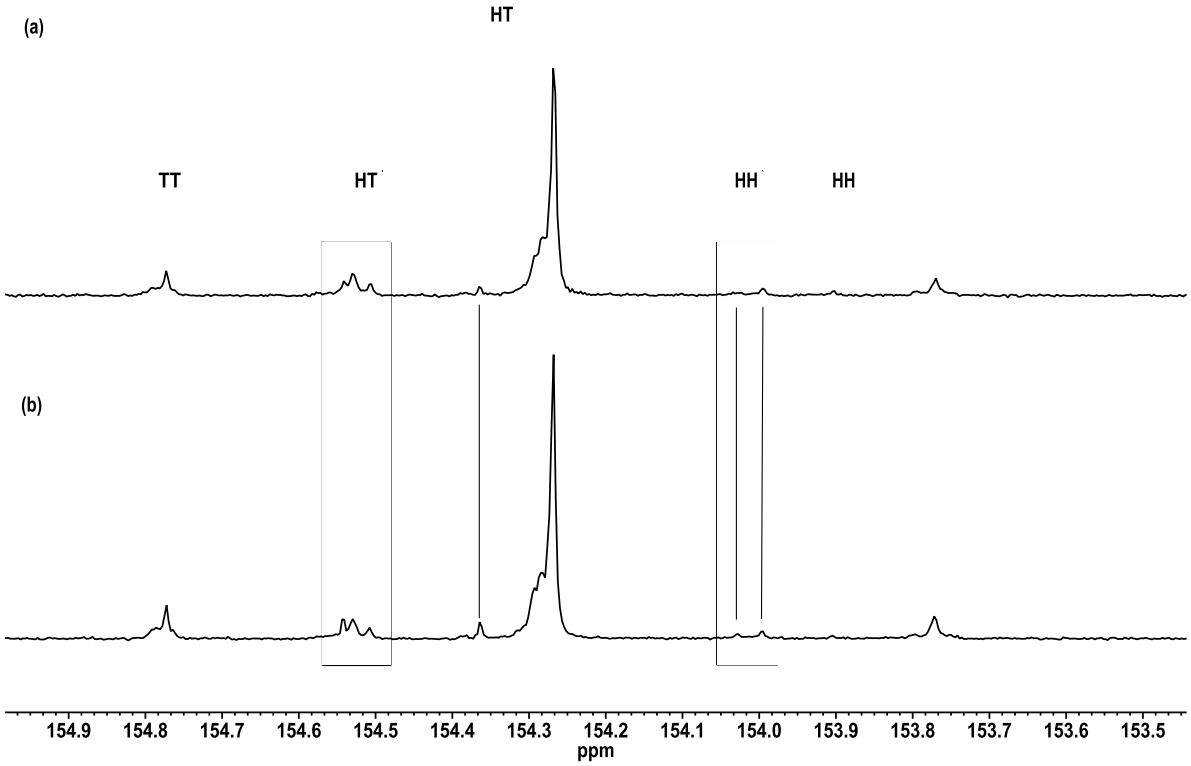

Figure 3.26: $^{13}C\{^1H\}$ NMR spectrum (125 MHz) of the carbonate carbons for PPC copolymer (a) synthesized using **19a** (b) synthesized using **26**, with 1400 equivalents PO and 50 bar CO_2 without cocatalyst (**Table 3.9**).

Although these reactions reflect a "mirror stereochemistry" of Chisholm´s system as discussed above with respect to the catalyst and propylene oxide configuration it is surprising to observe nearly no "abnormal" ring-opening of PO with retention of configuration in the

present system. Both catalysts **19a** and **26** produced very similar copolymers with respect to molecular weight and microstructure (**Figure 3.26**).

However, the copolymers feature an increased content of ether linkages compared the previously described systems, which is reflected in new peaks in HT region. That is, a group of peaks appeared at δ_C 154.5 - 154.6 ppm and a new shoulder of the **ii** signal is clearly seen at the low-field side in addition to the ii$_*$ signal. Unfortunately, the high amount of both regioerror and PO misinsertion (alternation error) prohibits the unambiguous assignment of each signal in these copolymers using the isolated error approach.

3.4 Copolymerization Reaction Mechanism

3.4.1 Proposed Initiation Step Mechanism

In order to select the best copolymerization condition for this study, the activity of **16b** was investigated using DMAP and [PPN]Cl as initiators in neat rac-PO (**Table 3.10**).

Table 3.10: Copolymerization of CO_2/rac-PO by (R,R)-Salen $Co^{(III)}Cl$ (**16b**)Complex System For 20 h using 1000 equivalent PO.

Entry	Cocat.	Cocat. Equiv.	Temp. °C	Pressure (bar)	Conv (%)[a]	PPC (%)[a]	Carbonate linkages (%)[a]	M_n (kg/mol)[b]	PDI (M_w/M_n)[b]
1	DMAP	0.5	50	50	0	----	----	----	----
2	DMAP	0.5	50	20	98	40	≥99	17.5	1.6
3	DMAP	0.5	30	20	Traces	----	----	----	----
4	DMAP	0.5	30	50	10	0	----	----	----
5	[PPN]Cl	1	30	30	82	≥99	≥99	36.5	1.7

[a]Determined by ^{1}H NMR spectroscopy.
[b]Determined by GPC in THF, calibrated with polystyrene standard.

It is shown that using DMAP as a neutral organic base cocatalyst with increasing the CO_2 pressure (**Table 3.10**, **entries 1** and **4**) deactivates the copolymerization reaction even at different reaction temperatures. Decreases in the CO_2 pressure to 20 bar enhanced the copolymerization reaction at high temperature (**Table 3.10**, **entry 2**) with high conversion but low selectivity in respect to the low reaction temperature (**Table 3.10**, **entry 4**). Based on results from DMAP, the binary catalytic system with [PPN]Cl was chosen for this copolymerization reaction which shows higher selectivity to produce alternating regioregular copolymers (**Table 3.10**, **entry 5**) The optimized [PPN]Cl to the catalyst molar ratio as reported previously by Coates et al.[54] which shows relatively same copolymerization results but at different reaction condition was also taken into consideration. Lu et al.[46] also reported high activity of some cobalt complexes systems even at lower CO_2 pressure using ammonium salts as cocatalysts, which is in contrast to the performance of cobalt complexes alone without initiators and which is active at high CO_2 pressure.[53] The catalytic system which is used in

this study is based on [PPN]Cl as initiator. The effect of the [PPN]Cl molar ratio to the catalyst on the kinetics of the reaction has been studied using in situ ATR-IR technique.

3.4.1.1 In situ ATR-IR measurements using cocatalysts

3.4.1.1.1 Reaction order in respect to [PPN]Cl

Decreasing the [PPN]Cl molar ratio to catalyst less than 1 equivalent shows low catalytic activity but increase in the polycarbonate selectivity over cyclic carbonate (**Figure 3.27**). It is clear that increasing the [PPN]Cl load increases the cPC formation at the beginning of the copolymerization reaction over PPC to the plateau region followed by increasing the polymer formation. This behavior is applied until the [PPN]Cl load is 2 equivalents of the catalyst, which depresses the polymer formation even after the cPC plateau region.

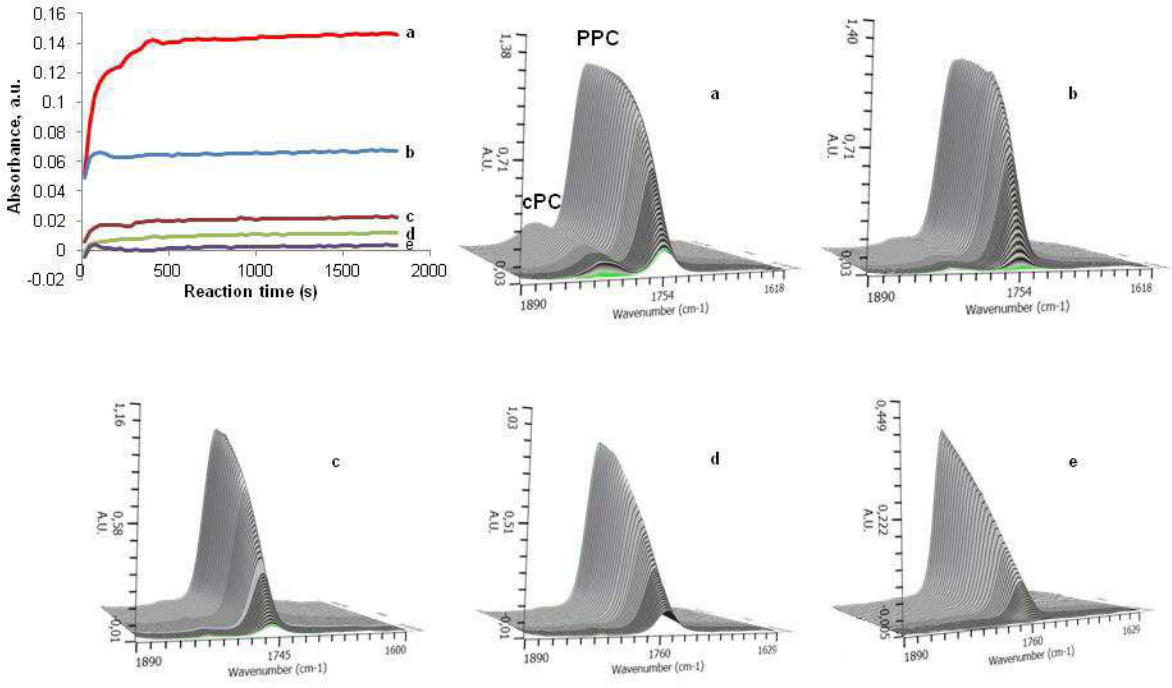

Figure 3.27: The cPC formation at 1810 cm^{-1} (over PPC) during the reaction initiation with time and different [PPN]Cl loading (82 mg(2 equiv.) —, 41 mg(1 equiv.) —, 20.5 mg(0.5 equiv.) —, 10.13 mg(0.25 equiv.) — and 5.13 mg(0.125 equiv.) —) using 45.7 mg of catalyst **16b** with 1000 equivalent rac-PO and the related 3D ATR-IR spectra.

The r_{obs} (**Figure 3.28**) and cocatalyst order has been measured to show first order (**Figure 3.29**) which is as expected since one cocatalyst is required to initiate the growth of one copolymer chain as monometallic or either bimetallic copolymerization mechanism.

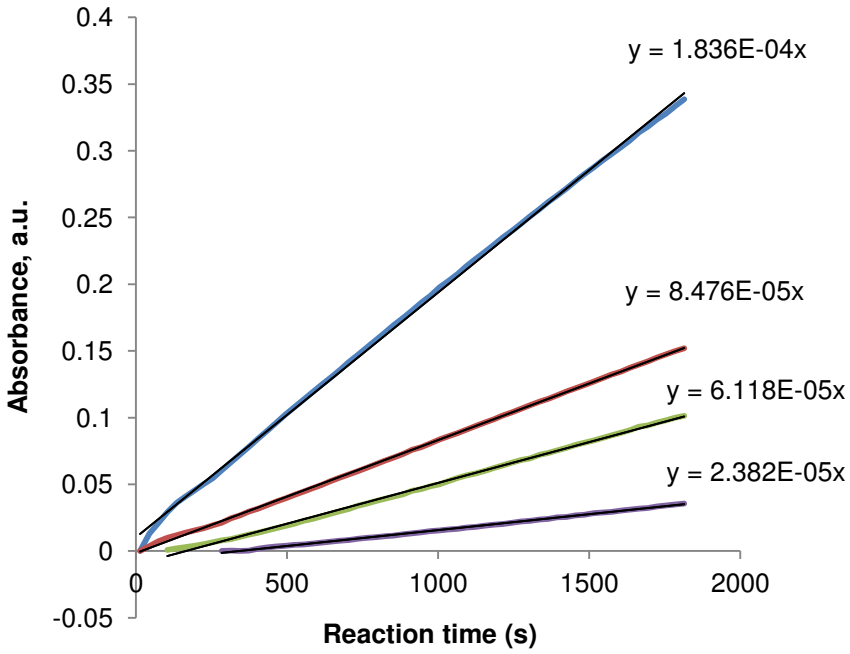

Figure 3.28: Determination of r_{obs} as change of absorbance at 1750 cm^{-1} at different [PPN]Cl loading (41 mg —, 20.5 mg —, 10.13 mg —, 5.13 mg —) using 45.7 mg catalyst **16b** with 1000 equivalents PO.

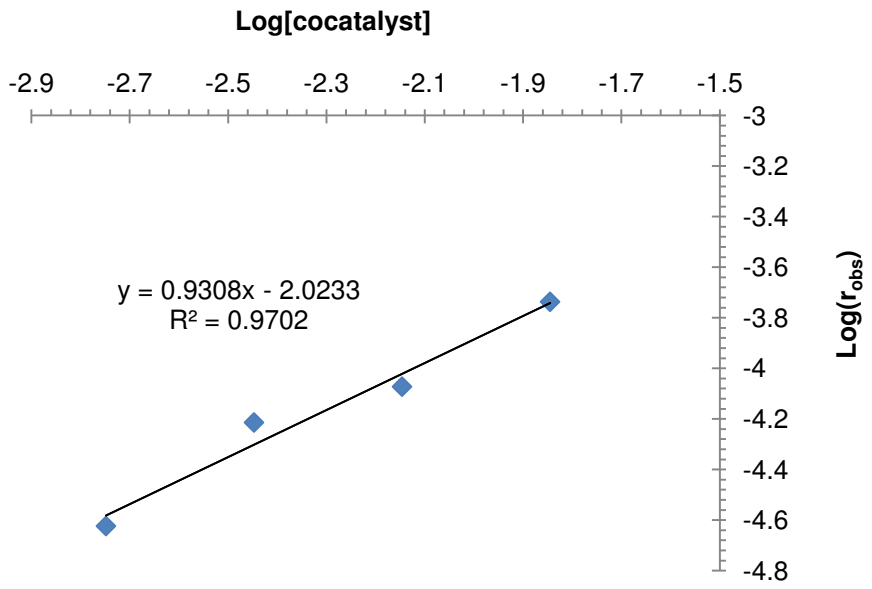

Figure 3.29: Determination of the cocatalyst order in the copolymerization reaction using 45.7 mg of catalyst **16b** with 1000 equivalents PO.

Applying the same reaction condition in the absence of the catalyst does not show any cPC formation, which clearly shows the effect of the catalyst as well. This means the formation of cPC is a competitive reaction at the initiation step which shifts the reaction to the formation of PPC copolymer. Based on the above observation, if the PO ring opening is followed by CO_2 insertion, the dissociated carboxylate group leads to intramolecular ring closure and cPC formation. On the other hand, insertion of two alternating PO units which is followed by CO_2 insertion which dissociates for another PO insertion does not lead to cPC because the ether bond cleavage by intramolecular reaction is not preferable (**Scheme 3.6**).

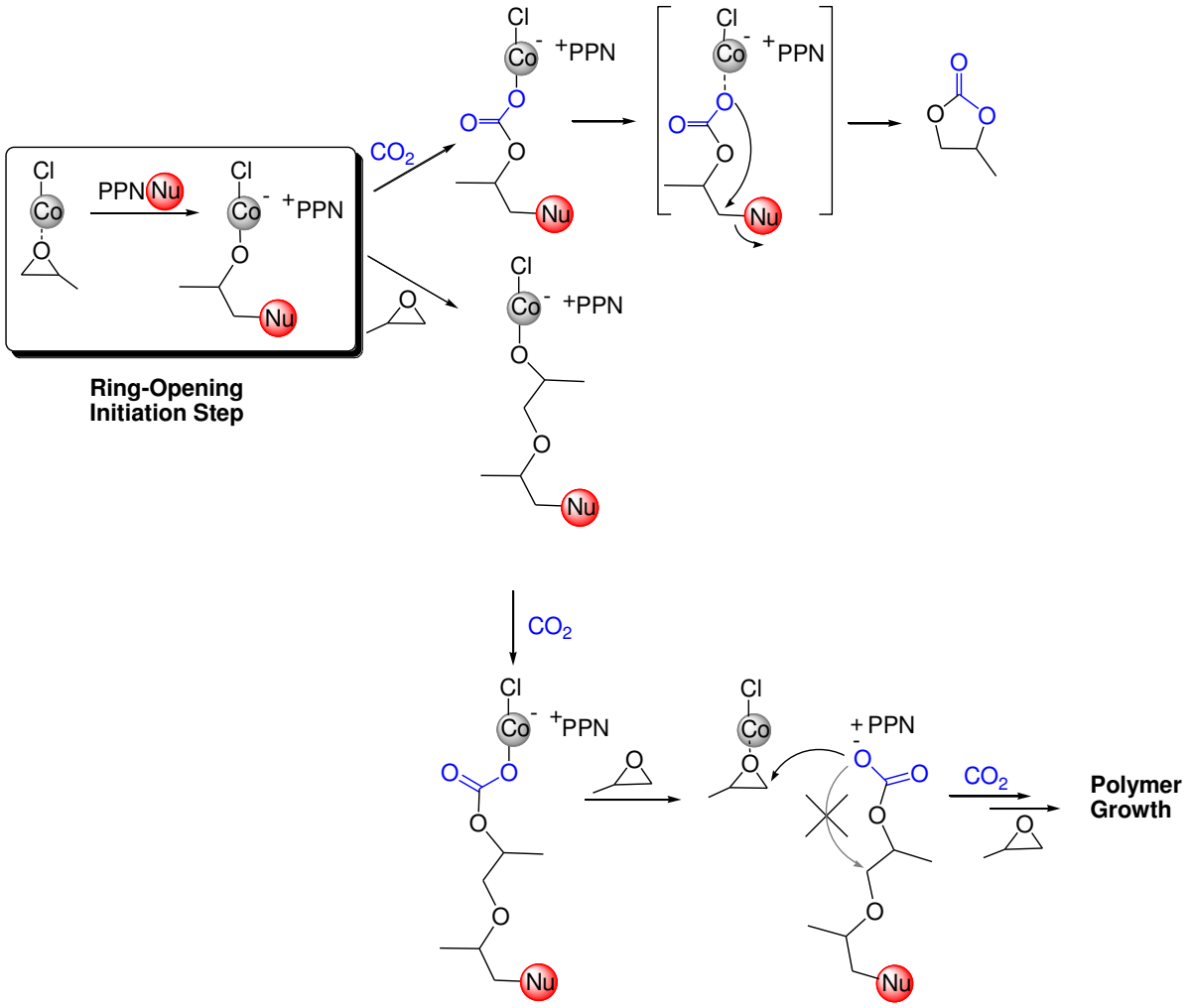

Scheme 3.6: Proposed mechanism for cPC and PPC formation.

However, at the early times of the copolymerization reaction with 1 equivalent cocatalyst molar ratio, broadening of the GPC chromatograms and PDI values were observed. On the other hand, using 0.5 or 0.25 equivalent cocatalyst shows the bimodality of the copolymer with relatively narrower PDI (**Table 3.2**). It is worthy to note that these bimodal copolymers show an increase in the intensity of the high M_n as a function of time which may attributed to the residual water in the system. This leads to the generation of propylene glycol which supports the copolymerization by the chain growth at both chain ends which is two times faster than chain growth at one end.[78]

3.4.1.1.2 Reaction order with respect to the catalyst

Consequently, the catalytic order has been measured using 1 equivalent cocatalyst relative to the catalyst. It was expected from **scheme 3.6** that the catalyst order would be second order. The calculations from the r_{obs} values at different enantiomeric pure (R,R)-configuration catalyst loading (**Figure 3.30**) show that it is first order in respect to the catalyst (**Figure 3.31**) which is consistent with what was previously published.[47,98,100]

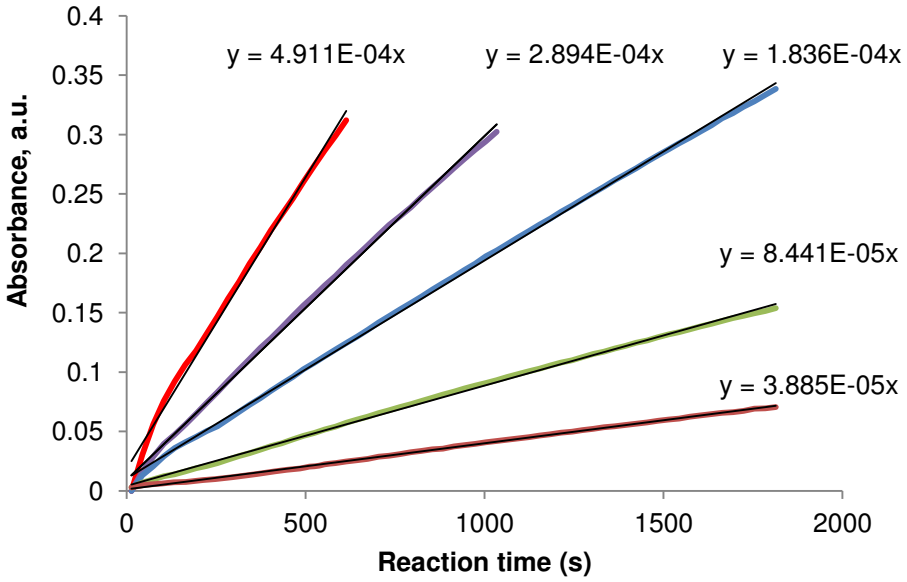

Figure 3.30: Determination of r_{obs} as change of absorbance at 1750 cm^{-1} at different catalyst loading (137.1 mg —, 91.4 mg —, 45.7 mg —, 22.5 mg —, 11.6 mg —) using catalyst **16b** with 1 equivalent [PPN]Cl and 5 mL rac-PO.

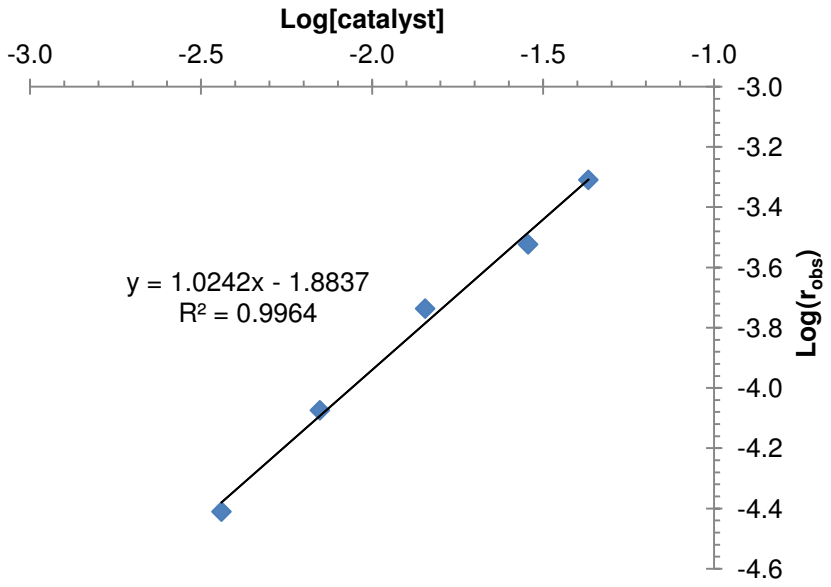

Figure 3.31: Determination of the reaction order with respect to the catalyst in the copolymerization reaction using catalyst **16b** with 1 equivalent [PPN]Cl.

Based upon the above results, a monometallic initiating process mechanism has been proposed for the PO/CO_2 copolymerization reaction (**Scheme 3.6**). It is noteworthy that during copolymerization of CO_2 and rac-PO using enantiomeric pure chiral catalyst, the enantioselectivity of the catalyst for the opposite PO configuration is pronounced.[48,54] Accordingly, the effect of using rac-catalyst on the rate of the reaction during the copolymerization of CO_2 and rac-PO was investigated (**Figure 3.32**).

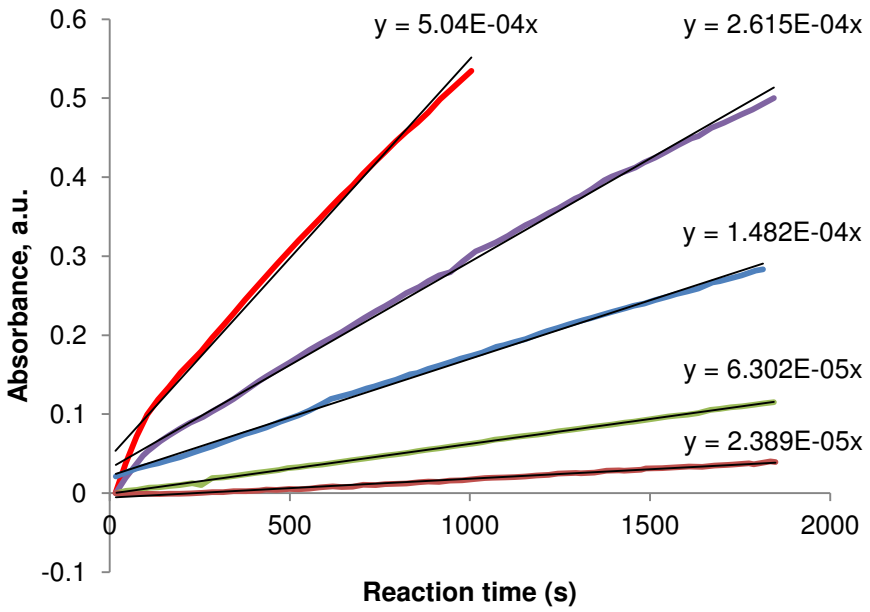

Figure 3.32: Determination of r_{obs} as change of absorbance at 1750 cm^{-1} at different catalyst loading (137.1 mg —, 91.4 mg —, 45.7 mg —, 22.5 mg —, 11.6 mg —) using catalyst **27** with 1 equivalent [PPN]Cl and 5 mL rac-PO.

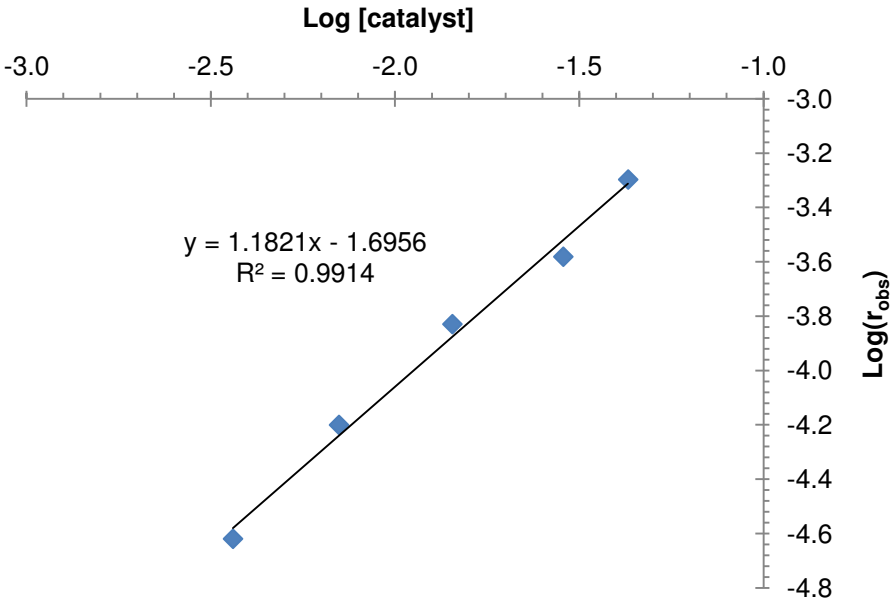

Figure 3.33: Determination of the reaction order with respect to the catalyst in the copolymerization reaction using **27** with 1 equivalent [PPN]Cl.

(**Figure 3.30** and **Figure 3.32**) demonstrate the same copolymerization reaction rates of both systems, reveals that the ring opening initiation rate process is independent of the catalyst chirality. However, the order of the reaction in respect to the catalyst (rac-catalyst) is also found first order (**Figure 3.33**).

3.4.1.2 In situ ATR-IR measurements without using cocatalyst

As shown previously, the rate law for the PO ring opening in the catalytic binary systems was found to be a first order dependence on the catalyst concentration and independent from the configuration of the catalyst. Accordingly, the initiation rate process without cocatalyst as initiator has been investigated using enantiomeric pure (R,R-Salen)$Co^{(III)}$Cl (**16b**) as an example. The in situ IR monitoring of PPC formation shows a long induction period of such a system (**Figure 3.34**) with respect to the binary catalytic system (**Figure 3.30** and **Figure 3.32**), which increase according to the decrease of catalyst loading.

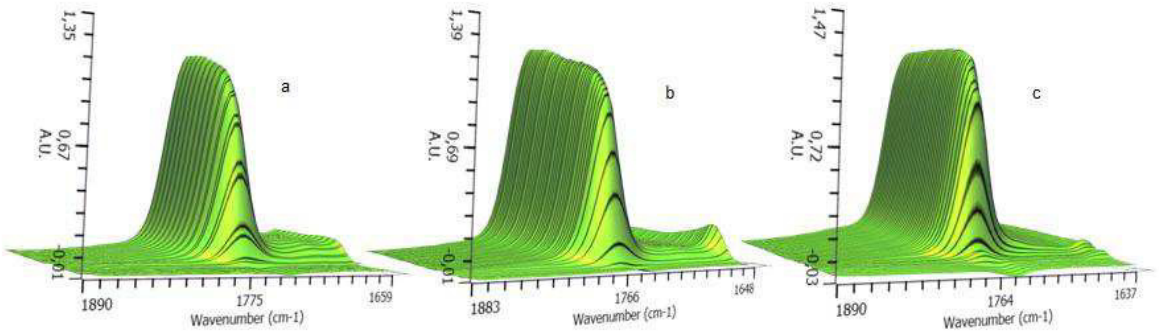

Figure 3.34: 3D ATR-IR spectra show change the induction period during CO_2/rac-PO copolymerization at different catalyst loading, a) 91.4 mg, b) 45.7 mg, c) 22.5 mg using catalyst **16b** and 5 mL rac-PO without cocatalyst.

However, **Figure 3.34** clearly shows that in the absence of the cocatalyst the formation of cPC during the copolymerization reaction is not pronounced, which indicates the crucial role of the cocatalyst for the formation of cPC as byproduct.

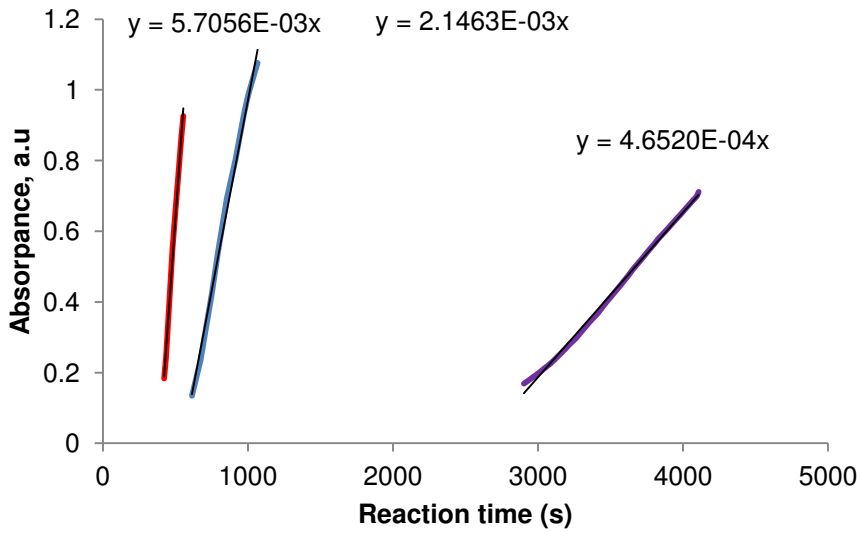

Figure 3.35: Determination of r_{obs} as change of absorbance at 1750 cm^{-1} at different catalyst loading (91.4 mg —, 45.7 mg —, 22.5 mg —) using catalyst **1** and 5 mL rac-PO without cocatalyst.

The calculations from the r_{obs} values at different enantiomeric pure (R,R)-configuration catalyst loadings (**Figure 3.35**) show there is second order rate law dependence on the catalyst loading with respect to epoxide ring opening (**Figure 3.36**).

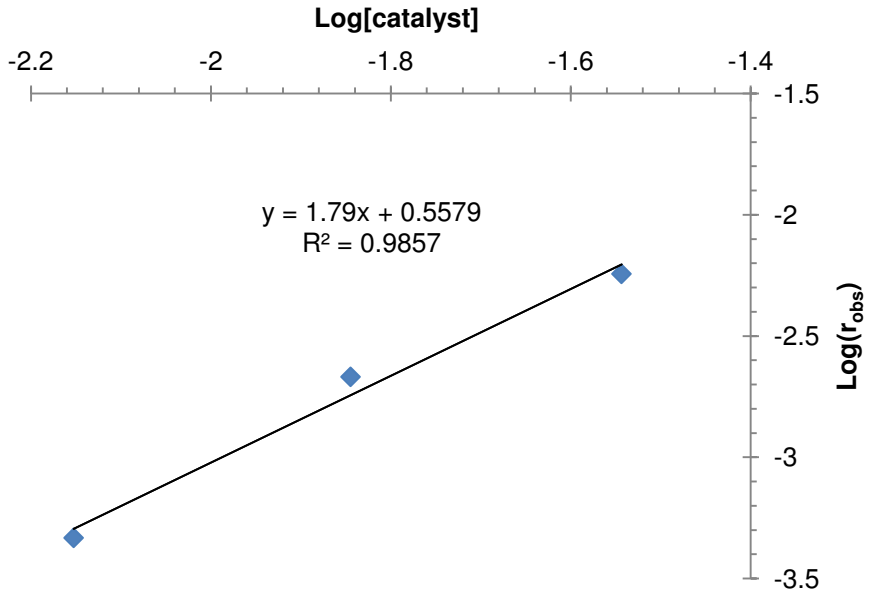

Figure 3.36: Determination of the reaction order with respect to the catalyst in the copolymerization reaction using **16b** without cocatalyst.

Therefore, the PO ring-opening involves a cooperative bimetallic mechanism as shown in **Scheme 3.7**.[101-103]

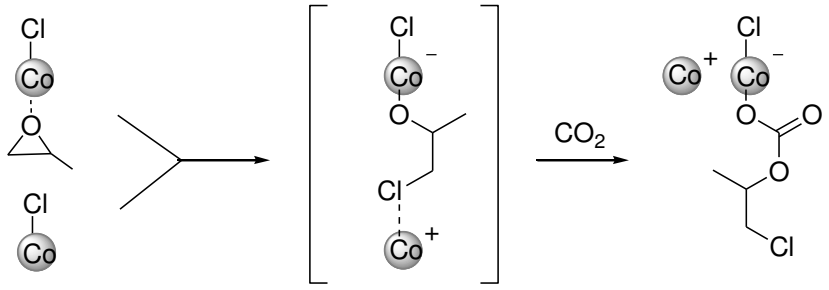

Scheme 3.7: Proposed bimetallic mechanism of PO ring opening.

3.4.2 Proposed Propagation Step Mechanism

Since the (R,R)-configuration catalyst prefers (S)-PO insertion, iso-enriched copolymer forms at the beginning of the reaction. At this stage, any (R)-PO insertion leads predominantly to a "normal" ring opening to form the HT regiostructure with a syndiotactic stereosequence. This misinsertion is then "corrected" by a (S)-PO insertion, thus producing an isotactic sequence with isolated stereoerrors. With gradual consumption of (S)-PO and increase of (R)-PO in the reaction feed, the relative insertion of the latter increases and the overall copolymer growth becomes slower. At high PO conversion, the "abnormal" ring opening becomes more pronounced, therefore increasing the HH and TT ratios in the copolymer (**Figure 3.37**). At this point, the copolymer can be described as an iso-enriched stereogradient copolymer. GC measurements of the degraded copolymers allowed the determination of K_{rel} according to the equation $K_{rel} = \ln[1-c(1+ee)]/\ln[1-c(1-ee)]$, where K_{rel} corresponds to the difference in energy between the diastereomeric transition states in the selectivity-determining step of the catalytic reaction.[104] The K_{rel} values (**Table 3.5**) showed that the insertion of (S)-PO is around five times more favored than (R)-PO at the beginning of the reaction. With consumption of (S)-PO, the K_{rel} values decrease correspondingly, which is a known issue.[104] Detailed $^{13}C\{^{1}H\}$

NMR spectroscopic analysis of the microstructure of the produced copolymers allowed to distinguish between the two operating mechanisms of copolymerization.

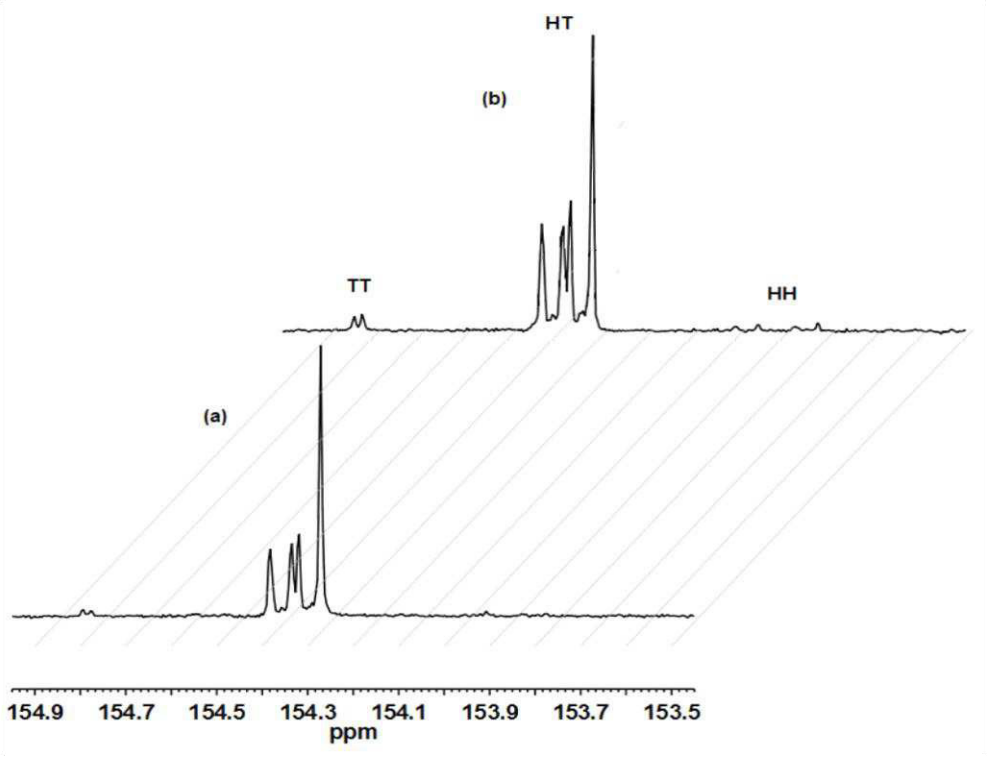

Figure 3.37: $^{13}C\{^{1}H\}$ NMR spectra (125 MHz, $CDCl_3$) of carbon carbonate region for iso-enriched PPC synthesized using **16b**, with 1 equivalent [PPN]Cl and 1000 equivalents PO at 30 °C and 30 bar CO_2 (a) for 30 min. and (b) for 4h.

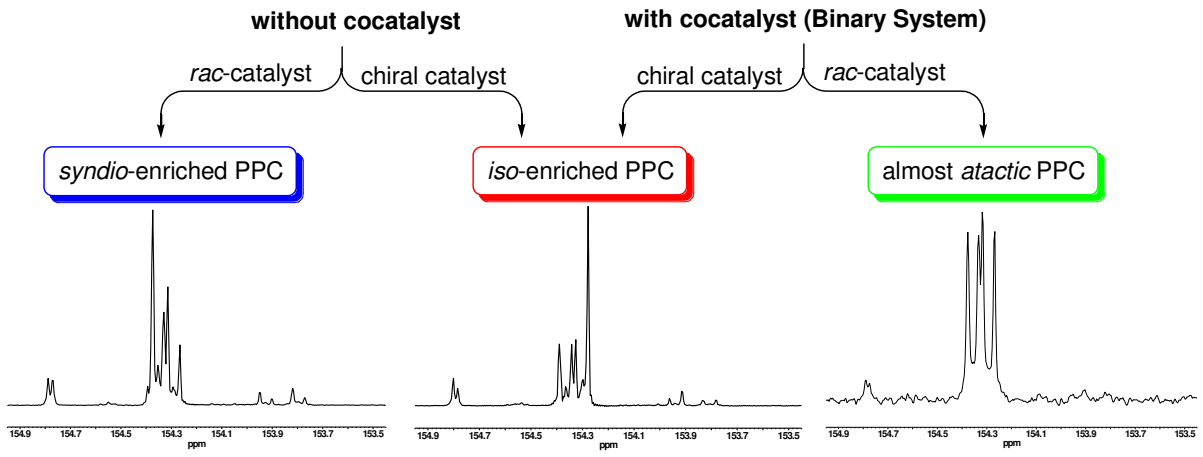

Scheme 3.8: Effect of the catalyst chirality and the catalyst system on the PPC microstructure

As shown in **Scheme 3.8**, the copolymerization mechanism with respect to the PPC microstructure can be proposed based on the two following facts:

a) Copolymerization reaction of rac-PO and CO_2 using the enantiomeric pure chiral-catalyst in presence or absence of [PPN]Cl as cocatalyst gives iso-enriched copolymer.
b) Copolymerization reaction of rac-PO and CO_2 using an equimolar mixture of (R,R)- and (S,S)-configuration catalysts leads to an almost atactic copolymer in the presence of [PPN]Cl as cocatalyst, whereas a syndio-enriched copolymer is formed in the absence of a cocatalyst

These above observations strongly support a dynamic nature of copolymerization, namely that the growing polymer chain can easily dissociate from one metal center and coordinate to the other active site, especially in the presence of a cocatalyst due to the formation of an anionic hexacoordinated species. This is closely associated with the so-called binary mechanism, according to which PO is activated by coordination to a metal center, followed by an attack of a non-coordinated nucleophilic polymer chain end. In this case, there is no or little chain end control of the microstructure, since the chiral center of the chain is distanced from the nucleophilic center of the chain (O atom of the carbonate group). Respectively, the ring-opening of coordinated (R)-PO at a (S,S)-catalyst or of (S)-PO at (R,R)-configuration by the non-coordinated chain end would proceed at an equal rate, leading to an almost atactic polymer (**Scheme 3.9**).

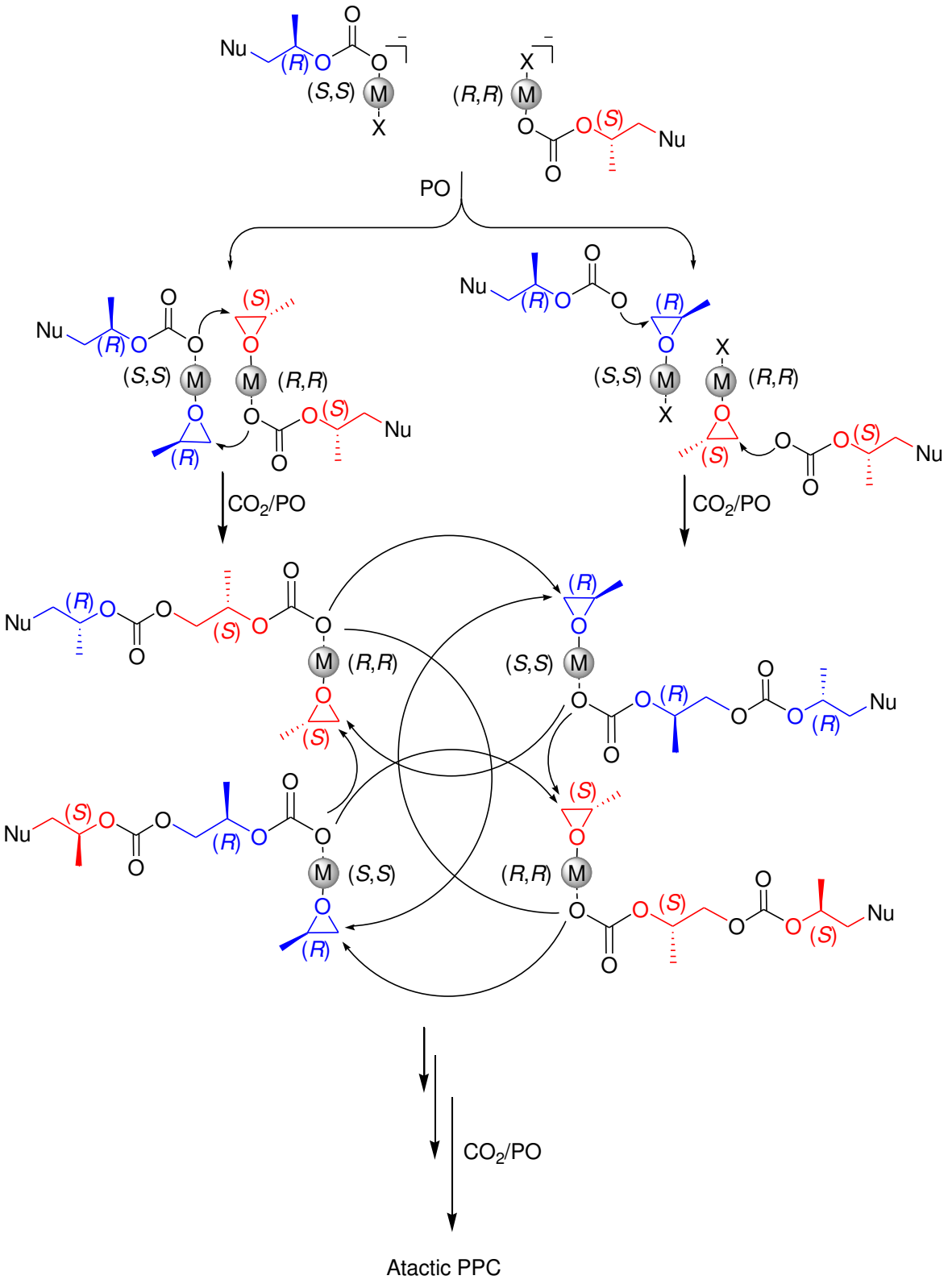

Scheme 3.9: Proposed mechanism leading to an almost atactic PPC.

However, in the absence of a cocatalyst, the dissociation of the polymer chain end from the metal center is slowed (anionic complexes are practically absent in the reaction media) and

copolymerization occurs via a bimetallic mechanism, according to which the carbonate chain end coordinated at one metal center attacks an activated PO at another metal site. This reaction pathway is generally slower than the binary propagation, but provides a good explanation for the formation of a syndio-enriched polymer (**Scheme 3.10**).

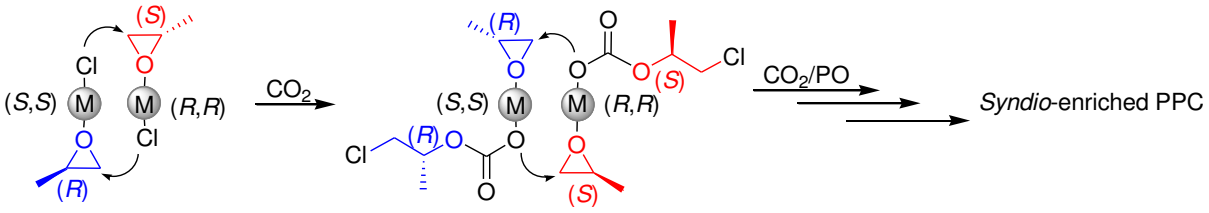

Scheme 3.10: Proposed copolymerization mechanism affording syndio-enriched PPC.

Moreover, the syndiotacticity of the obtained copolymer indicates that the copolymerization reaction preferably occurs via interaction of two catalyst molecules with opposite stereoconfigurations (i.e. (S,S)- and (R,R)-configuration). Independently, both bimetallic and binary mechanisms would lead to iso-enriched polymers if only one stereoisomer of the catalyst ((R,R) or (S,S)) is employed in the copolymerization of rac-PO and CO_2, that is largely due to the stereoselectivity in PO coordination. These conclusions are consistent with various previous reports on the copolymerization mechanism of PO and CO_2, which were based on studies of the reaction kinetics and other investigations.[78,105] From the above, the enantio- and stereoselectivity mechanism of the catalyst can be proposed as shown in **Scheme 3.11**. Since the (R,R)-configuration catalyst prefers (S)-PO insertion, it is clear that an isotactic copolymer forms at the beginning of the reaction. Any (R)-PO misinsertion leads to the methylene center ring-opening to form **HT** regiostructure with syndiotactic stereostructure which is corrected by (S)-PO insertion, which then produces an iso-enriched copolymer. At long reaction times with consumption of (S)-PO and increase of (R)-PO in the reaction feed, the misinsertion increases and the polymer growth becomes slower. At high PO conversion, a

methine-oxygen ring opining takes place, which then increases the **HH** and **TT** ratio in the copolymer which leads to produce stereogradient copolymer.

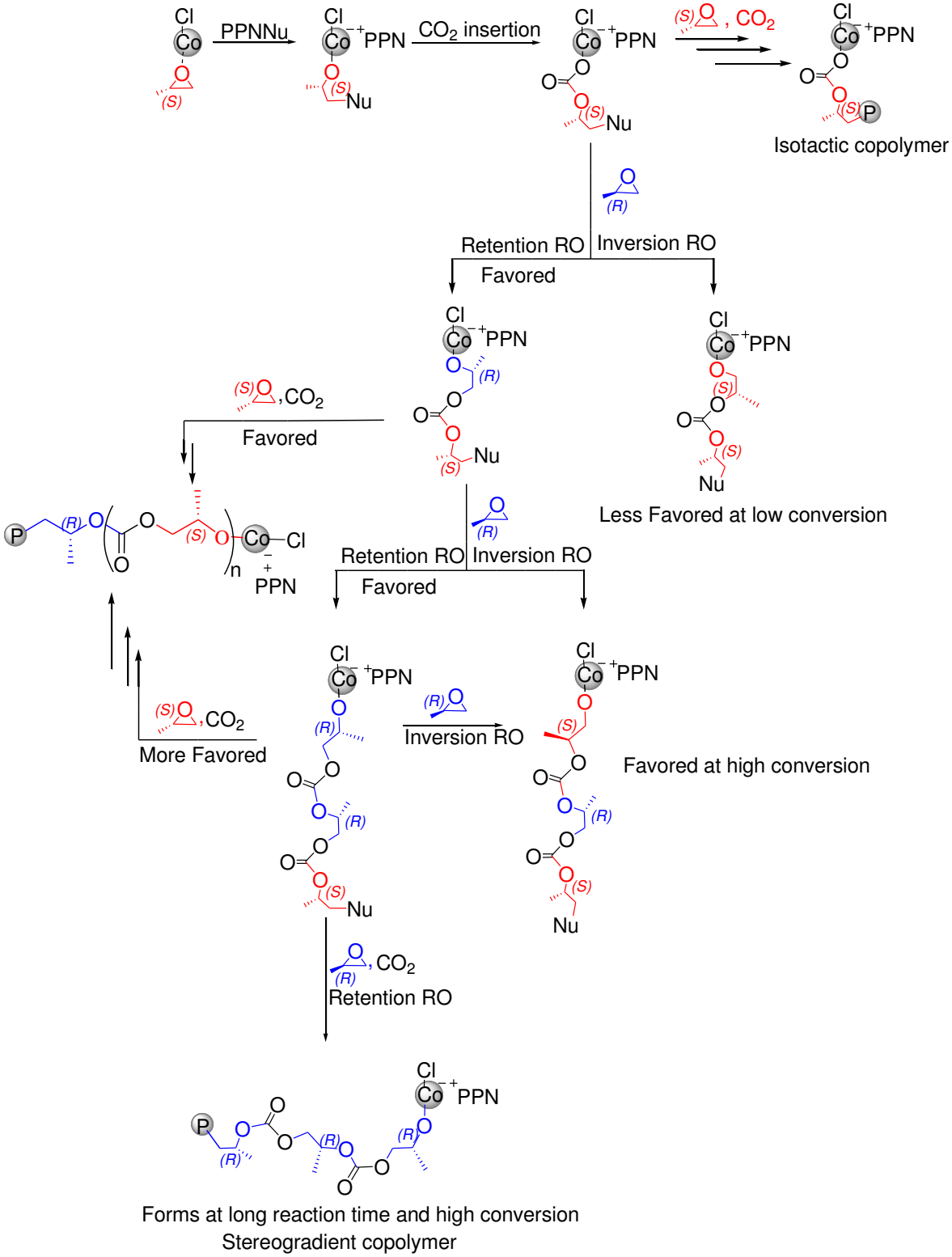

Scheme 3.12: Proposed stereo- and enantioselective ring opening using (R,R)-chiral salen cobalt complexes.

3.4.3 Catalyst Activity and Its Proposed Reduction Mechanism

The catalytic activity of the cobalt catalytic system has been studied with and without the presence of the cocatalyst. However, PPC showed an increase of the M_n as a function of time in the presence of [PPN]Cl (**Figure 3.38**).

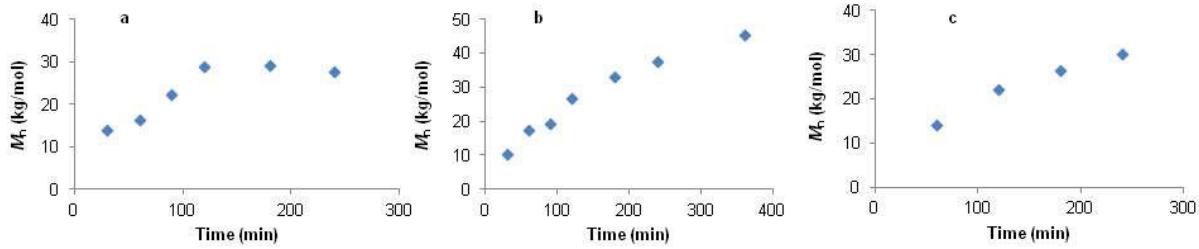

Figure 3.38: increase of the M_n of PPC as a function of time using cobalt catalyst **16b** and 1000 equivalent PO using, a)1 equivalent, b) 0.5 equivalent, c) 0,25 equivalent [PPN]Cl as cocatalyst with respect to the catalyst at 30 °C and 30 bar CO_2.

On the other hand, the catalyst did not show any catalytic activity after 2 h when the copolymerization reaction has been performed in absence of a cocatalyst using rac-catalyst as an example (**Table 3.11**).

Table 3.11: Copolymerization of CO_2/rac-PO using **27** without cocatalyst and 1000 equivalent PO.

entry	Temp. (°C)	Pressure (bar)	Time (h)	Conv (%)[a]	selectivity (% PPC)[a]	Carbonate linkages (%)[a]	M_n (kg/mol)[b]	PDI (M_w/M_n)[b]
1	30	50	2	26	95	≥ 98	17.7	1.3
2	30	50	4	24	96	≥ 98	21.4	1.4

[a]Determined by ^{1}H NMR spectroscopy.
[b]Determined by GPC in THF, calibrated with polystyrene standard.

However, in both catalytic systems red precipitates were observed and isolated, which were then characterized as the reduction of (R,R)-SalenCo$^{(III)}$Cl (**16b**) to (R,R)-LCo$^{(II)}$.[54] Suitable X-ray crystals have been grown from slow evaporation of CH_2Cl_2 solution and a crystal size of

0.15 x 0.25 x 0.69 mm^3 was used for measurement. Crystal data and detailed structure is summarized in **Table 3.12**. The space lattice and lattice parameters are the same as the previously reported X-ray single crystal data of the "mirror stereochemistry" of (S,S)-$LCo^{(II)}$ complex,[106] which is synthesized from direct complexation of the corresponding ligand with cobalt metal center. The perspective view of the red precipitate confirmed our expectation as shown in **Figure 3.39**; selected bond distances and angles are summarized in **Table 3.13**. However, reduction of $Co^{(III)}$ to $Co^{(II)}$ during the copolymerization reaction is slowed by addition of [PPN]Cl as cocatalyst. The ^1H NMR spectrum of the recovered reduced $Co^{(II)}$ did not show any indication to existence of Hydride co-ligand to the metal center in the high filed region which clearly excludes the β-H elimination mechanism during the copolymerization reaction. Accordingly, the reduction process of $Co^{(III)}$ to $Co^{(II)}$ during the copolymerization reaction is not yet clear.

Table 3.12: Crystallographic data for (R,R)-$LCo^{(II)}$

Empirical formula	$2(C_{36}H_5CoN_2O_2).CH_2Cl_2$
Formula weight	1292.38
Temp/K	123
Crystal system	Orthorhombic
Space group	$P2_12_12_1$
a/Å	9.9278(2)
b/Å	26.4156(6)
c/Å	26.9990(7)
V/ $Å^3$	7080.5(3)
Z	4
D_{calc}/g cm^{-3}	1.212
Absorption coefficient/mm^{-1}	0.593
F(000)	2768
R_{int}	0.033
R_1	0.0229
wR_2	0.0618

$^aR_1 = \sum|F_o| - |Fc|/ \sum|F_o|$. $^bwR_2 = \{[\sum w(F_o^2 - F_c^2)^2]/[\sum w(F_{o2})^2]\}^{1/2}$, $w = 1/[\sigma^2(F_o^2) + (aP)^2 + bP$, where $P = [\max(F_o^2),0) + 2(F_c^2)]/3$.

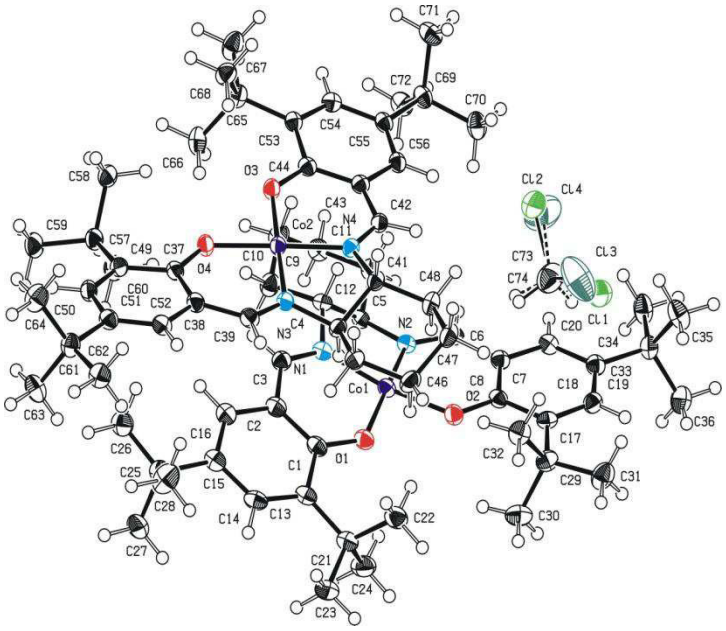

Figure 3.39: Molecular structure of (R,R)-LCo$^{(II)}$. Ellipsoids are shown at 50% probability level.

Table 3.13: Selected bond distances and bond angles of (R,R)-LCo$^{(II)}$

Bond distances (Å)		Bond Angles (°)	
Co1—O1	1.8494(11)	O1—Co1—O2	87.53(5)
Co1—O2	1.8510(11)	O3—Co2—O4	87.55(5)
Co2—O3	1.8560(11)	O1—Co1—N1	94.17(5)
Co2—O4	1.8536(11)	O3—Co2—N4	93.38(5)
Co1—N1	1.8653(13)	O1—Co1—N2	171.49(5)
Co1—N2	1.8626(13)	O3—Co2—N3	178.64(6)
Co2—N3	1.8646(14)	O2—Co1—N2	93.67(5)
Co2—N4	1.8681(14)	O4—Co2—N3	93.21(5)
		O2—Co1—N1	170.05(6)
		O4—Co2—N4	178.67(5)
		N1—Co1—N2	86.10(6)
		N3—Co2—N4	85.89(6)

The X-ray single crystal structure of the selected crystal (**Figure 3.39)** shows two adjacent molecules. The selected bond distances and bond angles around the metal center (**Table 3.13**) show that both molecules are distorted planar with significant differences in their bond angles for the oxygen and nitrogen atoms which are Trans to each other. Significantly, the distortion of the trans atoms around the Co1 metal center are more pronounced than the trans atoms around Co2. The bond distances and angles show a slight difference from those found in (S,S)-LCo$^{(II)}$, especially the bond angles between the trans atoms around Co2.[106] However, to

understand the reduction mechanism of $Co^{(III)}$ to $Co^{(II)}$, reaction of the catalyst with the copolymerization reaction reactants separately was studied. Upon adding excess amount of PO to the catalyst solution in $CDCl_3$, the solution color turned immediately from dark green to red which is an indication for reduction of $Co^{(III)}$ to $CO^{(II)}$. Despite the fact that the reaction of PO and the catalyst **16b** occurs in stoichiometric amount, many publications reported a catalytic rearrangement of epoxides.[107-113] Accordingly, reactions of PO with the catalyst in different molar ratios in $CDCl_3$ solution or at different reaction temperatures and different reactions´ time were studied. After allotted reaction time, the resulting products were collected under vacuum using finger trap immersed in liquid nitrogen and the crudes were studied by NMR spectrometer. All of the NMR spectra showed the same pattern regarding the major product, δ_H 4.00-3.89 (m, 1H), 3.53 (dd, J = 3.9 Hz, J = 11.1 Hz, 1H), 3.40 (dd, J = 6.9 Hz, J = 10.8 Hz, 1H), 1.22 (d, J = 6.30 Hz, 3H). However, the major product based on the NMR spectra has been identified as a result of ring-opening of epoxide resulting in either 1-methyl-2-chloro ethanol or the peroxide adduct of the latter. The existence of peroxide in the reaction solution has been tested with simple starch iodide paper, which showed a color change to bright blue indicating formation of peroxides in the reaction mixture. Formation of peroxide in the reaction as well as reduction of the catalyst can be explained by free radical formation due to M-O bond which forms after ring-opening of epoxide. However, novel materials can be synthesized by radical mediated cobalt complexes.[114-119]

3.5 Physical Properties of the obtained PPC

3.5.1 Thermal Properties of the PPC copolymers

DSC and TGA analyses have been applied for all the copolymers listed in **Table 3.2** and **Table 3.5**, which have been compared to the enantiomeric pure (R)-PPC (**Figure 3.40** and **Figure 3.41**).

Table 3.14: DSC and TGA measurements for the different copolymers obtained in Table 4.

entry	T_g	T_{d5}[a]	T_{d50}[a]	T_{d95}[a]
1	37	229.7	253.3	295.9
2	38	225.6	243.2	278.2
3	38	222.5	243.1	272.0
4	39	223.1	247.2	277.2
5	38	203.2	224.4	258.0
6	38	219.8	239.1	276.2
7	35	240.1	253.9	287.8
8	37	229.9	247.2	278.4
9	38	225.8	243.2	267.0
10	37	233.3	252.0	280.1
11	39	220.3	233.3	264.4
12	38	221.2	230.6	256.6
13	40	202.1	229.4	268.9
14	34	215.1	231.7	263.3
15	39	227.1	244.4	275.4
16	39	217.4	239.9	274.4
17	40	212.4	235.1	267.3
18[b]	39	240.6	255.8	288.4

[a] T_{d5}, T_{d50} and T_{d95} are the decomposition temperature at 5%, 50% and 95% weight loss, respectively. For the synthetic conditions, see the corresponding entry in **Table 3.2** and **Table 3.5**). [b](R)-PPC (**Table 3.3, entry 2**).

Table 3.14 clearly shows that there is no correlation between the microstructure, M_n and the physical properties of the iso-enriched stereogradient copolymers which are produced. DSC measurements in the range of -50 to 150 °C showed only glass transition temperature (T_g) without any indication of crystallization. Even a highly stereo- and regioregular PPC (**Table 3.14**, **entry 18**) obtained in our work could not be crystallized.[120]

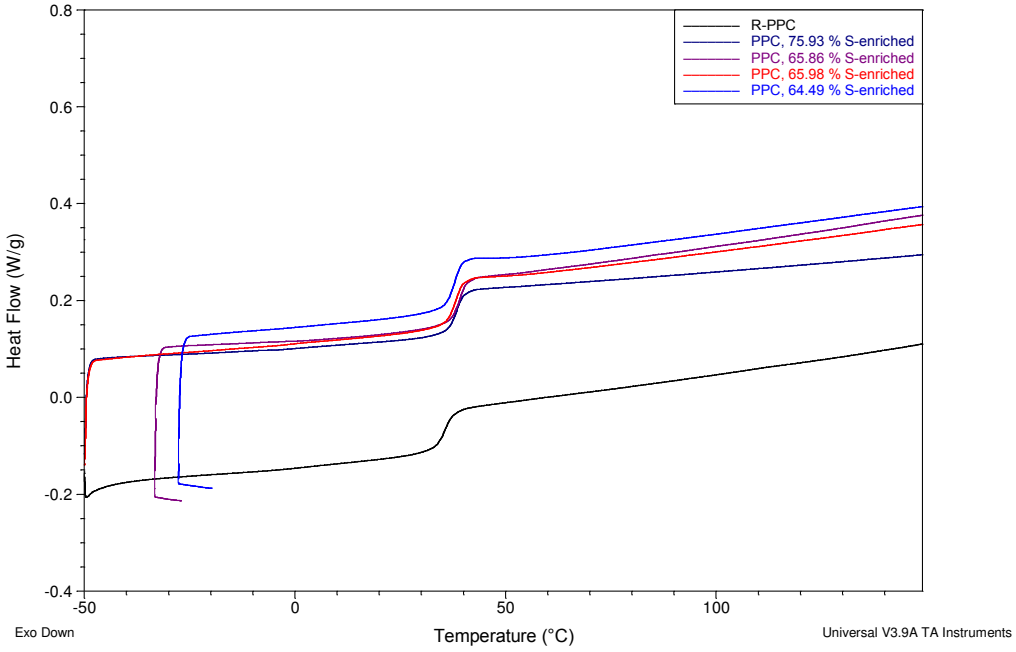

Figure 3.40: DSC thermograms for entantiomeric pure PPC and different (S)-enriched PPC.

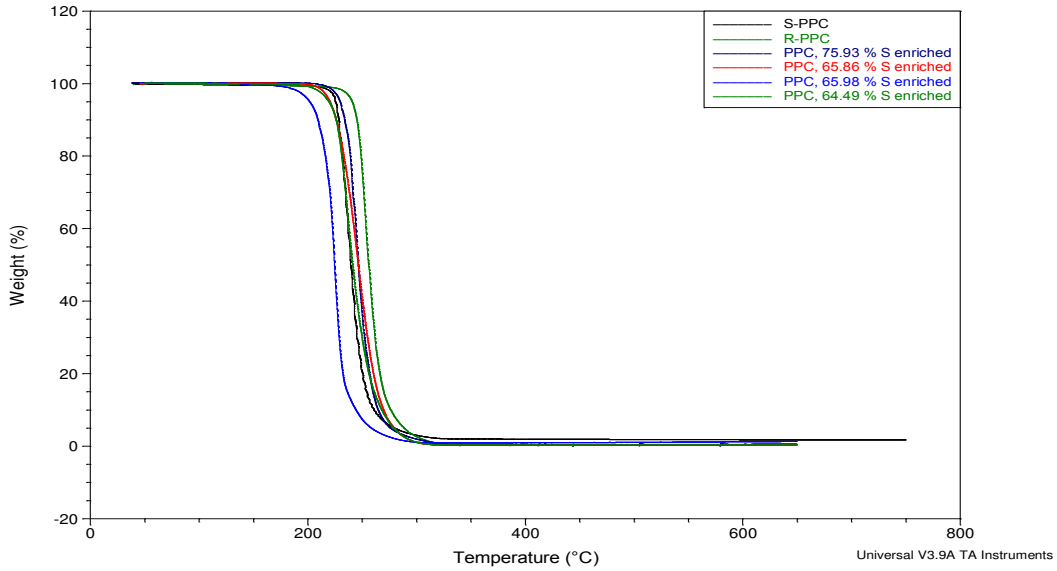

Figure 3.41: TGA thermograms for entantiomeric pure PPC and different (S)-enriched PPC.

The thermal degradation pathway, has been reported to occur by either main chain random scission or unzipping (back biting) degradation.[121-123] Herein, the decomposition pathway and

the decomposition products have been followed by TGA and TGA/Ms. A representative copolymer was divided into three samples and heated under N_2 to 150 °C, 200 °C and 240 °C. Upon cooling, the solidified residues were obtained for GPC measurement. Consequently, M_n was found to be 22.8 kg/mol (1% weight loss), 22.3 kg/mol (2% weight loss) and 12.3 kg/mol (30 % weight loss), respectively. On the other hand, the TGA/Ms measurements showed that the mass spectrum of the copolymer degradation is identical to the mass spectrum of the cPC degradation (**Figure 3.42**).

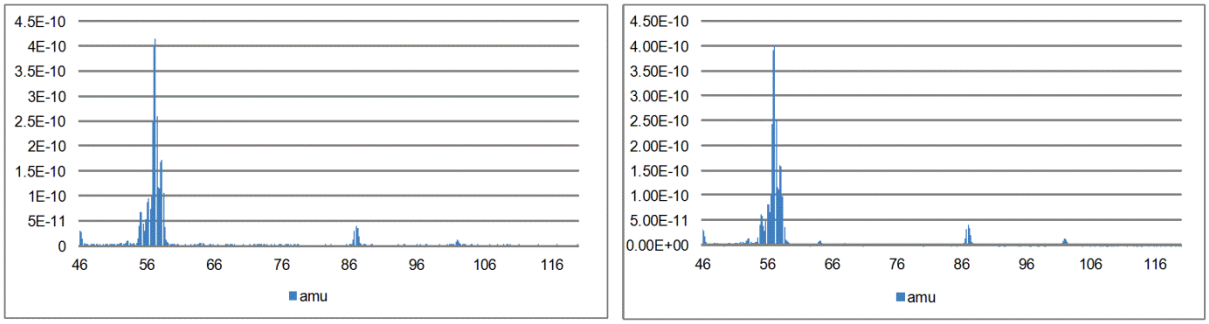

Figure 3.42: The Mass spectra, obtained from thermal degradation of PPC copolymer (Left), and cPC (Right).

Consequently, it was proposed that the thermal degradation of the obtained copolymers occur mainly through unzipping (back biting) degradation mechanism rather than the main chain random scission. However, the TGA thermograms did not correlate with the copolymers microstructure, since many parameters have been found to mainly influence the thermal stability of the PPC such as residual impurities (solvents, metal residues, acids, cPC byproduct), polyether inclusion, end groups, additives, molecular weight and purity of the PPC.[124-133]

3.5.2 PPC Morphology

The polymer morphology refers with the arrangement of the polymer chains in solid state. Arrangements and associations of a polymer's chains involve different morphologies such as crystalline or amorphous polymers.[134] Whereas the physical properties of a polymer are primarily dependent upon its morphology, the importance of studying the polymer morphology comes from the relationship between the polymer morphology and its physical properties, due to the dependence of polymer properties on the structure and morphology.[135,136] On the other hand, due to the utilization of crystalline or semicrystalline polymers in modern technology and sophisticated applications, a full understanding of the morphology and crystallization habits of polymers under different environments and conditions is essential.[137-140] Known commercially successful class of polymers are polycarbonates with useful properties such as heat capability, optical clarity, and toughness. Accordingly, controlling the chemical structure and morphology of polycarbonates is essential.[141] However, owing to the ease processing and the attractive properties of the semicrystalline polymers, these polymers are playing a crucial role in industry. In general, the degree of crystallinity varies from 0% for noncrystaline material such as atactic polystyrene to 70% for isotactic polypropylene.[142] Recently, Lu and co-workers have reported a crystalline poly(cyclohexene carbonate) (PCHC) from copolymerization CO_2 and cyclohexene oxide using unsymmetrical catalysts. [143,144] The crystallization behavior of PCHC is determined mainly by the relative stereochemistry of the cyclohexene units in the polymeric chains. Initially, the crystallization and melting behavior of the PCHCs were studied by means of DSC. Only a single glass transition peak was observed at around 115 °C for the atactic PCHC, demonstrating that this polymer is completely amorphous. It was found that the samples with less than 90% isotacticity did not show any crystallization. On the other hand, the obtained PCHC with RR:SS ratio 92:8 gave a T_g of 122 °C and a very small melting

endothermic peak at 207 °C with the melting enthalpy of (ΔHm) 3.92 J/g, indicating a very low degree of crystallinity. Regarding the higher isotactic PCHC (RR:SS ratio is 98:2), the T_g peak has disappeared and quite high crystallization peak was observed at 216 °C with melting enthalpy (ΔHm) 22.5 J/g. Moreover, WAXD was applied for isothermally crystallized isotactic PCHC at 180 °C. Regarding the polymer microstructure and its related physical properties, different PPC microstructures was synthesized from copolymerization of CO_2 and rac-PO as well as from CO_2 and enantiopure PO. The DSC measurements showed hat there is no correlation between the microstructure, M_n and the physical properties of the iso-enriched stereogradient copolymers which are produced as well as the enantiopure PPC (**Table 3.14, Figure 3.40**). upon above, different THF solution of (S)-PPC in different concentration were prepared and spin coated on Si wafer to study the morphology of the enantiopure PPC. These samples were annealed at different temperature ranged below and above the T_g, and then studied using AFM and HR-SEM.

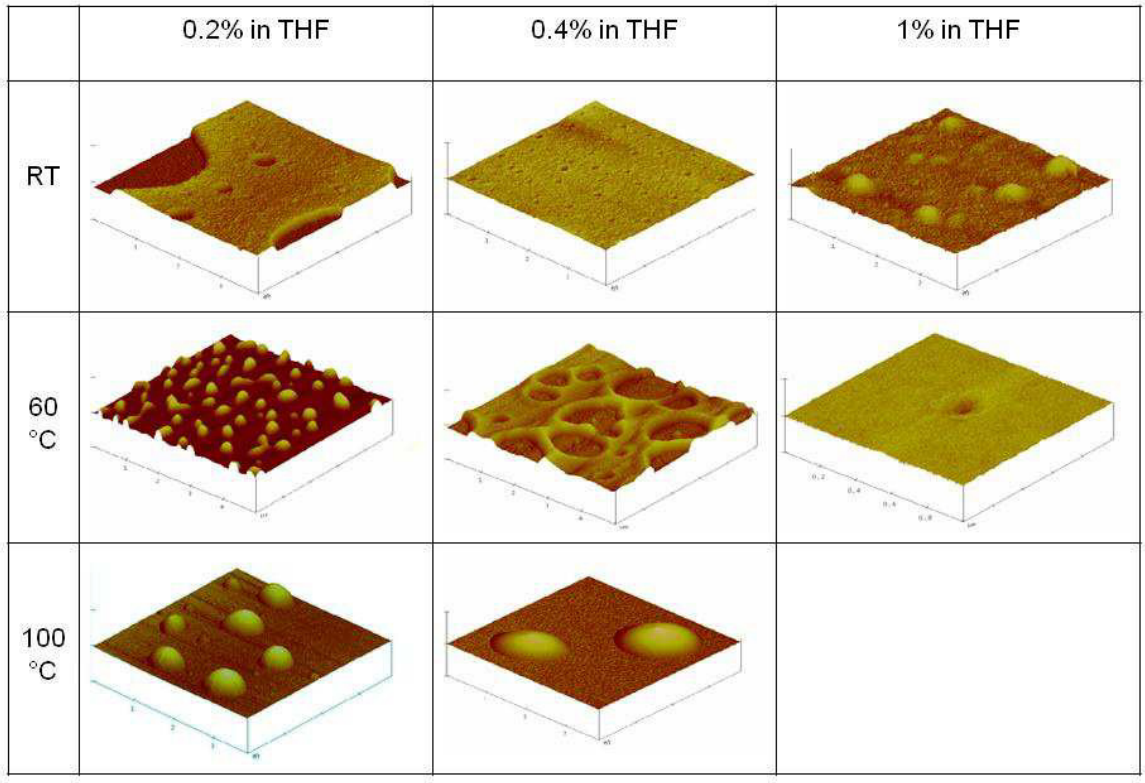

Figure 3.43: AFM of different (S)-PPC concentrations in THF on Si wafer after annealing at different Temperatures.

Figure 3.43 clearly shows that PPC polymers are amorphous even for high pure enantio- and stereostrucures polymer. Annealing of the PPC samples significantly pronounced the shrinkage behavior of this polymer rather polymer´s chain alignment.[120]

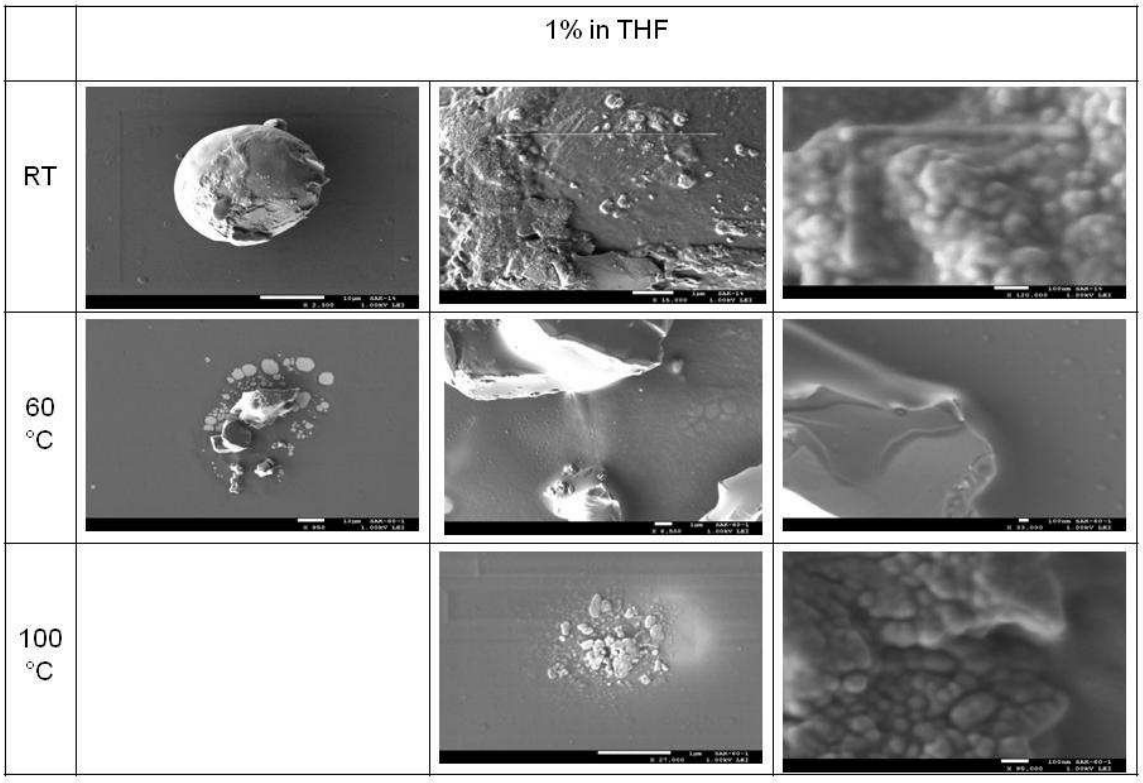

Figure 3.44: HR-SEM of 1% (S)-PPC in THF on Si wafer annealed at different temperatures.

For more understanding of the shrinkage behavior in microscale, a preventative samples were applied for SEM (**Figure 3.44**), which also confirms that PPC is amorphous polymer. However, the SEM showed empty areas on the Si wafer and a polymer clots as well. Accordingly, it is believed that the aggregate polymer is a result of shrinkage of PPC during the isothermal annealing.

4. Summary and outlook

The enantiopure 1,2-diaminocyclohexane was synthesized by resolution of the diamine using chiral tartaric acid. Accordingly, the chiral enantiopure salen ligands have been synthesized either by condensation reaction of the aldehyde with the corresponding 1,2-diaminitartrate compounds or using commercial enantiopure 1,2-diaminocyclohexane. The salen-metal complexes were then prepared under anaerobic atmosphere followed by oxidation by bubbling dry oxygen. The catalytic activity of cobalt and chromium complexes toward copolymerization of PO and CO_2 were studied. It is clearly shown that the reaction temperature, the catalyst molar ratio, CO_2 pressure and the initiator nature affect the catalytic activity. Comparing the polymer microstructures of the obtained PPC using different catalysts shows that using salen-Cr catalysts afford regioirregular PPC with respect to those obtained using salen-Co catalysts. The initiation reaction mechanism was studied using insitu-ATR IR using enantiopure cobalt catalyst **16b** or rac- catalyst **27**. The reaction mechanism was found first order with respect to the catalyst in presence of cocatalyst and second order in absence of cocatalyst. On the other hand, the propagation process was studied by analyzing different obtained PPC copolymer using a combination of GC and NMR spectroscopy. The selectivity of the chiral catalyst **16b** for (S)-PO over (R)-PO during the rac-PO/CO_2 copolymerization reaction led to the synthesis of stereogradient PPCs with different (S)-PO ratios in the copolymer chain. As incorporation of (S)-PO in the polymer chain is five times faster than (R)-PO; the copolymerization reaction becomes slower with an increase of (R)-PO concentration in the reaction feed, therefore indicating that (S)-PO insertion has a crucial influence on the microstructure. A change of cocatalyst loading did not show any effect on the PPC microstructure. Following of the (S)-PO/(R)-PO ratios in the polymer chain during the rac-PO/CO_2 copolymerization reaction using GC and 500 MHz NMR spectroscopy led to the understanding of PPC microstructure during copolymer growth and aided the assignment of

the carbonate carbon signal in the associated $^{13}C\{^{1}H\}$ NMR spectra taking into consideration the direction of the copolymer chain. However, studying the PPC microstructure using different catalytic systems led to understand the mechanism of the propagation process which proposed to be second order with respect to the catalyst. This study, raised a question about synthesize of new salen-type ligands to prepare either bimetallic metal centers or enhance the self assembly of the complexes to facilitate this propagation process as well as controlling the PPC microstructure. On the other hand, X-ray crystal structure confirmed the reduction of $Co^{(III)}$ during the copolymerization reaction to $Co^{(II)}$. Following the reduction phenomena by NMR showed formation of peroxide which is attributed to cobalt mediated radical formation as proposed in Scheme **4.1**.

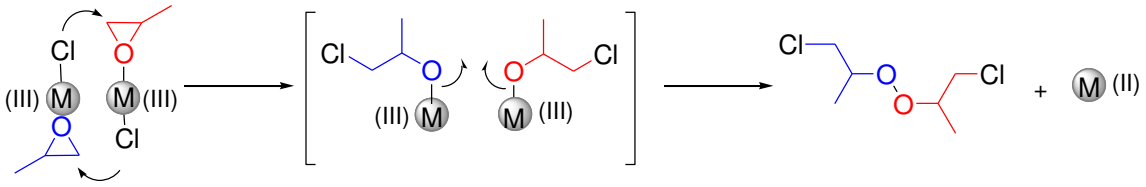

Scheme 4.1: proposed reduction mechanism of $Co^{(III)}$ to $Co^{(II)}$ during the copolymerization reaction.

However, it is recommended to make theoretical calculations to confirm the feasibility of this mechanism with respect to the copolymerization reaction. DSC measurements did not show any correlation between the glass transition temperature of the stereogradient copolymers and the microstructure, however TGA/MS measurements showed that main thermal decomposition pathway of PPC is a chain unzipping pathway, resulting in cPC. For more understanding the dynamic behavior of the polymer chain in solid state or solution, it is suggested to synthesize labeled polymers with fluorescent chromophores. The idea bases on Fluorescence Resonance Energy Transfer (FRET) between either two different mono labeled polymers or double labeled polymer with FRET-donor and FRET-acceptor and studying the polymer chain. The amount of the transferred energy, gives an indication for the interaction

amongst the polymer chains and the distance between each chain which may illustrate the physical properties of the polymer in solid state or in solution (**Chapter 8**).

5. Experimental Part

5.1 Methods and chemicals

All manipulations involving air- and/or moisture sensitive compounds were carried out using standard Schlenk/glovebox techniques under an argon atmosphere unless otherwise stated. Propylene oxide was purchased from Acros and distilled under argon atmosphere over CaH_2 prior to use. $Co(OAc)_2$ (anhydrous) was purchased from ABCR and stored in an argon-filled glove box. CO_2 of purity grade 4.5 was purchased from Westfalen AG and was applied in all experiments without additional purification. Dry solvents were obtained with an MBraun MB-SPS-800 solvent purification system. All other chemicals were purchased from Aldrich and used as received without further purification. The enantiomeric excess (ee) of cyclic propylene carbonate was determined by chiral gas chromatography (GC). Gas chromatograms were obtained on a Varian CP-3380 using a flame ionization detector, N_2 carrier gas and an Astec CHIRALDEX® A-TA capillary GC column (30 m x 0.25 mm). Reference experiments with cyclic propylene carbonate (rac-cPC) were first performed to determine retention times. ^1H and $^{13}C\{^1H\}$ NMR spectra were collected at ambient temperature using Bruker AV-III 300, AV-III 500 or AV-III 900 spectrometers. The spectra were referenced against an internal standard (TMS for ^1H NMR spectra and $CDCl_3$ for $^{13}C\{^1H\}$ NMR spectra). Number average molecular weights (M_n) and polydispersity indices (M_w/M_n) were determined against PS-standards by gel-permeation chromatography (GPC) using a Varian PL-GPC-50 Plus chromatograph equipped with Deflection RI detector. Tetrahydrofuran at 1 mL/min flow rate was used as eluent at 35 °C. Differential scanning calorimetry (DSC) measurements were performed on a TA DSC Q2000 in a temperature range from -50 to 150 °C in three cycles with a heating rate of 10 °C/min. Thermogravimetric analysis (TGA) was performed under an N_2 atmosphere on a TA TGA Q5000 in a temperature range between 40 °C and 650 °C with heating rate of 10 °C/min. Atomic force microscopy (AFM) scans were obtained with a

Nanoscope IIIa scanning probe microscope from Veeco Instruments (Mannheim, Germany). Scanning Electron Microscopy (SEM) pictures were taken with a JEOL JSM 5900 LV SEM microscope. MALDI-ToF MS measurements were performed on a Bruker Ultra flex ToF/ToF mass spectrometer. All samples were prepared in THF and dithranol doped with sodium trifluoroacetate. UV-Vis absorptions were performed using spectrophotometer 14 UV-Vis with band width 1nm. (R,R)-1,2-diammoniumcyclohexane mono-(+)-tartrate salt,[72] was synthesized according to relevant literature procedure.

5.2 Syntheses

5.2.1 Synthesis of (R,R)-*(−)-N,N′*-Bis(3,5-di-tert-butylsalicylidene)-1,2-cyclohexanediamine ((R,R)-LH_2)[72]

A three necked flask connected to a reflux condenser, and an addition funnel was charged with (R,R)-1,2-diammoniumcyclohexane mono-(+)-tartrate salt (5 g, 18.9 mmol), K_2CO_3 (5.2 g, 37.6 mmol), and distilled water (10 mL). The mixture was stirred until dissolution was achieved, and then ethanol (100 mL) was added. The resulting cloudy mixture was heated to 80 °C, and a solution of 3,5-di-tert-butyl-2-hydroxybenzaldehyd (8.9 g, 37.6 mmol) in ethanol (50 mL) was drop wise added. The funnel was then rinsed with ethanol (20 mL), and the yellow slurry was stirred at 80 °C for additional 2 h. the reaction mixture was then allowed to cool down slowly to ambient temperature. The mixture was then cooled in iced water with vigorous stirring for 2 h. The product was then collected by vacuum filtration and washed with ethanol (100 mL). The crude solid was redissolved in CH_2Cl_2 (100 mL) and washed with water (2 × 100 mL) and brine (100 mL). After drying over Na_2SO_4, the solution was filtered, and the solvent was removed under vacuum, and **(R,R)-LH_2** was isolated as a yellow powder (10.9 g, 98% yield).

mp: 207-208 °C.

^{1}H NMR (300 MHz, $CDCl_3$:) *δ 13.74 (*s, 2 H), 8.33 (s, 2 H), 7.33 (d, J = 2.5 Hz, 2 H), 7.01 (d, J = 2.5 Hz, 2 H), 3.36-3.33 (m, 2 H), 1.98-1.48 (m, 8 H), 1.44 (s, 18 H), 1.26 (s, 18H).

$^{13}C\{^{1}H\}$ NMR (75 MHz, $CDCl_3$): δ_C 165.94, 158.13, 139.99, 136.45, 126.86, 126.17, 117.97, 72.56, 35.09, 34.17, 33.42, 31.57, 29.58, 24.5.

EA for $C_{36}H_{54}N_2O_2$; Calculated: C, 79.07; H, 9.95; N, 5.12, Found: C, 79.32; H, 9.43; N, 5.10.

5.2.2 Synthesis of (S,S)-(+)-*N,N′*-Bis(3,5-di-tert-butylsalicylidene)-1,2-cyclohexanediamine ((S,S)-LH_2)

A two necked Schlenk flask connected to a reflux condenser, and an addition funnel was charged with 3,5-di-tert-butyl-2-hydroxybenzaldehyd (4 g, 17 mmol) in ethanol (100 mL). A solution of (S,S)-1,2-diaminocyclohexane (0.97 g, 8.5 mmol) in dry ethanol (40 mL) was drop wise added. The funnel was then rinsed with ethanol (20 mL), and the yellow slurry was stirred at 80 °C for additional 2 h. the reaction mixture was then allowed to cool down slowly to ambient temperature. The mixture was then cooled in iced water with vigorous stirring for 2 h. The product was then collected by vacuum filtration and washed with ethanol (100 mL), until the filtrate became clear. **(S,S)-LH_2** was then isolated as a yellow powder (4.1 g, 88% yield). The analyses are identical to which resulted from **(R,R)-LH_2**.

5.2.3 Representative Synthesis of (R,R)-$LCo^{(II)}$ and (S,S)-$LCo^{(II)}$

A two necked Schlenk flask connected to a reflux condenser was charged with the corresponding dry ligand (1.29 g, 2.4 mmol) in dry toluene (10 mL). A solution of $Co(OAc)_2$ (0.41 g, 2.4 mmol) in dry methanol (20 mL) was then transferred via a cannula under argon to the Schlenk flask, affording red precipitate. The mixture was then refluxed with stirring at 90 °C for 1h. After the reaction mixture was cooled down to 40 °C, the red precipitate was then filtered and washed with MeOH until the filtrate becomes clear. The product was dried at

40 °C under vacuum to constant weight. The product was collected as red powder (1.2 g, 83%).

EA for $C_{36}H_{52}CoN_2O_2$, Calculated: C, 71.62; H, 8.68; N, 4.64. Found: C, 71.68; H, 8.42; N, 4.53.

5.2.4 Representative Synthesis of (R,R)-LCo$^{(III)}$OTs (17a) and (S,S)-LCo$^{(III)}$OTs (17a`)

This product was synthesized as previously published with slight modification.[47,101] A round bottom flask was charged with a mixture of the corresponding $Co^{(II)}$ complex (6.0 g, 9.9 mmol) and p-toluenesulfonic acid monohydrate (1.89 g, 9.9 mmol). CH_2Cl_2 (200 ml) was added and the solution was stirred under dry oxygen atmosphere at room temperature for 3 h. The solvents were removed by rotary evaporation and the solid was further dried in vacuum. The resulting solid was suspended in hexane and collected by filtration. The collected product was then washed with a mixture of CH_2Cl_2/Hexane (25:75) and then dried at 40 °C under vacuum to constant weight to afford dark green product (6.6 g, 86%).

^{1}H NMR (DMSO-d6, 500 MHz): δ 7.82 (s, 2H), 7.46-7.41 (m, 6H), 7.07 (d, J=7.5Hz, 2H), 3.57-3.56 (m, 2H), 3.05-3.03 (m, 2H), 2.24 (s, 3H), 1.97-1.96 (m, 2H), 1.88-1.84 (m, 2H), 1.71 (s, 18H), 1.57-1.53 (m, 2H), 1.27 (s, 18H).

^{13}C{^{1}H} NMR (DMSO-d6, 125 MHz): δ_C 163.79, 161.21, 140.87, 136.63, 134.93, 128.43, 127.90, 127.18, 124.67, 117.64, 68.38, 34.93, 32.69, 30.64, 29.54, 28.65, 23.41, 19.95.

EA for $C_{43}H_{59}CoN_2O_5S$, Calculated: C, 66.65; H, 7.67; N, 3.61; S, 4.14. Found: C, 64.45; H, 7.57; N, 3.39; S, 4.81.

5.2.5 Representative Synthesis of (R,R)-LCo$^{(III)}$Cl (16b) and (S,S)-LCo$^{(III)}$Cl (16b`)

This product was synthesized following previously published literatures with slight modification.[47,101] The corresponding LCo$^{(III)}$OTs (5.68 g, 7.33 mmol) was dissolved in

CH_2Cl_2 (200 mL) and then transferred into a 500 mL separatory funnel. The organic layer was rinsed with saturated brine solution (3 × 400 mL). The organic layers were collected and dried over Na_2SO_4 and concentrated under reduced pressure. Upon adding hexane with vigorous stirring, the precipitate was formed. The resulting precipitate was further suspended in hexane and filtered. The collected solid was then dried at 40 °C under vacuum to constant weight to afford very dark green product (3.98 g, 85%).

1H NMR (DMSO-d6, 300 MHz): δ 7.83 (s, 2H), 7.44 (s, 2H), 7.32 (s, 2H), 3.84-3.63 (m, 2H), 3.09-3.06 (m, 2H), 2.02-1.97 (m, 2H), 1.97-1.83 (m, 2H), 1.72 (s, 18H), 1.63-1.52 (m, 2H), 1.31 (s, 18H).

EA for $C_{36}H_{52}ClCoN_2O_2$, Calculated: C, 67.65; H, 8.20; N, 4.38. Found: C, 67.25; H, 8.26; N, 4.28.

5.2.6 Representative Synthesis of (R,R)-LCr$^{(III)}$Cl (19a`) and (S,S)-LCr$^{(III)}$Cl (19a)

This product was synthesized following previously published literatures with slight modification.[43] A Schlenk flask was charged with the corresponding dry ligand (10.59 g, 19.37 mmol) and anhydrous $CrCl_2$ (2.38 g, 19.37 mmol) in glove box. The Schlenk flask was then taken out the glove box and dry, degassed THF (200 mL) was then added under argon. The resulting dark brown solution was stirred at ambient temperature for 3h and then dry O_2 was bubbled into solution for 2h. t-butyl methyl ether (1000 mL) was then added to the reaction solution and washed with saturated NH_4Cl solution (3 × 600 mL) and brine (3 × 600 mL). The organic phase was dried over N_2SO_4 and volatiles were removed under reduced pressure. The resulting product was then recrystalized from acetonitrile. The collected solid was then dried at 40 °C under vacuum to constant weight to afford orange-brown product (7.3 g, 60%).

EA for $C_{36}H_{52}ClCrN_2O_2.H_2O.THF.CH_3CN$, Calculated: C, 67.07; H, 8.62; N, 5.26. Found: C, 67.40; H, 8.52; N, 5.01.

5.2.7 Representative procedure for CO_2/PO copolymerization reaction

All polymerization experiments were performed in 100 mL steel autoclaves equipped with a magnetic stirring bar. The autoclave was prepared by heating at 130 °C overnight and cooling under vacuum to ambient temperature. The autoclave was charged with a mixture of the catalyst and cocatalyst in appropriate amount under an argon atmosphere. Dry PO (5 mL, 71.5 mmol) was then transferred by syringe under a flow of argon. The mixture solution was stirred about 10 minutes and then was put into a pre-heated oil bath to appropriate temperature and pressurized to appropriate pressure with CO_2. After the allotted reaction time, the autoclave was cooled to 0 °C and the pressure slowly released. An aliquot of the crude copolymer was taken for NMR spectroscopic analysis. The crude polymer was then dissolved in a minimal volume of dichloromethane and precipitated with methanolic HCl solution (2.2 M, 100 mL). This process was repeated three times to completely remove the catalyst and the obtained colorless polymer was dried at 60 °C under vacuum to constant weight.

5.2.8 Representative CO_2/PO copolymerization for enantioselectivity analysis

All polymerization experiments were performed in 100 mL steel autoclaves equipped with a magnetic stirring bar. The autoclave was prepared by heating at 130 °C overnight and cooling under vacuum to ambient temperature. The catalyst **16b** (45.7 mg, 71.5 × 10^{-6} mol), bis(triphenylphosphine)iminium chloride ([PPN]Cl) (1.0, 0.5, or 0.25 molar ratio with respect to the catalyst) and propylene oxide (5.0 mL, 71.5 mmol, 1000 equivalents with respect to catalyst) were transferred to the autoclave under argon atmosphere. The autoclave was closed and then heated to 30 C in an oil bath with stirring, followed by pressurization to 30 bar with

CO_2. After the allotted reaction time, the autoclave was cooled to 0 °C and the pressure slowly released. An aliquot of the crude copolymer was taken for NMR spectroscopic analysis. The crude polymer was then dissolved in a minimal volume of dichloromethane and precipitated with methanolic HCl solution (2.2 M, 100 mL). This process was repeated three times to completely remove the catalyst and the obtained colorless polymer was dried at 60 °C under vacuum to constant weight. The isolated PPC was weighed to calculate the yield and analyzed by ^{1}H and $^{13}C\{^{1}H\}$ NMR spectroscopy.

5.2.9 Degradation of PPC for GC analysis

Degradation of the PPC was performed as previously published with a slight modification.[67] A Schlenk flask was charged with PPC (0.5 g) and purged with argon. Dry THF (25 mL) was then added, followed by LiOtBu solution in THF (0.3 mL, 2.2 M, 0.66 mmol) and dry tert-butanol (1.0 mL) under argon atmosphere. The reaction mixture was allowed to stir at 40 °C in a closed system. An NMR sample was then taken after 24 h to ensure the complete degradation of the polymer to cyclic propylene carbonate (cPC). All volatiles were then removed under reduced pressure and the residue dissolved in anhydrous chloroform (10 mL). For GC analysis 1 mL of this solution was diluted in chloroform (10 mL) and filtered using 0.20 μm syringe filter prior to injection.

^{1}H NMR of cPC ($CDCl_3$, 300 MHz): *δ 1.50 (d, 3H, CH_3)*, 4.03 (t, 1H, CH_2), 4.56 (t, 1H, CH_2), 4.86 (m, 1H, CH).

6. Acknowledgment

This dissertation is carried out from June 2009 until December 2012 in department of macromolecular chemistry of the Technical University of Munich (TUM), Germany.

First of foremost I would like to thank God who has been my source of strength and to whom I owe all that I have been able to do and accomplish. My deepest appreciation and utmost gratitude goes to my supervisor Prof. Dr. Dr. hc. Bernhard Rieger for his invaluable support, his great ideas, his motivating support and patient guidance during the course of this dissertation.

I would like to express my greatest gratitude to all those who have helped and supported me throughout my research work.

My greatest thanks to my mother, my wife and brothers and sisters for their appreciated support and interest who inspired me and encouraged me to go my own way, without whom I would be unable to complete my project.

I gratefully thank Dr. Carsten Troll for his technical help and support, which helped me to overcome all the technical difficulties. I would like also to thank Dr. Sergei Vagin and Dr. Carly Anderson for their supports, fruitful discussions and good ideas.

I am grateful to Prof. Bassam Eleswed (Albalqa applied University, Jordan) for the fruitful collaboration and the statistical measurements in this work. I also owe my deepest gratitude to Ursula Zinth who undertook to help me measuring the Fluorescence Resonance Energy Transfer (FRET) measurements in department of biophysical chemistry.

I would like to thank all of my colleagues at the Technical University of Munich, specifically my current and former lab mates for their friendship and the friendly atmosphere of working, who motivated me during my work.

7. References

(1) Ipcc Special Report on Renewable Energy Sources and Climate Change Mitigation; Cambridge University Press: United Kingdom and New York, NY, USA, **2011**.

(2) Davis, S. J.; Caldeira, K.; Matthews, H. D. Science **2010**, 329, 1330-1333.

(3) Ha-Duong, M.; Grubb, M. J.; Hourcade, J. C. Nature **1997**, 390, 270-273.

(4) Hoffert, M. I.; Caldeira, K.; Jain, A. K.; Haites, E. F.; Harvey, L. D. D.; Potter, S. D.; Schlesinger, M. E.; Schneider, S. H.; Watts, R. G.; Wigley, T. M. L.; Wuebbles, D. J. Nature **1998**, 395, 881-884.

(5) Kerr, R. A. Science **2011**, 331, 1510-1511.

(6) Kerr, R. A. Science **2008**, 322, 1178-1179.

(7) Cokoja, M.; Bruckmeier, C.; Rieger, B.; Herrmann, W. A.; Kuehn, F. E. Angew. Chem., Int. Ed. **2011**, 50, 8510-8537.

(8) Sakakura, T.; Choi, J.-C.; Yasuda, H. Chem. Rev. **2007**, 107, 2365-2387.

(9) Huang, K.; Sun, C.-L.; Shi, Z.-J. Chem. Soc. Rev. **2011**, 40, 2435-2452.

(10) Carbon Dioxide as Chemical Feedstock; Aresta, M., Ed.; Wiley-VCH: Weinheim, 2010.

(11) Luinstra, G. A. Polym. Rev. **2008**, 48, 192-219.

(12) Inoue, S.; Koinuma, H.; Tsuruta, T. Makromol. Chem. **1969**, 130, 210-20.

(13) Inoue, S.; Koinuma, H.; Tsuruta, T. J. Polym. Sci., Part B **1969**, 7, 287-92.

(14) Kember, M. R.; Buchard, A.; Williams, C. K. Chem. Commun. **2011**, 47, 141-163.

(15) Kobayashi, M.; Inoue, S.; Tsuruta, T. Macromolecules **1971**, 4, 658-9.

(16) Kobayashi, M.; Tang, Y.-L.; Tsuruta, T.; Inoue, S. Makromol. Chem. **1973**, 169, 69-81.

(17) Kuran, W.; Pasynkiewicz, S.; Skupinska, J.; Rokicki, A. Makromol. Chem. **1976**, 177, 11-20.

(18) Kuran, W.; Pasynkiewicz, S.; Skupinska, J. Makromol. Chem. **1977**, 178, 47-54.

(19) Kuran, W.; Pasynkiewicz, S.; Skupinska, J. Makromol. Chem. **1976**, 177, 1283-92.

(20) Kobayashi, M.; Inoue, S.; Tsuruta, T. J. Polym. Sci.: Polym. Chem. Ed.**1973**, 11, 2383-2385.

(21) Darensbourg, D. J.; Zimmer, M. S. Macromolecules **1999**, 32, 2137-2140.

(22) Eberhardt, R.; Allmendinger, M.; Zintl, M.; Troll, C.; Luinstra, G. A.; Rieger, B. Macromol. Chem. Phys. **2004**, 205, 42-47.

(23) Ree, M.; Bae, J. Y.; Jung, J. H.; Shin, T. J. J. Polym. Sci., Part A Polym. Chem. **1999**, 37, 1863-1876.

(24) Klaus, S.; Lehenmeier, M. W.; Herdtweck, E.; Deglmann, P.; Ott, A. K.; Rieger, B. J. Am. Chem. Soc. **2011**, 133, 13151-13161.

(25) Darensbourg, D. J.; Holtcamp, M. W.; Struck, G. E.; Zimmer, M. S.; Niezgoda, S. A.; Rainey, P.; Robertson, J. B.; Draper, J. D.; Reibenspies, J. H. J. Am. Chem. Soc. **1999**, 121, 107-116.

(26) Darensbourg, D. J.; Holtcamp, M. W. Macromolecules **1995**, 28, 7577-7579.

(27) Darensbourg, D. J.; Zimmer, M. S.; Rainey, P.; Larkins, D. L. Inorg. Chem. **2000**, 39, 1578-1585.

(28) Darensbourg, D. J.; Zimmer, M. S.; Rainey, P.; Larkins, D. L. Inorg. Chem. **1998**, 37, 2852-2853.

(29) Cheng, M.; Lobkovsky, E. B.; Coates, G. W. J. Am. Chem. Soc. **1998**, 120, 11018-11019.

(30) Allen, S. D.; Moore, D. R.; Lobkovsky, E. B.; Coates, G. W. J. Am. Chem. Soc. **2002**, 124, 14284-14285.

(31) Kim, J. G.; Cowman, C. D.; LaPointe, A. M.; Wiesner, U.; Coates, G. W. Macromolecules **2011**, 44, 1110-1113.

(32) Byrne, C. M.; Allen, S. D.; Lobkovsky, E. B.; Coates, G. W. J. Am. Chem. Soc. **2004**, 126, 11404-11405.

(33) Cheng, M.; Moore, D. R.; Reczek, J. J.; Chamberlain, B. M.; Lobkovsky, E. B.; Coates, G. W. J. Am. Chem. Soc. **2001**, 123, 8738-8749.

(34) Eberhardt, R.; Allmendinger, M.; Luinstra, G. A.; Rieger, B. Organometallics **2003**, 22, 211-214.

(35) Moore, D. R.; Cheng, M.; Lobkovsky, E. B.; Coates, G. W. Angew. Chem. Int. Ed. **2002**, 41, 2599-2602.

(36) Kröger, M.; Folli, C.; Walter, O.; Döring, M. Adv. Syn. Catal. **2005**, 347, 1325-1328.

(37) Kröger, M.; Döring, M. Catal. Today **2006**, 115, 146-150.

(38) Kröger, M.; Folli, C.; Walter, O.; Döring, M. J. Organomet. Chem. **2006**, 691, 3397-3402.

(39) Nozaki, K.; Nakano, K.; Hiyama, T. J. Am. Chem. Soc. **1999**, 121, 11008-11009.

(40) Nakano, K.; Nozaki, K.; Hiyama, T. J. Am. Chem. Soc. **2003**, 125, 5501-5510.

(41) Cheng, M.; Darling, N. A.; Lobkovsky, E. B.; Coates, G. W. Chem. Commun. **2000**, 2007-2008.

(42) Lu, X.-B.; Darensbourg, D. J. Chem. Soc. Rev. **2012**, 41, 1462-1484.

(43) Martinez, L. E.; Leighton, J. L.; Carsten, D. H.; Jacobsen, E. N. J. Am. Chem. Soc. **1995**, 117, 5897-5898.

(44) Tokunaga, M.; Larrow, J. F.; Kakiuchi, F.; Jacobsen, E. N. Science **1997**, 277, 936-938.

(45) Schaus, S. E.; Brandes, B. D.; Larrow, J. F.; Tokunaga, M.; Hansen, K. B.; Gould, A. E.; Furrow, M. E.; Jacobsen, E. N. J. Am. Chem. Soc. **2002**, 124, 1307-1315.

(46) Lu, X.-B.; Wang, Y. Angew. Chem., Int. Ed. **2004**, 43, 3574-3577.

(47) Lu, X.-B.; Shi, L.; Wang, Y.-M.; Zhang, R.; Zhang, Y.-J.; Peng, X.-J.; Zhang, Z.-C.; Li, B. J. Am. Chem. Soc. **2006**, 128, 1664-1674.

(48) Li, B.; Wu, G.-P.; Ren, W.-M.; Wang, Y.-M.; Rao, D.-Y.; Lu, X.-B. J. Polym. Sci., Part A Polym. Chem. **2008**, 46, 6102-6113.

(49) Min, S. S. J. K.; Seong, J. E.; Na, S. J.; Lee, B. Y. Angew. Chem., Int. Ed. **2008**, 47, 7306-7309.

(50) Nakano, K.; Hashimoto, S.; Nozaki, K. Chem. Sci. **2010**, 1, 369-373.

(51) Ren, W.-M.; Zhang, X.; Liu, Y.; Li, J.-F.; Wang, H.; Lu, X.-B. Macromolecules **2010**, 43, 1396-1402.

(52) Ren, W.-M.; Liu, Y.; Wu, G.-P.; Liu, J.; Lu, X.-B. J. Polym. Sci., Part A Polym. Chem. **2011**, 49, 4894-4901.

(53) Qin, Z.; Thomas, C. M.; Lee, S.; Coates, G. W. Angew. Chem. Int. Ed. **2003**, 42, 5484-5487.

(54) Cohen, C. T.; Chu, T.; Coates, G. W. J. Am. Chem. Soc. **2005**, 127, 10869-10878.

(55) Lu, X.-B.; Darensbourg, D. J. Chem. Soc. Rev. **2012**, 41, 1462-1484.

(56) Qin, Z.; Thomas, C. M.; Lee, S.; Coates, G. W. Angew. Chem., Int. Ed. **2003**, 42, 5484-5487.

(57) Cohen, C. T.; Thomas, C. M.; Peretti, K. L.; Lobkovsky, E. B.; Coates, G. W. Dalton Trans. **2006**, 237-249.

(58) Paddock, R. L.; Nguyen, S. T. Macromolecules **2005**, 38, 6251-6253.

(59) Shi, L.; Lu, X.-B.; Zhang, R.; Peng, X.-J.; Zhang, C.-Q.; Li, J.-F.; Peng, X.-M. Macromolecules **2006**, 39, 5679-5685.

(60) Li, B.; Zhang, R.; Lu, X.-B. Macromolecules **2007**, 40, 2303-2307.

(61) Nakano, K.; Nakamura, M.; Nozaki, K. Macromolecules **2009**, 42, 6972-6980.

(62) Ren, W. M.; Zhang, W. Z.; Lu, X. B. Sci. China: Chem. **2010**, 53, 1646-1652.

(63) Aida, T.; Inoue, S. Macromolecules **1982**, 15, 682-684.

(64) Inoue, S.; Koinuma, H.; Tsuruta, T. Polym. J. **1971**, 2, 220-4.

(65) Inoue, S.; Hirano, T.; Tsuruta, T. Polym. J. **1977**, 9, 101-6.

(66) Lednor, P. W.; Rol, N. C. J. Chem. Soc., Chem. Commun. **1985**, 598-9.

(67) Chisholm, M. H.; Navarro-Llobet, D.; Zhou, Z. Macromolecules **2002**, 35, 6494-6504.

(68) Byrnes, M. J.; Chisholm, M. H.; Hadad, C. M.; Zhou, Z. Macromolecules **2004**, 37, 4139-4145.

(69) Inoue, S.; Koinuma, H.; Yokoo, Y.; Tsuruta, T. Makromol. Chem. **1971**, 143, 97-104.

(70) Kuran, W.; Listos, T. Macromol. Chem. Phys. **1994**, 977-984.

(71) Nakano, K.; Nozaki, K.; Hiyama, T. Macromolecules **2001**, 34, 6325-6332.

(72) Larrow, J. F.; Jacobsen, E. N.; Gao, Y.; Hong, Y.; Nie, X.; Zepp, C. M. J. Org. Chem. **1994**, 59, 1939-1942.

(73) Eberhardt, R.; Allmendinger, M.; Rieger, B. Macromol. Rapid Commun. **2003**, 24, 194-196.

(74) van Meerendonk, W. J.; Duchateau, R.; Koning, C. E.; Gruter, G.-J. M. Macromolecules **2005**, 38, 7306-7313.

(75) Kember, M. R.; Jutz, F.; Buchard, A.; White, A. J. P.; Williams, C. K. Chem. Sci. **2012**, 3, 1245-1255.

(76) Kember, M. R.; Williams, C. K. J. Am. Chem. Soc. **2012**, 134, 15676-15679.

(77) Kember, M. R.; White, A. J. P.; Williams, C. K. Macromolecules **2010**, 43, 2291-2298.

(78) Klaus, S.; Vagin, S. I.; Lehenmeier, M. W.; Deglmann, P.; Brym, A. K.; Rieger, B. Macromolecules **2011**, 44, 9508-9516.

(79) Rao, D.-Y.; Li, B.; Zhang, R.; Wang, H.; Lu, X.-B. Inorg. Chem. **2009**, 48, 2830-2836.

(80) Darensbourg, D. J. Inorg. Chem. **2010**, 49, 10765-10780.

(81) Decortes, A.; Castilla, A. M.; Kleij, A. W. Angew. Chem., Int. Ed. **2010**, 49, 9822-9837.

(82) Brule, E.; Guo, J.; Coates, G. W.; Thomas, C. M. Macromol. Rapid Commun. **2011**, 32, 169-185.

(83) Klaus, S.; Lehenmeier, M. W.; Anderson, C. E.; Rieger, B. Coord. Chem. Rev. **2011**, 255, 1460-1479.

(84) Martin, R.; Kleij, A. W. ChemSusChem **2011**, 4, 1259-1263.

(85) Peters, M.; Koehler, B.; Kuckshinrichs, W.; Leitner, W.; Markewitz, P.; Mueller, T. E. ChemSusChem **2011**, 4, 1216-1240.

(86) Quadrelli, E. A.; Centi, G.; Duplan, J.-L.; Perathoner, S. ChemSusChem **2011**, 4, 1194-1215.

(87) Hirano, T.; Inoue, S.; Tsuruta, T. Makromol. Chem. **1975**, 176, 1913-1917.

(88) Parker, R. E.; Isaacs, N. S. Chem. Rev. **1959**, 59, 737-799.

(89) Rokicki, A.; Kuran, W. Makromol. Chem. **1979**, 180, 2153-61.

(90) Nakano, K.; Hashimoto, S.; Nakamura, M.; Kamada, T.; Nozaki, K. Angew. Chem., Int. Ed. **2011**, 50, 4868-4871.

(91) Kember, M. R.; Jutz, F.; Buchard, A.; White, A. J. P.; Williams, C. K. Chem. Sci. **2012**, 3, 1245-1255.

(92) Wu, G.-P.; Ren, W.-M.; Luo, Y.; Li, B.; Zhang, W.-Z.; Lu, X.-B. J. Am. Chem. Soc. **2012**, 134, 5682-5688.

(93) Wu, G.-P.; Wei, S.-H.; Lu, X.-B.; Ren, W.-M.; Darensbourg, D. J. Macromolecules **2010**, 43, 9202-9204.

(94) Wu, G.-P.; Wei, S.-H.; Ren, W.-M.; Lu, X.-B.; Xu, T.-Q.; Darensbourg, D. J. J. Am. Chem. Soc. **2011**, 133, 15191-15199.

(95) Darensbourg, D. J.; Wilson, S. J. J. Am. Chem. Soc. **2011**, 133, 18610-18613.

(96) Wu, G.-P.; Wei, S.-H.; Ren, W.-M.; Lu, X.-B.; Li, B.; Zu, Y.-P.; Darensbourg, D. J. Energy Environ. Sci. **2011**, 4, 5084-5092.

(97) Salmeia, K. A.; Vagin, S.; Anderson, C. E.; Rieger, B. Macromolecules **2012**, 45, 8604-8613.

(98) Chisholm, M. H.; Zhou, Z. J. Am. Chem. Soc. **2004**, 126, 11030-11039.

(99) Thakur, K. A. M.; Kean, R. T.; Hall, E. S.; Kolstad, J. J.; Lindgren, T. A.; Doscotch, M. A.; Siepmann, J. I.; Munson, E. J. Macromolecules **1997**, 30, 2422-2428.

(100) Darensbourg, D. J.; Yarbrough, J. C. J. Am. Chem. Soc. **2002**, 124, 6335-6342.

(101) Nielsen, L. P. C.; Stevenson, C. P.; Blackmond, D. G.; Jacobsen, E. N. J. Am. Chem. Soc. **2004**, 126, 1360-1362.

(102) Nielsen, L. P. C.; Zuend, S. J.; Ford, D. D.; Jacobsen, E. N. J. Org. Chem. **2012**, 77, 2486-2495.

(103) Paddock, R. L.; Nguyen, S. T. J. Am. Chem. Soc. **2001**, 123, 11498-11499.

(104) Keith, J. M.; Larrow, J. F.; Jacobsen, E. N. Adv. Syn. Catal. **2001**, 343, 5-26.

(105) Ren, W.-M.; Wu, G.-P.; Lin, F.; Jiang, J.-Y.; Liu, C.; Luo, Y.; Lu, X.-B. Chem. Sci. **2012**, 3, 2094-2102.

(106) Leung, W.-H.; Chan, E. Y. Y.; Chow, E. K. F.; Williams, I. D.; Peng, S.-M. J. Chem. Soc., Dalton Trans. **1996**, 1229-1236.

(107) Södergren, M. J.; Bertilsson, S. K.; Andersson, P. G. J. Am. Chem. Soc. **2000**, 122, 6610-6618.

(108) Morgan, K. M.; Gronert, S. J. Org. Chem. **2000**, 65, 1461-1466.

(109) Kulasegaram, S.; Kulawiec, R. J. J. Org. Chem. **1997**, 62, 6547-6561.

(110) Prantz, K.; Mulzer, J. Chem. Rev. **2010**, 110, 3741-3766.

(111) Suda, K.; Kikkawa, T.; Nakajima, S.-i.; Takanami, T. J. Am. Chem. Soc. **2004**, 126, 9554-9555.

(112) Suda, K.; Baba, K.; Nakajima, S.-i.; Takanami, T. Tetrahedron Lett. **1999**, 40, 7243-7246.

(113) Suda, K.; Baba, K.; Nakajima, S.-i.; Takanami, T. Chem. Commun. **2002**, 2570-2571.

(114) Debuigne, A.; Poli, R.; De Winter, J.; Laurent, P.; Gerbaux, P.; Wathelet, J.-P.; Jérôme, C.; Detrembleur, C. Macromolecules **2010**, 43, 2801-2813.

(115) Affo, W.; Ohmiya, H.; Fujioka, T.; Ikeda, Y.; Nakamura, T.; Yorimitsu, H.; Oshima, K.; Imamura, Y.; Mizuta, T.; Miyoshi, K. J. Am. Chem. Soc. **2006**, 128, 8068-8077.

(116) Setsune, J.-i.; Ito, S.; Takeda, H.; Ishimaru, Y.; Kitao, T.; Sato, M.; Ohya-Nishiguchi, H. Organometallics **1997**, 16, 597-605.

(117) Gridnev, A. A.; Ittel, S. D.; Fryd, M.; Wayland, B. B. Organometallics **1996**, 15, 222-235.

(118) Lu, H.; Dzik, W. I.; Xu, X.; Wojtas, L.; de Bruin, B.; Zhang, X. P. J. Am. Chem. Soc. **2011**, 133, 8518-8521.

(119) Lyaskovskyy, V.; Suarez, A. I. O.; Lu, H.; Jiang, H.; Zhang, X. P.; de Bruin, B. J. Am. Chem. Soc. **2011**, 133, 12264-12273.

(120) Luinstra, G. A. Polym. Rev. **2008**, 48, 192-219.

(121) Liu, B.; Chen, L.; Zhang, M.; Yu, A. Macromol. Rapid Commun. **2002**, 23, 881-884.

(122) Li, X. H.; Meng, Y. Z.; Zhu, Q.; Tjong, S. C. Polym. Degrad. Stab. **2003**, 81, 157-165.

(123) Lu, X. L.; Zhu, Q.; Meng, Y. Z. Polym. Degrad. Stab. **2005**, 89, 282-288.

(124) Dixon, D. D.; Ford, M. E.; Mantell, G. J. J.Polym. Sci.: Polym. Lett. Ed. **1980**, 18, 131-134.

(125) Kuran, W.; Listos, T. Macromol. Chem. Phys. **1994**, 195, 1011-15.

(126) Liu, B.; Zhao, X.; Wang, X.; Wang, F. J. Appl. Polym. Sci. **2003**, 90, 947-953.

(127) Peng, S.; An, Y.; Chen, C.; Fei, B.; Zhuang, Y.; Dong, L. Polym. Degrad. Stab. **2003**, 80, 141-147.

(128) Gao, L. J.; Du, F. G.; Xiao, M.; Wang, S. J.; Meng, Y. Z. J. Appl. Polym. Sci. **2008**, 108, 3626-3631.

(129) Gao, L. J.; Xiao, M.; Wang, S. J.; Meng, Y. Z. J. Appl. Polym. Sci. **2008**, 108, 1037-1043.

(130) Spencer, T. J.; Kohl, P. A. Polym. Degrad. Stab. **2011**, 96, 686-702.

(131) Yao, M.; Mai, F.; Deng, H.; Ning, N.; Wang, K.; Fu, Q. J. Appl. Polym. Sci. **2011**, 120, 3565-3573.

(132) Yu, T.; Luo, F.-L.; Zhao, Y.; Wang, D.-J.; Wang, F.-S. J. Appl. Polym. Sci. **2011**, 120, 692-700.

(133) Barreto, C.; Hansen, E.; Fredriksen, S. Polym. Degrad. Stab. **2012**, 97, 893-904.

(134) Iler, H. D.; Rutt, E.; Althoff, S. J. Chem. Edu. **2006**, 83, 439.

(135) Ma, Z.; Hong, Y.; Nelson, D. M.; Pichamuthu, J. E.; Leeson, C. E.; Wagner, W. R. Biomacromolecules **2011**, 12, 3265-3274.

(136) Potts, J. R.; Shankar, O.; Du, L.; Ruoff, R. S. Macromolecules **2012**, 45, 6045-6055.

(137) Li, H.; Yan, S. Macromolecules **2011**, 44, 417-428.

(138) Yu, T.; Zhou, Y.; Zhao, Y.; Liu, K.; Chen, E.; Wang, D.; Wang, F. Macromolecules **2008**, 41, 3175-3180.

(139) Zhai, W.; Yu, J.; Ma, W.; He, J. Macromolecules **2005**, 40, 73-80.

(140) Yoon, P. J.; Hunter, D. L.; Paul, D. R. Polymer **2003**, 44, 5323-5339.

(141) Brunelle Daniel, J. Advances in Polycarbonates; American Chemical Society, **2005**; Vol. 898; pp 1-5.

(142) Collier, J. R. Ind. Eng. Chem. **1994**, 61, 50-65.

(143) Lu, X.-B.; Ren, W.-M.; Wu, G.-P. Acc. Chem. Res. **2012**, 45, 1721-1735.

(144) Wu, G.-P.; Ren, W.-M.; Luo, Y.; Li, B.; Zhang, W.-Z.; Lu, X.-B. J. Am. Chem. Soc. **2012**, 134, 5682-5688.

8. Annex

In this part of the work, we focused on the dynamic and folding behavior of the PPC chains in THF solution by using labeled polymers and applying the FRET technique. The idea bases on Fluorescence Resonance Energy Transfer (FRET) between either two different mono labeled polymers or double labeled polymer with FRET-donor and FRET-acceptor. The amount of the transferred energy, gives an indication for the interaction amongst the polymer chains and the distance between each chain which may illustrate the physical behavior of the polymer in solution.

8.1 Fluorescence Resonance Energy Transfer (FRET)

The interaction of the molecules with photons of appropriate energy, can result in a chain of photophysical events, such as internal conversion or vibrational relaxation, fluorescence, intersystem crossing and phosphorescence as shown in the Jablonski diagram (**Figure 8.1**).[1,2] Excited molecules can also relax to the ground state through non-radiative paths or quenching by other molecules or ions (not shown in **Figure 8.1**).

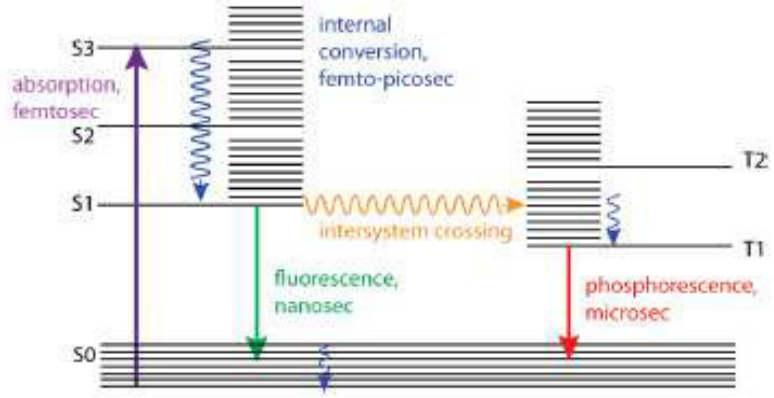

Figure 8.1: Jablonski diagram and a time scale of photophysical processes of organic molecules.[2]

The fluorescence of organic molecules corresponds to the radiative transition from its first singlet state S1 into the ground singlet state S0 (**Figure 8.1**) is characterized by three parameters:[2]

(i) Fluorescence spectrum I(λ) : fluorescence intensity as a function of a wavelength.

(ii) Quantum yield Φ: the ratio of the total number of emitted photons (nf) released in the process of fluorescence to the total number of molecules promoted to the excited state (n).

(iii) Fluorescence lifetime τ.

The time resolved fluorescence decay can be experimentally monitored by Time Correlated Single Photon Counting (TCSPC).

Excitation energy can be transferred from an excited donor molecule to an acceptor molecule through fluorescence resonance energy transfer (FRET) (see **Figure 8.2**). The rate of energy transfer depends on the distance r between donor and acceptor through the following equation:[3]

$$k_{ET} = \frac{1}{\tau}\left(\frac{R_0}{r}\right)^6 \quad (5)$$

Here τ is the fluorescence lifetime of the donor in absence of the acceptor and R_0 is the Förster distance, which in terms depends on the spectral overlap of the two chromophores. The efficiency of energy transfer (E) for a donor-acceptor pair at a fixed distance r is:

$$E = \frac{R_0^6}{R_0^6 + r^6} = 1 - \frac{\tau_{DA}}{\tau} \quad (6)$$

τ_{DA} is the lifetime of the donor in presence of the acceptor.

FRET is widely used to determine distances between two chromophores attached to proteins or DNA and to monitor interaction- or binding events between molecules in vitro and in vivo.[2,4,5]

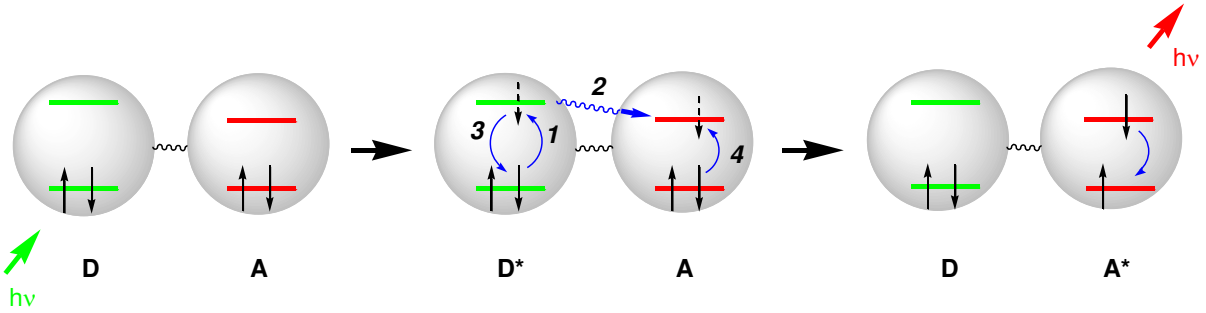

Figure 8.2: Diagram of FRET. Upon excitation by the photon, the electron of the donor is promoted to the excited state (1), followed by the energy transfer to the acceptor excited orbital (2), simultaneous return of the excited electron back to the ground state (3), and excitationof an acceptor (4).[2]

In this chapter, the PPC chains interaction as well the PPC copolymer folding and conformation using chromophore-labeled PPC were studied.

8.2 Results and Discussion

8.2.1 Synthesis of labeled PPC

The donor chromophore (3-(1-naphthyl)propylene oxide) was synthesized in two steps. firstly, by reaction of 1-bromonaphthalene with Mg under anhydrous condition, followed by ring opening of epichlorohydrin to form the required 1-(3-chloro-2-hydroxypropyl)naphthalene which is purified on silica to obtain very viscous yellow oil. Secondly, reaction of 1-(3-chloro-2-hydroxypropyl)naphthalene with aqueous NaOH solution led to intra-molecular ring closure resulting in the required epoxide product. All of the analytical results integrate well with the calculated percentage of each atom in the product. To this end, PPC-donor polymers in different chain length have been synthesized using different catalytic systems and reaction condition as shown in **Table 8.1**.

Table 8.1: Copolymerization of CO_2/rac-PO using 1-(3-chloro-2-hydroxypropyl)naphthalene as donor chromophore.

entry	catalyst system	Pressure(bar)	Temp. (°C)	Time (h)	Conv (%)[c]	M_n(kg/mol)[d]	PDI(M_w/M_n)[d]
1	16b/[PPN]Cl[a]	30	30	2	40	15.7	1.4
2	19a`/DMAP[b]	50	50	4	17	5.7	1.2

[a]catalyst:cocatalyst:donor:PO = 1:1:1:1000. [b]catalyst:cocatalyst:donor:PO = 1:0.5:1:500. [c]Based on isolated yield.[d]Determined by GPC in THF solution, against polystyrene standard.

Labeling of PPC polymer with donor chromophore resulting in **PPC-donor** polymers was confirmed by the absorption spectrum of the labeled polymer in THF solution (**Figure 8.3**).

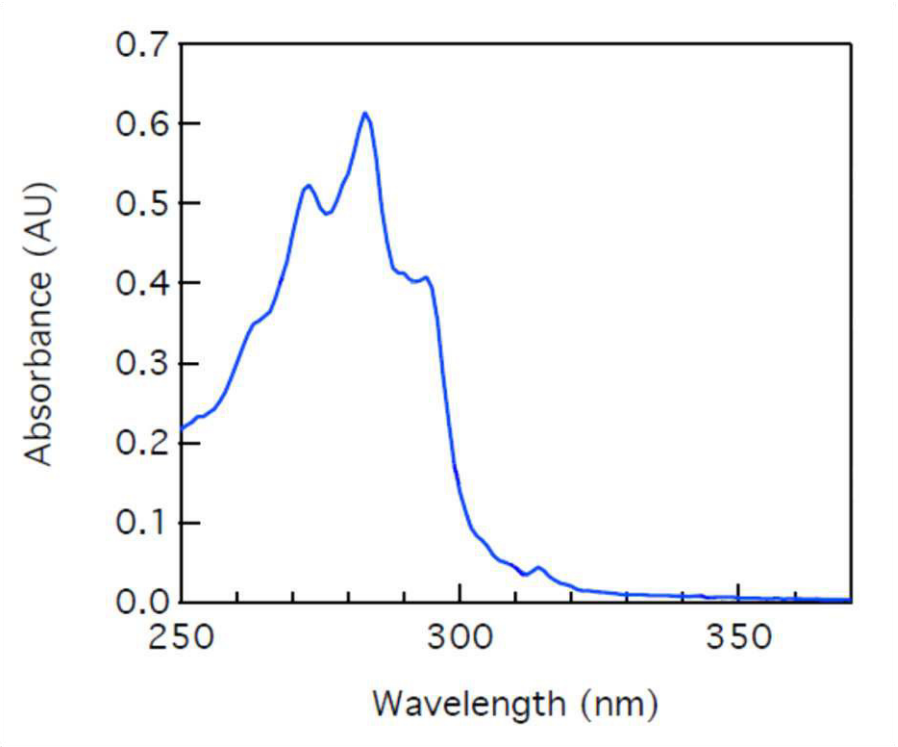

Figure 8.3: UV absorption spectrum of PPC-Donor polymer in THF solution.

The polymeric materials were analyzed by MALDI-ToF MS to determine the PPC-Donor end groups, at least for those chains that are volatilized. In the mass spectrum of the low molecular weight copolymer, two set of masses were found. Although only one combination of the end groups can be expected, the MALDI-ToF MS spectrum showed bimodal molecular weight distribution. **Figure 8.4** shows perfect alternative polycarbonate chains units, with –naphthalene and –H end-groups. The expected chain ends originating from ionization by Na^+

of a **PPC-Donor** of repeating propylene carbonate units resulting from the catalyst-Cl co-ligand initiating moiety and a proton on the other side originating from hydrolysis of the carbonato-catalyst bond during the workup process. However, **Figure 8.4** shows existence the polymer chain units in different structures regarding the formation of ether linkages in a range from 4-12% maximum per chain. Accordingly, corporation of naphthalene end-group was confirmed by MALDI-ToF MS.

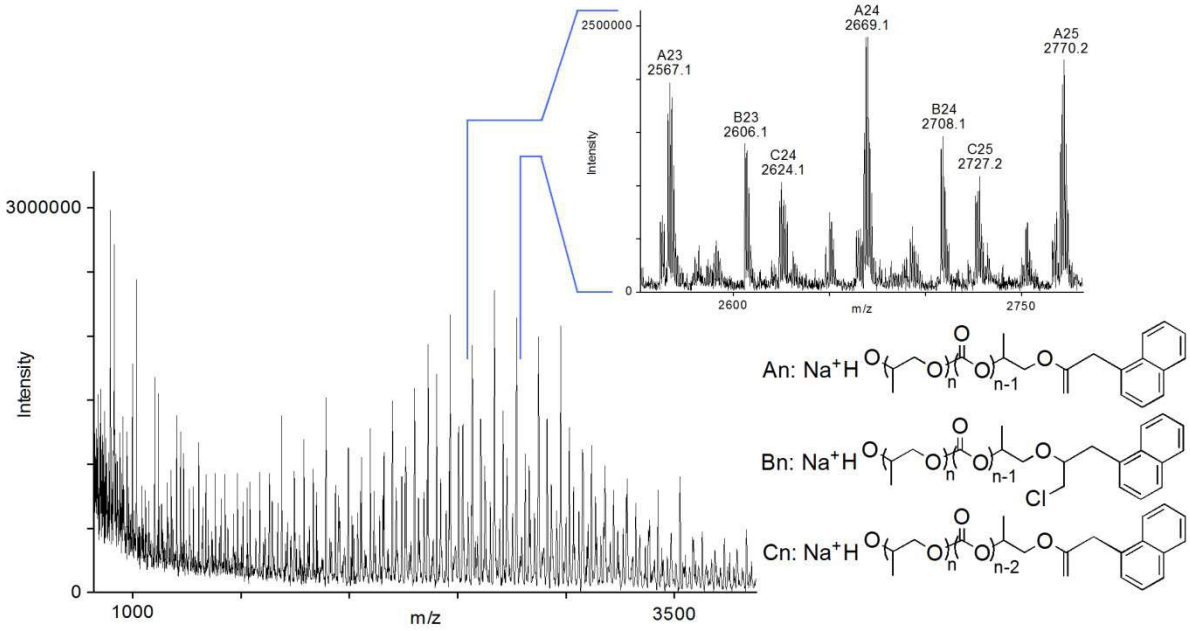

Figure 8.4: MALDI-ToF mass spectrum of mono labeled **PPC-Donor**polymer and the series assignments.

The mono labeled PPC-Dansyl (**Acceptor-PPC**) polymers were synthesized by simple reaction of PPC polymers with dansyl chloride in dry acetone using dry triethyl amine as organic base.

8.2.2 FRET Measurements of labeled PPC

The fluorescence decay time of the **PPC-donor** in THF was found to be 20 ns. The fluorescence decay of **PPC-donor/acceptor-PPC** mixture in THF solution did not show any indication for resonance energy transfer even for high excess of **acceptor-PPC** with respect to

PPC-donor, exhibiting that the PPC polymer chains do not show a polymer alignment alongside the polymer chains. This can be assigned to the polymer chain folding, which may prevent the chromophores encountering. Accordingly, double labeled PPC copolymers using donor (naphthalene group) and acceptor (dansyl group) chromophores (**Acceptor-PPC-Donor**, one at each end) with different chain length were synthesized. The double labeled PPCs were synthesized in two steps, namely first by synthesizing the mono labeled PPC-donor polymer using different catalytic system. The isolated polymers were then reacted simply with dansyl chloride in dry acetone using dry triethylamine as organic base, resulting in double labeled PPC (**Acceptor-PPC-Donor**) with different chain length (**Table 8.2**).

Table 8.2: GPC trace results of the **Acceptor-PPC-Donor** polymers.

run	catalyst system	M_n(kg/mol)[c]	PDI(M_w/M_n)[c]
1	16b/[PPN]Cl[a]	16.8	1.6
2	19a`/DMAP[b]	6.4	1.2

[a]catalyst:cocatalyst:donor:PO = 1:1:1:1000. [b]catalyst:cocatalyst:donor:PO = 1:0.5:1:500. [c]Determined by GPC in THF solution, against polystyrene standard.

Existence of both donor and acceptor on both terminal sides of PPC polymers was confirmed by the absorption spectrum of the double-labeled PPC polymer (**Acceptor-PPC-Donor**) in THF solution with respect to the PPC-**donor** polymer (**Figure 8.5**).

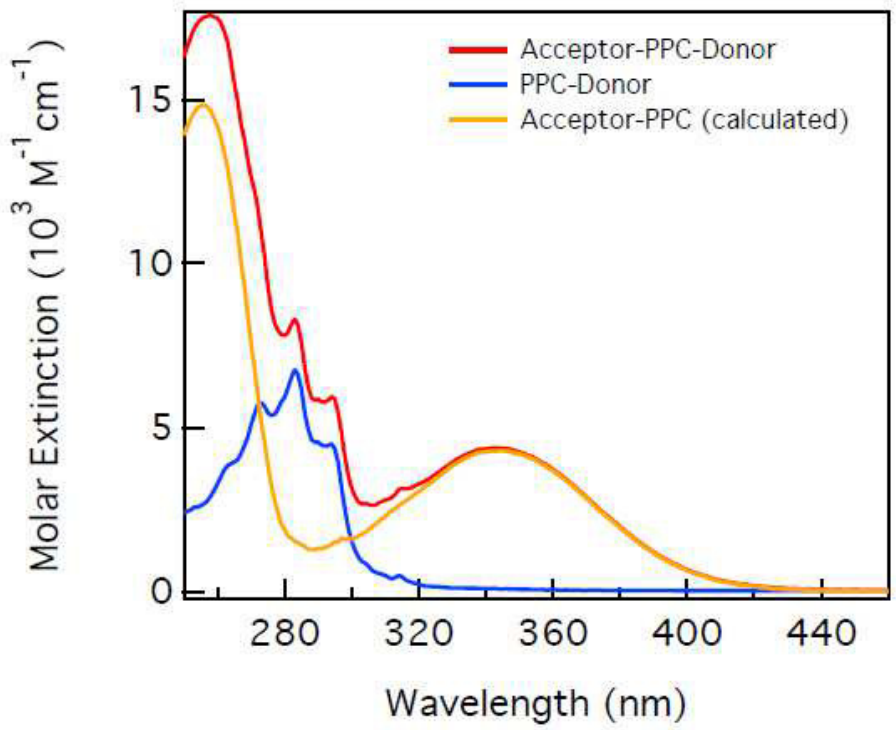

Figure 8.5: Absorption spectrum of labeled PPC polymers in THF solution in the uv region.

The Förster distance of the donor-acceptor pair attached to PPC was determined from the spectral overlap (**Figure 8.6**) to be $R_0 = 1.94$ nm.

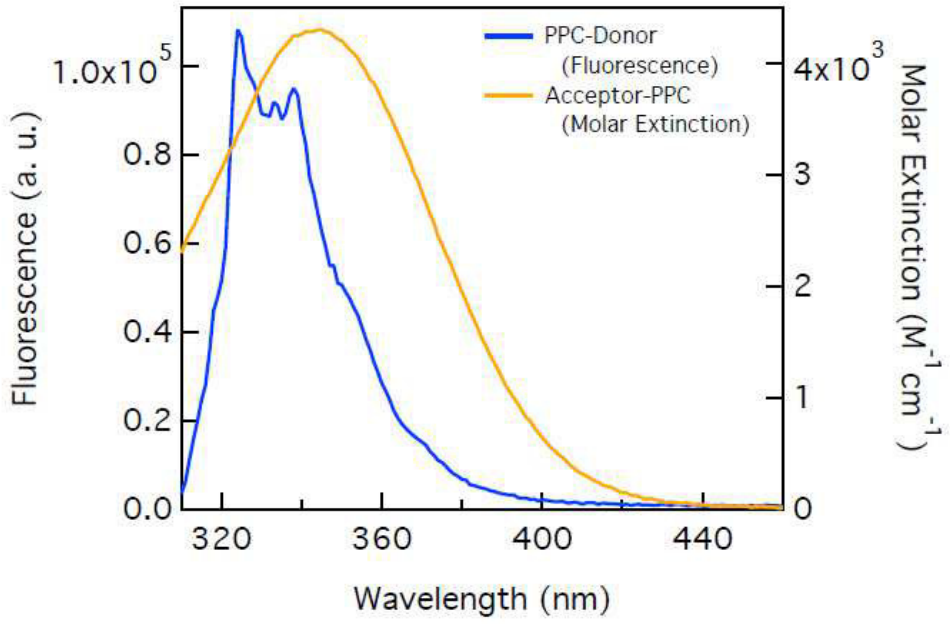

Figure 8.6: overlapping of fluorescence emission spectrum of **PPC-Donor** ($\lambda_{exitation}$ = 281 nm) and absorption of **Acceptor-PPC**

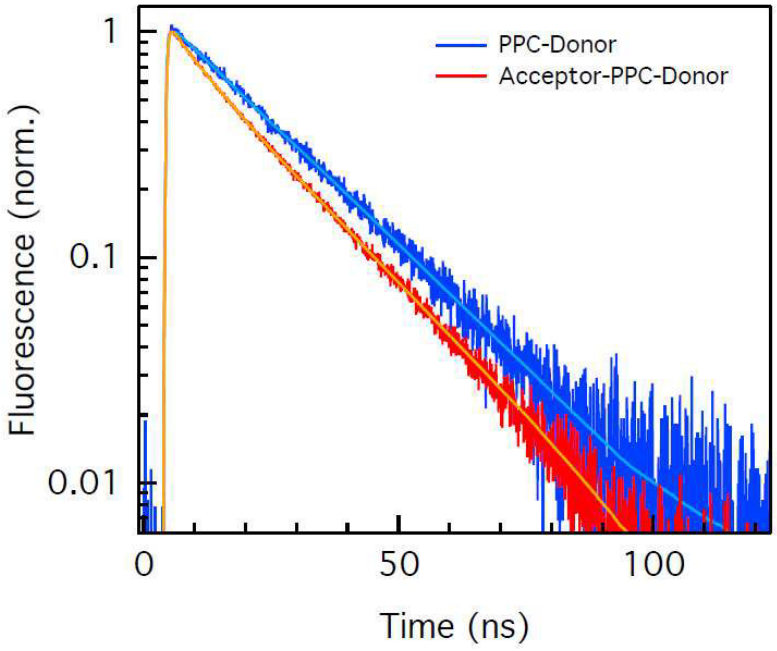

Figure 8.7 Normalized time-resolved emission decay of labeled PPC.

For the **Acceptor-PPC-Donor** polymer with relative high M_n (Table 8.2, entry 1) no FRET was observed in TCSPC measurements (data are not shown), revealing that the two chromophores are not close enough for FRET. On the other hand, the **Acceptor-PPC-Donor** polymer with relative low M_n (Table 8.2, entry 2) showed a reduction of the fluorescence lifetime due to FRET occurrence as indicated in **Figure 8.7**.

The fluorescence lifetime decay of the donor showed a large amount (59%) of donor only decay with τ_1 = 19.8 ns. Two fast phases where present in the sample with relative amplitudes of 27% and decay time τ_2 = 9.74 ns and 14% with τ_3 =1.07 ns respectively. By calculating the corresponding donor-acceptor distances from the FRET-efficiency, distances of 1.93 nm and 1.2 nm are found for these two phases. It is possible that these two phases in the fit belong to one conformational species, which has a broad donor-acceptor distance distribution.

The 59% of donor-only decay can be proposed based on the two following possibilities:

a) The acceptor is too far from the donor (≳5 nm).

b) The lack of the acceptor in the labeled polymer either due to bleaching or due to the incomplete labeling.

From the UV-Vis spectrum of **Acceptor-PPC-Donor** (**Figure 8.5**, red trace) it seems unlikely that incomplete labeling occurred for more than around 15% of the molecules and typically bleaching should not affect more than 5% of the sample. However, 20% maximally of the sample were lacking the acceptor and are uninformative about the polymer conformation and are discarded. Assuming that 20% of the overall polymer sample either does not have an acceptor or the acceptor was bleached, half of the remaining 80% of the sample can undergo FRET. It is likely that the observed FRET is due to some intermolecular or intramolecular chain interaction of the polymers sample. A possible explanation is that the polymer chains align alongside each other in both directions with equal probability resulting in decay with the donor only lifetime without FRET when donor comes close to donor or with a faster decay due to FRET, when donor is close to acceptor. We also tried to fit the fluorescence lifetime data presuming a random coil distribution of end-to-end distances. This did not lead to any physically meaningful results, so it seems unlikely that PPC in solution adopts conformations like a random coil. However, the FRET measurements in this work was conducted in THF solution, accordingly it is suggested to imply the same FRET measurements in solid sate to depict a clear picture for the interaction between the polycarbonates chains in solution and in solid state as well.

8.3 Experimental Part

8.3.1 Chemicals and Methods

All manipulations involving air- and/or moisture sensitive compounds were carried out using standard Schlenk/glovebox techniques under an argon atmosphere unless otherwise stated. Propylene oxide and epichlorohydrin were purchased from Acros and distilled under argon atmosphere over CaH_2 prior to use. 1-Bromonaphthalene was purchased from ABCR and

freshly distilled under vacuum and stored under argon. CO_2 of purity grade 4.5 was purchased from Westfalen AG and was applied in all experiments without additional purification. Dry solvents were obtained with an MBraun MB-SPS-800 solvent purification system. All other chemicals were purchased from Aldrich and used as received without further purification. MALDI-ToF MS measurements were performed on a Bruker Ultra flex ToF/ToF mass spectrometer. All samples were prepared in THF and dithranol doped with sodium trifluoroacetate. Fluorescence lifetime measurements were performed using TCSPC technique with FluoTime 200. The emission was exited by laser pulses with wavelength of 281 nm with pulse width < 635ps. Emission wave length was selected by monochromater (348 nm and 520 nm for donor and acceptor, respectively). Fluorescence measurement measurements were performed using fluorolog with excitation band width 1nm and emission band width 2nm. UV-Vis absorptions were performed using spectrophotometer 14 UV-Vis with band width 1nm.

8.3.2 Syntheses

8.3.2.1 Synthesis of 1-(3-chloro-2-hydroxypropyl)naphthalene

8.3.2.1.1 Method A

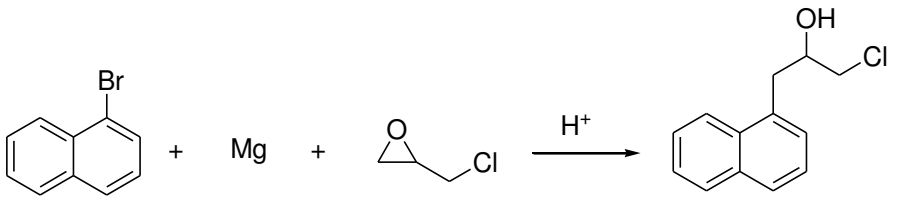

A two necked Schlenk flask connected to a reflux condenser, and an addition funnel was charged with magnesium turning (2.26 g, 93 mmol) and one iodine crystal in dry THF (100 mL). A solution of 1-bromonaphthalene (6.5 mL, 9.65 g, 46.6 mmol) in dry THF (50 mL) is added in small portions by dropping funnel until the reaction initiated. The reaction

temperature was allowed to cool down and all the 1-bromonaphthalene solution was then added in one shot. The funnel was then rinsed with dry THF (20 mL), and the slurry was refluxed with stirring for 1 h. The reaction mixture was then allowed to cool down slowly to ambient temperature. Epichlorohydrin was then added at once under argon at 0 °C. The reaction mixture was allowed to reach room temperature and stirred over night. Aqueous HCl solution (3 M, 100 mL) was then slowly added at 0 °C and the organic was extracted with diethyl ether (2 × 100 mL). The combined organic layers were collected, washed with water and then dried over anhydrous Na_2SO_4. After filtration, the volatiles were removed and the product was purified by flash chromatography (EtOAc 0—10% in Hexane) affording viscous yellow oil (3.0 g, 30% yield).

R_f (SiO_2, 2:8 EtOAc:Hexane) = 0.32

^{1}H NMR ($CDCl_3$, *300 MHz) δ 8.06*-8.09(m, 1H), 7.90-7.87(m, 1H), 7.81-7.78(m, 1H), 7.59-7.49(m, 2H), 7.47-7.39(m, 2H), 4.28-4.21(m, 1H), 3.66(dd, J= 4.1, 11.1Hz, 1H), 3.58(dd, J=5.9, 11.1 Hz, 1H), 3.37(dd, J= 6.3, 13.9 Hz, 1H), 3.30(dd, J= 6.9, 13.9 Hz, 1H),2.24(s, 1H, OH).

^{13}C NMR ($CDCl_3$, 75 MHz) δ_C 134.08, 133.28, 132.09, 129.03, 127.87, 127.85, 126.38, 125.91, 125.63, 123.69, 71.48, 49.60, 37.89.

EA for $C_{13}H_{13}ClO$, Calculated: C, 70.75; H, 5.94. Found: C, 71.17; H, 6.00.

8.3.2.1.2 Method B

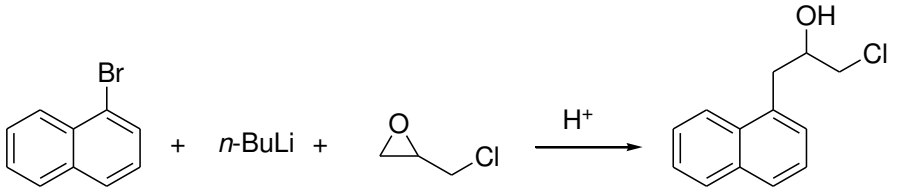

A two necked Schlenk flask connected to a reflux condenser, and an addition funnel was charged with dry 1-bromonaphthalene (7.0 mL, 10.4 g, 50.2 mmol) in dry THF (200 mL)

under Argon. n-BuLi (2.5 M, 24.1 mL, 60.2 mmol) was then added drop-wise by additional funnel at -83 °C with stirring. After complete addition, the funnel was then rinsed with dry THF (10 mL) and the reaction mixture was stirred for 1 h. Dry epichlorohydrin (3.9 mL, 4.64 g, 50.2 mmol) was then added in one shot and the reaction mixture was stirred at -83 °C for additional 2h. Aqueous HCl solution (3 M, 100 mL) was then slowly added at 0 °C and the organic was extracted with diethyl ether (2 × 100 mL). The combined organic layers were collected, washed with water and then dried over anhydrous Na_2SO_4. After filtration, the volatiles were removed and the product was purified by flash chromatography (EtOAc 0─10% in Hexane) affording viscous yellow oil (1.0 g, 10% yield).

The analytical results of method B are similar to the method A.

8.3.2.2 Synthesis of 3-(1-naphthyl)propylene oxide

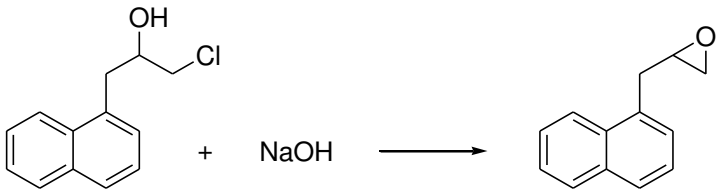

Two neck round bottom flask connected to condenser was charged with 1-(3-chloro-2-hydroxypropyl)naphthalene (5.0 g, 22.7 mmol) suspended in hexane (50 mL). Solution of NaOH (1.2 g, 32 mmol) in water (10 mL) was then added slowly with vigorous stirring. After complete addition, the reaction mixture was stirred at 70 °C for 5h. The reaction temperature was cooled down to ambient temperature and the organic phase was separated, washed with water (3 × 100 mL) and dried over N_2SO_4. After filtration, the volatiles were removed and the product was purified by flash chromatography (EtOAc 0─10% in Hexane) affording colorless oil (1.0 g, 25% yield).

b.p. 85 °C (0.01 mbar)

R_f (2:8 EtOAc: Hexane) = 0.58

^{1}H NMR ($CDCl_3$, *300 MHz) δ 8.11 (d, J =8.2 Hz, 1H), 7.93 (d, J =7.9 Hz , 1H), 7.83(m ,* 1H),7.63-7.48(m, 4H), 3.49-3.27 (m, 3H), 3.85 (dd, J=4.3, 4.1Hz, 1H), 2.63 (dd, J =2.0, 4.2Hz, 1H).

^{13}C NMR ($CDCl_3$, *75 MHz)* δ_C 133.72, 133.47, 132.10, 128.69, 127.37, 126.81, 126.03, 125.60, 125.48, 123.68, 51.93, 47.11, 35.56.

EA for $C_{13}H_{12}O$, Calculated: C, 84.75; H, 6.57; O, 8.68. Found: C, 84.93; H, 6.54; O, 8.53.

8.3.2.3 Representative procedure for synthesis of labeled PPC

8.3.2.3.1 Labeled PPC with 3-(1-naphthyl)propylene oxide

All polymerization experiments were performed in 100 mL steel autoclaves equipped with a magnetic stirring bar. The autoclave was prepared by heating at 130 °C overnight and cooling under vacuum to ambient temperature. The autoclave was charged under an argon atmosphere with a solution of catalyst and cocatalyst in appropriate amount and 1 equivalent of 3-(1-naphthyl)propylene oxide with respect to the catalyst in dry CH_2Cl_2 (2.5 mL). The mixture was then stirred at room temperature for 10 min. Dry PO (2.5 mL, 35.75 mmol) was then transferred by syringe under a flow of argon. The mixture solution was stirred about 10 minutes and then placed into a pre-heated oil bath to appropriate temperature and pressurized to appropriate pressure with CO_2. After the allotted reaction time, the autoclave was cooled to 0 °C and the pressure slowly released. An aliquot of the crude copolymer was taken for NMR spectroscopic analysis. The crude polymer was then dissolved in a minimal volume of dichloromethane and precipitated with methanolic HCl solution (2.2 M, 100 mL). This process was repeated three times to completely remove the catalyst and the obtained colorless polymer was dried at 60 °C under vacuum to constant weight.

8.3.2.3.2 Labeled PPC with dansyl chloride

A two necked Schlenk flask connected to a reflux condenser was charged with dansyl chloride (0.97 g, 3.6 mmol) and PPC (2 g) under argon. Dry acetone (20 mL) was then transferred by syringe followed by addition of dry triethylamine (0.5 mL, 3.6 mmol). The resulting yellow solution was then refluxed for 2 h. The reaction solution was cooled to ambient temperature and the polymer was precipitated by addition of methanol. The crude polymer was then dissolved in a minimal volume of dichloromethane and precipitated with methanol. This process was repeated three times to completely remove the excess dansyl chlordie and the obtained pale yellow polymer was dried at 60 °C under vacuum to constant weight.

8.3.2.3.3 Double-labeled PPC with dansyl chloride and 3-(1-naphthyl)propylene oxide

The resulting labeled polymer in 8.3.2.3.1 was treated as shown in 8.3.2.3.2, resulting in yellow polymer.

8.4 References

(1) Jablonski, A. Nature **1933**, 131, 839-840.

(2) Berezin, M. Y.; Achilefu, S. Chem. Rev. **2010**, 110, 2641-2684.

(3) Lakowicz, J. R. Principles of Fluorescence Spectroscopy; third ed.; Springer: USA, **2006**.

(4) Sinkeldam, R. W.; Greco, N. J.; Tor, Y. Chem. Rev. **2010**, 110, 2579-2619.

(5) Zhang, H.; Liu, Y.; Yao, D.; Yang, B. Chem. Soc. Rev. **2012**, 41, 6066-6088.